Integrating apatite (U-Th)/He and fission track dating for a comprehensive thermochronological analysis: refining the uplift history of the Teton Range

Summer Jasmine Brown

Thesis submitted to the faculty of the Virginia Polytechnic Institute and State University
in partial fulfillment of the requirements for the degree of

Master of Science
In
Geosciences

James A. Spotila
Richard D. Law
Jefferey M. Rahl

04/29/2010
Blacksburg, Virginia

Keywords: Teton Range, apatite, thermochronometry, exhumation

Integrating apatite (U-Th)/He and fission track dating for a comprehensive thermochronological analysis: refining the uplift history of the Teton Range

Summer Jasmine Brown

ABSTRACT

Uplift of the Teton Range is primarily controlled by displacement across the range-front Teton normal fault. The Tetons comprise the footwall block while the hanging wall encompasses Jackson Hole valley and a portion of the Snake River. Relative to the rest of the Rocky Mountains, the Tetons experienced the majority of uplift very recently, substantiating the need for a detailed investigation integrating structural analysis and bedrock thermochronometry. New low-temperature cooling ages are documented in three vertical transects across the Teton Range and at low elevations parallel to the Teton fault. Samples adjacent to the Teton fault are consistently young (~9 Ma) and represent a minimum estimate for the onset of Teton fault-related uplift. Modeling of time-temperature histories supports a ~9-11 Ma onset of rapid uplift, indicating that the Teton fault likely originated as a Basin and Range-type structure. A maximum throw of ~8 km occurs proximal to the Grand Teton, while the average throw for the entire ~100 km along-strike fault length is ~3.3 km. Thus, the geometry of the Teton fault is comparable to traditional scaling relationships dictating a correlation between fault length and displacement.

Inversion of the typical (U-Th)/He (AHe) and fission track (AFT) relationship in a few of the Teton Range samples is a result of intense zoning, primarily in apatite from Precambrian layered gneisses. Nonetheless, both the AHe and AFT ages consistently indicate slight differential uplift of the Tetons between the Late Oligocene and Middle Miocene. HeFTy models indicate that doming of the Precambrian-Paleozoic unconformity occurred prior to ~50 Ma. However, by ~15 Ma, rapid cooling of the Mount Moran section essentially "flattened" the unconformity. Thus, the modern domed shape is a result of displacement across the Teton fault, allowing the unconformity to be used as a proxy for fault deformation. Moreover, reconstruction of the unconformity and volume calculations produced an average depth to incision of ~0.3 km and a long-term erosion rate of 0.18 mm/yr. Compared to the long-term uplift rate of 0.22 mm/yr, this provides a quantitative explanation for the modern Teton topography.

ACKNOWLEDGEMENTS

Jim, you essentially let me take charge of this project, and although you had to steer me back on course once in a while, it was just the right amount of involvement. I never wanted an advisor who would dictate all of my actions every single day, and it was one of the main reasons I came back to Virginia Tech to work with you. My committee has been equally helpful, providing excellent feedback and plenty of good faith. Jeff came into this project with only a year left, and although we hadn't even met, your enthusiasm for my progress was much needed and very reassuring. Rick you let me take over Structure Lab, join you in Scotland for two field seasons, and I have thoroughly enjoyed spending many evenings with you and your family. Chris Krugh at the University of Wyoming completed the fission track portion of the project and I truly appreciate him taking time from his own work to process the Teton samples.

Lisa, you have been the other half of this project, and your familiarity with the Tetons and the permitting process made my transition quite easy. I will always be indebted to you for the impromptu night we spent on Mount Moran. Although we didn't have our own sleeping bags, tent, warm clothes, or any real food for that matter, you never once complained. Aaron taught me apatite separation and picking techniques, and no matter how bad that would get, when I heard Phil shouting expletives, I always thought, "well, at least I know how to use Illustrator".

I have found the support staff in our department to be a tremendous help. Connie, you have rescued me numerous times over the past seven years. Additionally, Miles and Mark L. have been invaluable assets through multiple instances of hard drive failure and printing frustrations.

Whereas many graduate students find teaching a weighty responsibility, I often found it justified my presence at Virginia Tech, especially when I hit obstacles during the course of my thesis. Although I never expected it, the support my students provided by acknowledging my efforts to improve them as budding geologists, draftsmen, and writers kept me going. I never imagined I would have students sincerely thank me for giving out D's and F's on first drafts!

My parents played a large role in getting me here; mostly, for never really questioning my decisions, whether it was choosing geology as a major or calling from the Outer Banks at seventeen to announce that my car broke down and that I was going to live and work there for the rest of the summer. Some were well-planned and others were absurdly spontaneous, but by allowing me the freedom to make my own choices, you gave me an independence that carries me further than six years of classes and seminars. My grandparents set the bar high from the start, and their own academic endeavors fascinated me. Spending summer days on a college campus with my grandmother and seeing my grandfather's archeological excursions on the regional news was nothing short of awesome. Their constant travels to exotic countries inspired me to find a career allowing the same.

My siblings and friends have allowed me to enjoy a life outside of geology, which it seems is a rarity in this profession. When I need an impromptu road trip, hike, or back-porch wine drinking session, one of you always is up to the challenge, ready to supply hours of excellent conversation, and never once uttering the words apatite or exhumation. Cassie, as my sister, you are certainly the foil in my life story, but you are the only person I've met with my exact sense of humor and the past twenty four years would not have been nearly as enjoyable without you. Some close friends also assisted in the thesis work. Philip Mothena, volunteered to travel to the Tetons to help carry rocks, and has since become the standard in field assistant

excellence. My roommate Allison not only kept our apartment tidy, but with her own degree in English was essentially my personal editor and secretary.

Finally, Ryan, you have kept me going the past five years. You have put up with my crazy sleeping and working schedule, provided coffee on early mornings, and helped with my home improvement ventures, all while being the ultimate geological reference. By dragging me to meetings early on, you have given me quite the repertoire of connections in the geology world, and I owe the majority of my success and confidence to you. I hope in fifty years we are still leaping out of the car (okay, maybe crawling), you with your hammer and me with my camera, racing to great road cuts on our cross-country travels.

Table of Contents

List of Tables and Figures

1. INTRODUCTION

Basin and Range type normal faults are prevalent across the western United States, often in areas with preexisting Sevier and Laramide deformation. The Teton Range lies near the eastern flank of the Basin and Range province and within the Sevier Idaho-Wyoming thrust belt. The Laramide orogeny is primarily responsible for bringing Precambrian metamorphic and plutonic rocks, those composing the core of the Tetons, to the surface (Figure 1A & B). Many studies have examined the relative influence of these previous episodes of deformation on the Tetons, and more recently, the possibility of uplift related to migration of the Yellowstone hotspot (e.g. Pierce and Morgan, 2009). The majority of Teton uplift is governed by displacement across the Teton fault, a range front normal fault spanning the entire eastern length of the Teton Range (Figure 1C). Similar faults have been observed encircling the Snake River Plain, supporting the notion of uplift related to encroachment of a hotspot (Anders et al., 1989; Anders and Sleep, 1992; Pierce and Morgan, 1992), and thus making the Tetons particularly important as they represent the interface of four distinct tectonic provinces.

The dramatic relief of the Teton Range suggests recent uplift (Figure 2), and although the Teton normal fault is the source, disagreements exist regarding the timing of initiation and displacement magnitude across this structure (Smith et al., 1993a; Byrd et al., 1994). Attempts to correlate the Precambrian-Paleozoic unconformity, present at high elevations in the hanging wall, with the assumed footwall position beneath Quaternary sediments in Jackson Hole, have produced multiple estimates for displacement on the Teton fault. Throw estimates range from 2.5 km to 9 km (Behrendt et al., 1968; Love, 1977; Gilbert et al., 1983; Smith, 1991; Byrd et al., 1994) while derivations of the onset of faulting span between 13 and 2 Ma (Barnosky, 1984; Byrd et al., 1994; Love et al., 2003; Morgan and McIntosh, 2005; Leopold et al., 2007; Pierce and Morgan, 2009). Consequently, disputes exist regarding the long-term vertical slip rate, and range from 0.5 to 1.2 mm/yr.

In an effort to resolve some of these discrepancies, Roberts and Burbank (1993) analyzed apatite fission tracks (AFT) suggesting early exhumation of the southern Tetons and, although beyond the scope of AFT, hypothesized rapid recent uplift of the northern portion of the range. However, assumptions made based on the AFT data of Roberts and Burbank (1993) are questionable, in need of further examination and possibly reinterpretation. Also, advances in the use of fission track dating, and the renaissance of apatite (U-Th)/He (AHe) techniques (e.g.

Farley, 2000), have redefined the expectations of a comprehensive thermochronological study. For fission track dating, apatite has a closure temperature of ~110°C, implying that AFT ages from the previous transects do not clearly define the onset of Teton uplift because there is no record of cooling below ~110°C. Since many important tectonic and erosional processes occur in the upper 5 km of the crust, it is necessary to incorporate other methods to bridge gaps left by previous low-temperature studies.

Low-temperature cooling data can potentially provide insight into faulting kinematics, particularly in relatively young settings (Ehlers et al., 2001), as footwall topographic relief seems to be directly correlated to fault development in extensional systems (Densmore et al., 2005). Over the past decade, there has been increased interest in the formation and growth of normal faults, especially in Basin and Range type scenarios involving relatively simple fault block geometries (e.g. Reiners et al., 2000). Nonetheless, the fundamental mechanisms involving the initial kinematics are not well understood. In the case of the Teton fault, it is important to determine if the progression of uplift along the Teton escarpment was along-strike growth or a constant-length increase in relief and offset. Although recent uplift of the Teton Range is influenced by it's proximity to the Yellowstone hotspot (Figure 1A), the fault-controlled footwall uplift provides an opportunity to utilize low-temperature dating to compare the leading fault development models and examine the early history of the Teton fault. Additionally, the structural geometry can strongly influence ages and thus requires a thorough understanding of the fault history to correctly interpret low temperature data.

Here we present apatite (U-Th)/He ages from a series of bedrock transects along and across the Teton Range that document the most recent stages of exhumation and further demonstrate the applicability of AHe for constraining normal fault evolution. Vertical transect AHe data indicates relatively rapid uplift of the northern Tetons, supporting early predictions made by Roberts and Burbank (1993). Data from a series of new AFT samples, however, prove to be more complicated, in some case involving inversions of the typical young AHe and old AFT age relationship. Additionally, conflicts between older AFT (Roberts and Burbank, 1993) and the new AFT ages suggest that further examination of both datasets is necessary, requiring in-depth exploration of the differences in methods.

Figure Captions

Figure 1: The Teton Range is located in northwestern Wyoming and is governed by displacement on the Teton normal fault. A) Location map of the Teton Range in northwestern Wyoming showing extent of Basin and Range, Snake River Plain, Yellowstone System, and Sevier thrusts (after Smith and Seigal, 2000). Notable range-forming normal faults are shown. B) Simplified geologic map of the Teton Range (after Love et al., 1992). C) Block model of the Teton normal fault with the Tetons in the footwall and Jackson Hole valley in the hanging wall. The highest peaks are centrally located along strike.

Figure 2: Photos show the dramatic topography of the Teton Range. A) View of the Teton Range showing rugged topography and eastern range front taken from Signal Mountain. Photo by Jeff Gardner, 2009, used with permission. B) Grand Teton from Buck Mountain. Notch left of summit is the Upper Saddle. Photo by Summer Brown, 2008. C) View north from Upper Saddle of Grand Teton. High peak near center of photograph is Mount Moran. Photo by Jeff Gardner, 2009, used with permission.

Figure 1. The Teton Range is located in northwestern Wyoming and is governed by displacement on the Teton normal fault.

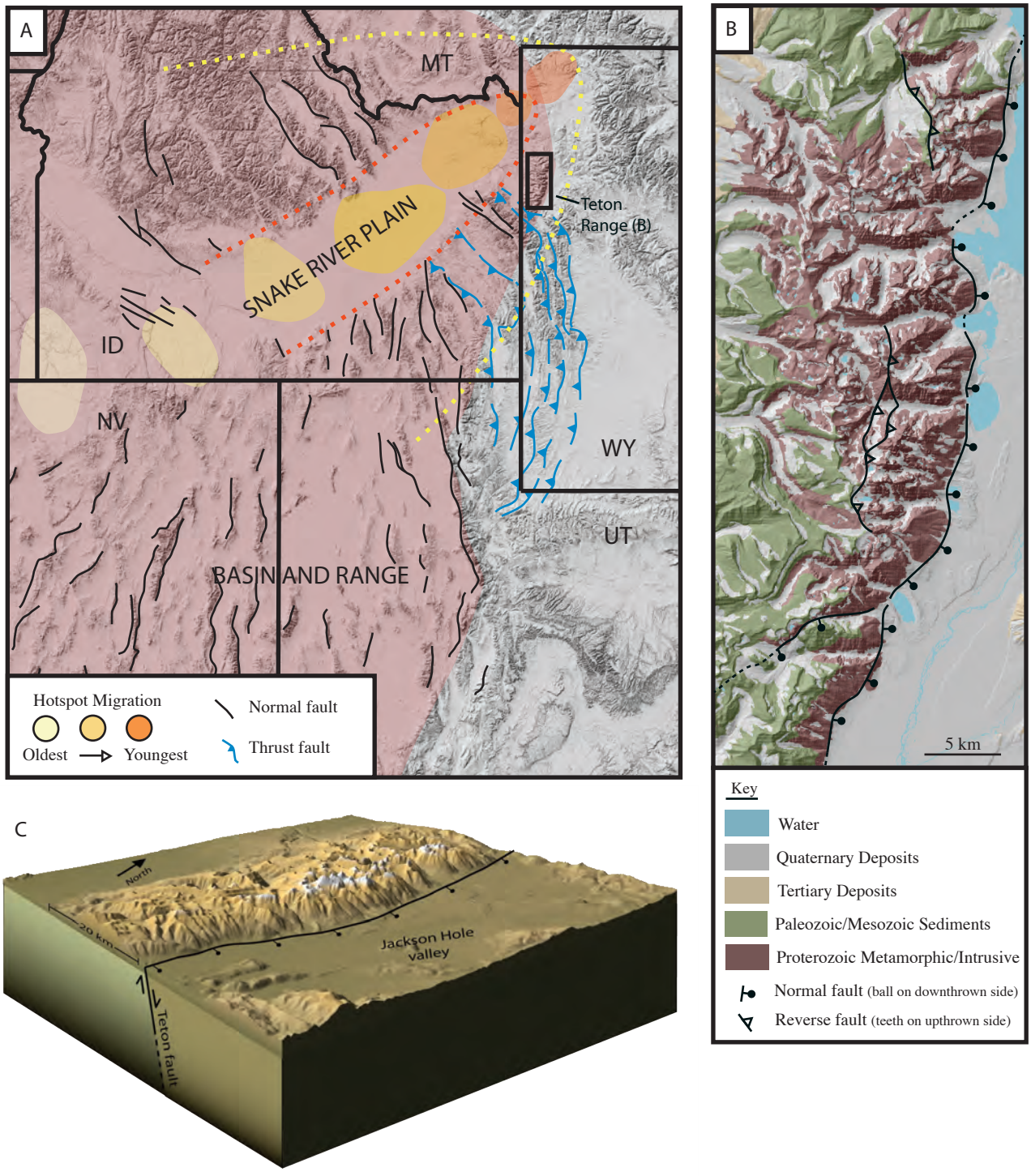

Figure 2. Photos show the dramatic relief of the Teton Range. A) Rangefront view with Grand Teton in center (Jeff Gardner, 2009). B) View of the Grand Teton from Buck Mountain (Jeff Gardner, 2009). C) Looking north from Grand Teton (Summer Brown, 2008).

2. BACKGROUND

2.1 The Behavior of Large, Range-Bounding Normal Faults

There is generally a direct relationship between displacement and fault length in most faults. Historically, this relationship has been represented by:

$$D = cL^n$$

where D is the maximum displacement, L is the length of the fault trace, c is a constant, and n is between 1 and 1.5 (Walsh and Watterson, 1988; Cowie and Scholz, 1992; Gillespie et al., 1992; Dawers et al., 1993; Schlische et al., 1996; Walsh et al., 2002). Densmore et al. (2004) documented a correlation between throw and fault length for 11 faults surrounding the Snake River Plain, where n is 1 and c is 0.33. This is consistent with earlier work by Schlische et al. (1996) examining fault scaling over eight orders of magnitude (Figure 3A). Because fault growth is recognized to be the result of repeated earthquake events, documenting the relationship between the magnitude and frequency of earthquakes and fault growth is an essential first step to understanding the behavior of fault systems. A constant slip to length ratio of 5×10^{-5} has been found to represent a linear relationship between slip and fault-rupture length of actual rupture events (Wells and Coppersmith, 1994). Conventional models propose that faults are significantly shorter in early stages, and grow in length as displacement accrues (Walsh and Watterson, 1988; Cowie and Scholz, 1992) (Figure 3B). However, these established fault models show a much higher displacement to length ratio than the individual rupture events, suggesting a need for a different approach. An alternative model, consistent with the aforementioned displacement data, suggests that fault lengths are established early and rapidly because the subsequent interaction between adjacent faults reduces any lateral propagation (Walsh et al., 2002).

Another relevant topical issue related to normal fault behavior deals with their along strike integration and segmentation. Although segmented faults are common, the kinematics of the linkage and growth of the segments are poorly understood. Early models involve propagation of spatially and mechanically independent segments, which incidentally overlap, resulting in a single larger displacement structure (Morley et al., 1990; Cartwright et al., 1995, 1996; Dawers and Anders, 1995). Most importantly, these models require that overlap of the faults occur entirely by chance. A different account, first proposed by Childs et al. (1995, 1996b), suggested that fault segments initiate and grow individually, but that they are

kinematically related from initiation, "soft-linked" by ductile strain of the material between them and are therefore "coherent" (Figure 3C) (Walsh et al., 2003). Fault arrays often display a displacement deficit between fault segments (discontinuous deformation), which often seem to be accommodated through an increase in folding and bed rotation (continuous deformation). If the calculated displacement still reveals a deficit when both continuous and discontinuous deformation are considered, then the isolated fault models are a viable option. However, more often than not, examination of continuous deformation within the relay zones negates the presence of a displacement deficit, thereby supporting the coherent fault model (Walsh et al., 2003 and references therein).

Recently, many studies have focused on refining uplift histories of normal fault settings using thermochronometry. In active settings, the thermal regime is often complicated, requiring a multidimensional approach (Ehlers et al., 2001). Because of the block geometry of Basin and Range normal faults, they are often the focus of work examining both the exhumation history and the kinematics of faulting (Stockli et al., 2000, 2005; Armstrong et al., 2003; Ehlers et al., 2003). The footwall blocks remain mostly intact through faulting, exhumation, and tilting (e.g. Stewart, 1980) and models indicate that the theoretical ratio of hanging wall subsidence to footwall uplift is about 4:1 (King et al, 1988; King and Ellis, 1990; Ellis and King, 1991). Therefore, if fault slip and magnitude of offset are ample enough to exhume the footwall block from depth, then thermochronometry can be used to directly date the timing of faulting (e.g. Fitzgerald et al., 1991). However, it is necessary to take fault geometry into consideration when interpreting low-temperature data. The effect of rapid faulting on geotherm shape can also affect thermochronometer interpretation as, for example, when there is heat transfer due to the juxtaposition of a hot footwall and cold hanging wall. Thus, it is important to consider the rate and character of exhumation and denudation when interpreting time-temperature histories, and the inherent constraints of normal fault blocks provide a manageable setting for this approach.

2.2 Rocks of the Teton Range

The erosion-resistant Precambrian rocks comprise the highest peaks of the Teton Range and are part of the Wyoming Craton. The oldest units (>2680 Ma), observed in the north, south, and the eastern part of the central Tetons, are Archean layered gneisses, including biotite gneiss, plagioclase gneiss, amphibole gneiss, and some amphibolite (Reed and Zartman, 1973). Two

other concomitant units include the Rendezvous Metagabbro exposed on Rendezvous Mountain and in Granite Canyon, and Webb Canyon Gneiss found in the northern Tetons between upper Moran Canyon and Webb Canyon (Love et al., 1992). The latest Archean unit, prominent in the central range, is the Mount Owen Quartz Monzonite (2545 Ma), which is also associated with a series of intrarange pegmatites (Reed and Zartman, 1973; Love et al., 1992; Love et al., 2003). The youngest Precambrian rocks (765 Ma) are easily identifiable black diabase dikes cross-cutting the faces of Mount Moran, the Grand Teton, and Middle Teton (Reed and Zartman, 1973). Because most samples collected for this study were extracted from the eastern face of the escarpment, layered gneiss and quartz monzonite are the predominant lithologies analyzed for apatite.

The Precambrian-Paleozoic unconformity is exposed in the northwestern, western, and southern flanks of the Tetons, and as the top few meters of Mount Moran (Love et al., 1992). The oldest sedimentary rocks observed in the Tetons are mid-Cambrian sandstones and shales with the Flathead Sandstone typically marking the unconformity. A series of early Paleozoic strata encompassing sandstone, shale, limestone, and dolomite document the advance of western seas into present day Wyoming (Love et al., 2003). Subduction on the western margin of North America and the associated volcanic arc, in addition to rise of the Ancestral Rocky Mountains, contributed further material during the late Paleozoic and early Mesozoic. Throughout the Cretaceous, continued deposition of sandstones and shales occurred in the inland seaway until the beginning of the Targhee uplift. A series of clastics, dominated by highland derived conglomerates with sparsely interbedded bentonite, mark the Laramide orogeny during the Late Cretaceous. Eocene strata are distinguished by a transition to predominantly volcanics, evidencing the eruptions from the nearby Absaroka Range. The encroachment of the predecessor fields to Yellowstone is first apparent in Tertiary deposits, as thick volcanics, including the Conant Creek and Kilgore tuffs, blanketed the northern Tetons (Love et al., 2003). In the early Pliocene the Shooting Iron Formation was deposited in a lake occupying southern Jackson Hole, and is the focus of recent estimates of the onset of Teton uplift (Pierce and Morgan, 2009). The first documented eruption from the present Yellowstone caldera, the 2.05 Ma Huckleberry Ridge Tuff (Lanphere et al., 2002), is visible in the northwestern parts of the range and is widespread north of the Tetons and Jackson Hole (Love, 1977).

Due to its conspicuous presence throughout the Tetons, the aforementioned Precambrian-

Paleozoic unconformity is ideal for structural reconstructions. In the footwall, the unconformity is dome shaped, visible at high elevations in the central Tetons, and appearing again in the west and on the northern and southern flanks of the range (Figure 4A & B). In the hanging wall the unconformity is deformed by a series of folds and faults that most likely predate the Teton fault (Behrendt et al., 1968; Byrd et al., 1994). It is unclear when exactly deformation of the unconformity occurred, although Roberts and Burbank (1993) suggest that it occurred during the Laramide, based on the differential pattern of fission track ages. However, new fission track data raises questions regarding the previous ages and interpretations.

2.3 Tectonic History

Multiple periods of deformation are responsible for shaping the Tetons, but can generally be divided into three major episodes: Sevier (Late Jurassic to early Paleogene), Laramide (Late Cretaceous to early Tertiary), and Post-Laramide (Figure 5). The Sevier orogeny is characterized by a series of northeast verging folds and thrusts, most notably, the Jackson thrust, which marks the southern terminus of the Tetons. Most of the thrusts associated with the Sevier transported only thin sheets of sedimentary rocks, and are not documented within the Teton Range. The start of Teton-Gros Ventre uplift marks the transition into the Laramide orogeny. This broad, gentle, northwest-southeast trending uplift encompassed the present day Tetons and Gros Ventre Range. Laramide age thrusts trend roughly northwest-southeast and are well-documented within the Tetons. The Cache Creek fault lies just north of the Sevier Jackson thrust near Teton Pass, and is responsible for nearly 20 km of uplift and the surfacing of the Precambrian basement rocks that compose the core of the Teton Range. Two other intra-range Laramide thrusts include the Buck Mountain fault and the Forellen Peak fault (Figure 6). Extensive work by Smith (1991) concluded that the Buck Mountain fault dips ~57° to the east with a throw of ~1 km. As the Buck Mountain fault is exposed immediately to the west of the Grand Teton, thrusting could have contributed to the development of the highest Teton peak. The Forellen Peak fault is similar in character to the Buck Mountain fault, and is exposed north of Mount Moran; however, as presently mapped, probably did not play as large a role in the growth of the high elevation central peaks.

The most prominent of the post-Laramide structures is the Teton fault. Arguably the single most contributing factor to the present appearance of the Teton Range, the N10ºE striking

normal fault separates the Tetons from Jackson Hole. The Teton Range composes the west-tilted footwall block while the hanging wall encompasses Jackson Hole and the Snake River Plain. From observations of the ~2 Ma Huckleberry Ridge Tuff, postemplacement tilt estimates of the hanging wall are thought to be approximately 10° to the west (Byrd et al., 1994). Previous efforts to deduce the age, geometry, and offset of the Teton fault have resulted in a wide array of poorly constrained estimates. Lavin (1957) developed a series of gravity driven forward models and suggested that the Teton fault dips 60° to 90°. Early seismic work by Behrendt et al. (1968) using forward modeling and delay time analysis viewed the dip as 35° to 45°, but stated that an interpretation involving a series of steeply dipping normal faults could provide an alternative explanation. A trench at Granite Canyon revealed a late Quaternary fault dip of 75°-85° (Byrd, 1995). Other estimates range between 45° and 75° from seismic refraction, gravity, and inverse ray-tracing models (Smith et al., 1993b; Byrd et al., 1994). Thus, most recent work assumes the Teton fault to be defined by a series of stepped, steeply dipping (>45°) down-to-the-east normal faults (Love et al., 2003; Hampel et al., 2007; White et al., 2009).

The surface expression of the Teton fault is approximately 55 km long, with the southern end coinciding with the Jackson and Cache Creek thrusts, leading some to believe that it soles into the Cache Creek thrust at depth (Sales, 1983; Royse, 1983; Lageson, 1992; White et al., 2009). Alternatively, others have proposed that the Teton fault is actually 90-100 km long, and offsets the thrust, but that such is difficult to discern due to the intense effects of Pliocene and Pleistocene glaciation (Love and Albee, 1972; Love et al., 1973; Smith et al., 1977; Doser and Smith, 1983; Byrd et al., 1994). The range front is marked by numerous instances of offset alluvial fans and terraces (e.g. Machette et al., 2001; Nash and Beaujon, 2006) that define the surficial expression of the Teton fault and have been extensively studied to discern along-strike changes in slip rate. Variations in slip rate along the Teton fault relate well to topography; the highest scarps coincide with the central high peaks, with both slip rate and topography tapering off to the north and south (Smith et al., 1993a; Byrd et al., 1994; Machette et al., 2001; Foster et al., 2010).

In terms of displacement, stratigraphic reconstruction relying on the presumed depth of the unconformity in Jackson Hole (from the geophysical studies of Behrendt et al., 1968) produced a range of throw estimates between 6 and 9 km (Behrendt et al., 1968; Love, 1977; Smith, 1991; Love et al., 2003). By projecting the ~2 Ma Huckleberry Ridge Tuff, exposed east

of Jackson Hole, west towards the Teton fault others have suggested a throw of ~3 km (Figure 7) (Gilbert et al., 1983; Smith et al., 1993b). More recently, Byrd et al. (1994) suggested a length-averaged throw of 2.5 to 3.5 km and a maximum throw of 8 km. As many of these efforts involve the assumed presence of the unconformity in Jackson Hole, it is worth noting that this surface is highly variable due to repeated episodes of deformation and includes several areas of downwarping. Seismic data (Behrendt et al., 1968) indicate a large trough roughly parallel to the Teton fault where the unconformity is estimated to be ~3 km below sea level. A broad area between the Whetstone anticline and the Buffalo Fork thrust fault and another east of the north end of the Bacon Ridge anticline have unconformity depths estimated at 3.4 km and 4.5 km below sea level, respectively. Approximately 2 km of the vertical displacement is thought to be footwall uplift, while the remaining displacement is accommodated by hanging wall subsidence (Roberts and Burbank, 1993).

Current age of onset of Teton fault activity estimates range from 13 Ma to 2 Ma, and are based on relationships between prominent stratigraphic horizons and angular unconformities (Barnosky, 1984; Love, 2003; Smith et al., 1993b). These arguments generally involve the Miocene Colter and Teewinot formations or the Conant Creek Tuff. Although it is not explicitly stated that the Teton fault was active by the deposition of the Teewinot Formation (12 to 7.5 Ma; Perkins and Nash, 1994; Love et al., 1997), it is clearly evident from the asymmetric stratigraphy that deposition within Teewinot Lake was most active along the western margin, near the present Teton fault (Love et al., 2003). Conversely, the lack of coarse detritus within the Teewinot Formation could also indicate that the Tetons were not significantly elevated (Love, 1977), although this is generally discredited by the lack of such detritus in present day range front lake deposits (Shuey et al., 1977). Morgan and McIntosh (2005) argue that the presence of the 4.45 Ma Kilgore Tuff in Jackson Hole indicates that the northern Teton Range was not yet a pronounced barrier, as it originated from the Heiss volcanic field northwest of the Tetons. Pollen in the Shooting Iron Formation (Jackson Hole lake sediments) were dated by Leopold et al. (2007), and based on the unconformity with the Teewinot Formation could indicate that the majority of Teton uplift occurred after ~2 Ma. This is in agreement with recent work by Pierce and Morgan (2009) comparing fault ages to distance from the Yellowstone hotspot. Calculations involving the angle of the Huckleberry Ridge Tuff suggest that much, if not all, of the displacement on the Teton fault has occurred within the past ~ 2 Ma (Byrd et al., 1994).

As a result of the extensive range of timing and displacement estimates across the Teton fault, disputes also exist regarding the long-term vertical slip rate. Given the estimate of 2.5 to 3.5 km (Byrd et al., 1994) of displacement since 2 Ma, the maximum long-term rate is calculated to be ~0.6-0.9 mm/yr. White et al. (2009) calculated an average Quaternary rate of 1.2 mm/yr based on displacement measurements within a glacial moraine at Granite Canyon. Other estimates range from 0.5 to 1.2 mm/yr (Love, 1977; Smith et al., 1993a). Additionally, recent numerical modeling of postglacial conditions within the Teton and Yellowstone region by Hampel et al. (2007) suggest that much of the ~70% of postglacial slip occurred within a few thousand years immediately following glaciation, thus implying that slip estimates based on moraine offset may only represent isolated periods of increased fault movement related to isostatic rebound following deglaciation (Byrd et al., 1994; Lageson et al., 1999).

2.4 Uplift of the Teton Range

The only previous effort at documenting the uplift of the Teton Range through thermochronometry used fission track dating to analyze samples from three vertical transects including Mount Moran, Buck Mountain, and Rendezvous Peak (Roberts and Burbank, 1993). Rendezvous Peak samples ranged from 82.5 ± 9.0 at the top to 72.0 ± 6.2 Ma at the base. Buck Mountain samples ranged from 79.9 ± 8.8 Ma at the top to 66.5 ± 14.3 Ma at the base. The highest elevation sample from the Mount Moran section yielded a fission track age of 67.0 ± 8.6 Ma, whereas the lowest elevation sample was 25.8 ± 8.0 Ma. Along with a clear trend of increasing age with increasing elevation, there is a noticeable spatial variation in ages from north to south. The north-south trend was interpreted as differential uplift, with early uplift of the southern Tetons from ~80 to 60 Ma. Because of the close proximity, Roberts and Burbank (1993) applied a series of numerical heat-flow models to address the possibility of thermal perturbation from the Yellowstone magma body, as an alternative explanation for the young northern samples. They concluded that the amount of thermal energy produced was not sufficient to reach the Mount Moran area and at that point, the hotspot was located too far from the Tetons to generate significant heating. Thus, they imply that the fission track ages can be interpreted as cooling and exhumation. It was also inferred that doming of the unconformity probably occurred in the Laramide, since there is not a strong correlation between the AFT ages and structural depth. Additionally, during this time the unconformity was tilted at depth; the

present day southern Tetons were about 3.5 km below the surface and the Mount Moran portion was 4.5 km beneath the surface. However, because the unconformity is currently level in the north and south, Roberts and Burbank hypothesized that rapid uplift of the northern Tetons must have occurred since the early Miocene to bring the unconformity to its present position. This is somewhat problematic, because if the Teton fault initiated during the Miocene, then greater fault displacement would be expected in the northern Tetons; conversely, maximum displacement is observed in the central range, near the Grand Teton (Love et al., 1992). As all of their samples are older than ~25 Ma, they clearly predate the onset of Teton uplift suggesting any uplift related to the Teton fault is beyond the scope of apatite fission track dating.

The variation in arguments for the timing and displacement magnitude across the Teton fault have lead to the emergence of two uplift scenarios: (1) the Teton fault was a 12 to 9 Ma Basin and Range structure that has since experienced increased uplift related to the Yellowstone hotspot or (2) initiation of the Teton fault between 6 and 2 Ma as a result of it's proximity to Yellowstone. It is widely accepted that encroachment of the Yellowstone hotspot played a large role in the recent development of the Teton fault. Uplift of the crust proximal to the Yellowstone area has resulted in a crescent-shaped pattern of normal faults radiating out from the hotspot track (Figure 1A). When the estimated ages of the faults are compared to the distance from the assumed present day hotspot location, a clear trend emerges indicating the direct relationship between the Teton fault and the Yellowstone region (Figure 8) (Pierce and Morgan, 2009). The data trend also provides further evidence supporting young (<2 Ma) displacement accumulation on the Teton fault. Chemical analyses of the tuff deposits in Jackson Hole suggest a transition from a compressional to an extensional regime between 18 Ma and 13 Ma (Barnosky, 1984, 1986; Barnosky and Labar, 1989). It is also important to note that seismic velocity models (White et al., 2009) indicate a belt of seismicity extending north from the Teton fault beneath the southern portion of the Yellowstone caldera, possibly reflecting an earlier Basin and Range-type zone of weakness (Smith and Arabasz, 1991).

2.5 Geomorphology of the Tetons

The interaction between climate, topography, erosion, and tectonics governs the relief of mountain ranges (e.g., Berger et al., 2008), and is often the basis for examination of relatively young mountain ranges, such as the Tetons (Foster et al., 2008, 2010; Tranel et al., in review).

Field observations and models show focused erosion at the zone where net accumulation of snow is equal to ablation, the equilibrium line altitude (ELA) (e.g. Berger and Spotila, 2008). Additionally, rock erosion is greater at elevations where there is a longer occupation of ice. Although available evidence suggests extensive glacial activity in northwestern Wyoming during the late Pliocene and throughout the Pleistocene, the focused erosion of the Pleistocene glaciations is responsible for shaping the modern Teton landscape. While the sedimentary and volcanic rocks above the unconformity are relatively easily eroded, glacial activity is the basis for the majority of erosion of the otherwise resistant Precambrian rocks. The Bull Lake glaciation occurred between 160 to 130 ka and contributed to scouring the eastern front of the Tetons. Evidence for this episode is documented through weathered moraines, and as glacial till and loess deposits. The Pinedale glaciation, the last glacial maximum (LGM), lasted from about 44 ka to 14 ka (Licciardi et al., 2005). The Pinedale is notably responsible for the formation of Jackson Lake, Jenny Lake, and many of the other smaller, range-front lakes along the Teton fault.

Maximum topography in the Tetons is thought to be roughly parallel to both the extent of the LGM and the long-term ELA (Foster et al., 2010), supporting previous work theorizing a "glacial buzzsaw" limiting elevation (Brozovic et al, 1997; Mitchell and Montgomery, 2006; Foster et al., 2008). However, the presence of Mount Moran and the Grand Teton towering hundreds of meters over the rest of the range requires an alternative explanation. Foster et al. (2010) concluded that a complex combination of rock mass strength and varied glacial erosion within different portions of the Teton Range is responsible for the appearance of Mount Moran and the Grand Teton. Tilting of the footwall coupled with climate (e.g. wind direction, precipitation) governs the size and health of glaciers, thus affecting the efficiency of glacial erosion. The elevation of these peaks also produces positive feedback, by providing an orographic barrier that encourages further steepening from focused precipitation on the flanks. Foster et al. (2010) asserts that the Tetons have achieved a topographic steady-state. Nonetheless, recent field observations (Tranel et al., in review) evidencing lichen cover and limited fresh surfaces on peaks and ridges, as well as widespread evidence of glacial erosion in the valleys, suggests that long term erosion rates in the valleys are nearly three times as rapid as those at the peaks. This implies that steady-state was only recently achieved in the Teton Range and is further documented by field observations adjacent to the Grand Teton within Garnet

Canyon (Tranel et al., in review). In addition to the correlation between glacial erosion and topography, numerical modeling by Hampel et al. (2007) indicates that deglaciation had a large impact on the tectonics of the Teton Range, leading to a postglacial slip-rate increase on the Teton fault immediately following the LGM.

Figure Captions

Figure 3: Normal fault models. Scaling properties of normal faults have been extensively studied. A) Displacement-length scaling relationship of faults from numerous locations around the world (Schlische et al., 1996 and references therein). B) Fault growth model. (1) Fault length increases as displacement accrues. (2) Fault length is established early, as interaction between segments reduces lateral propagation. C) In the isolated fault model, faults initiate as separate segments and overlap entirely by chance. In the coherent model, the array is related from the beginning as faults are "soft-linked" by the ductile deformation occurring between them. From Walsh et al. (2003).

Figure 4: The Paleozoic-Precambrian unconformity is domed and visible throughout the Teton Range. A) Precambrian basement overlain by Paleozoic and younger sedimentary and volcanic rocks. Photo by Summer Brown, 2008. B) Domed shape of the unconformity as viewed from Jackson Hole.

Figure 5: Modified regional tectonic map of Love et al. (2003). Tectonic map shows the Sevier, Laramide, and Post Laramide structures, as well as relevant peaks.

Figure 6: Intra-range faults are noted throughout the Teton Range. Teton Range faults are from the geology map of Love et al., (1992). (A) JT - Jackson thrust; CCF - Cache Creek fault. (B) Buck Mountain Thrust System, throw of ~1 km (Smith, 1991). (C) Forellen Peak Fault.

Figure 7: Orientation of Jackson Hole sediments and proposed Teton fault dip. Schematic cross section shows Teton fault orientations and projected dips of the Huckleberry Ridge Tuff and Conant Creek Tuff from the Jackson Lake Dam. Subsurface geology from seismic work of Behrendt et al. (1968).

Figure 8: Correlation between age of faults and proximity to Yellowstone following Pierce and Morgan (2009).

Figure 3. Normal fault models.

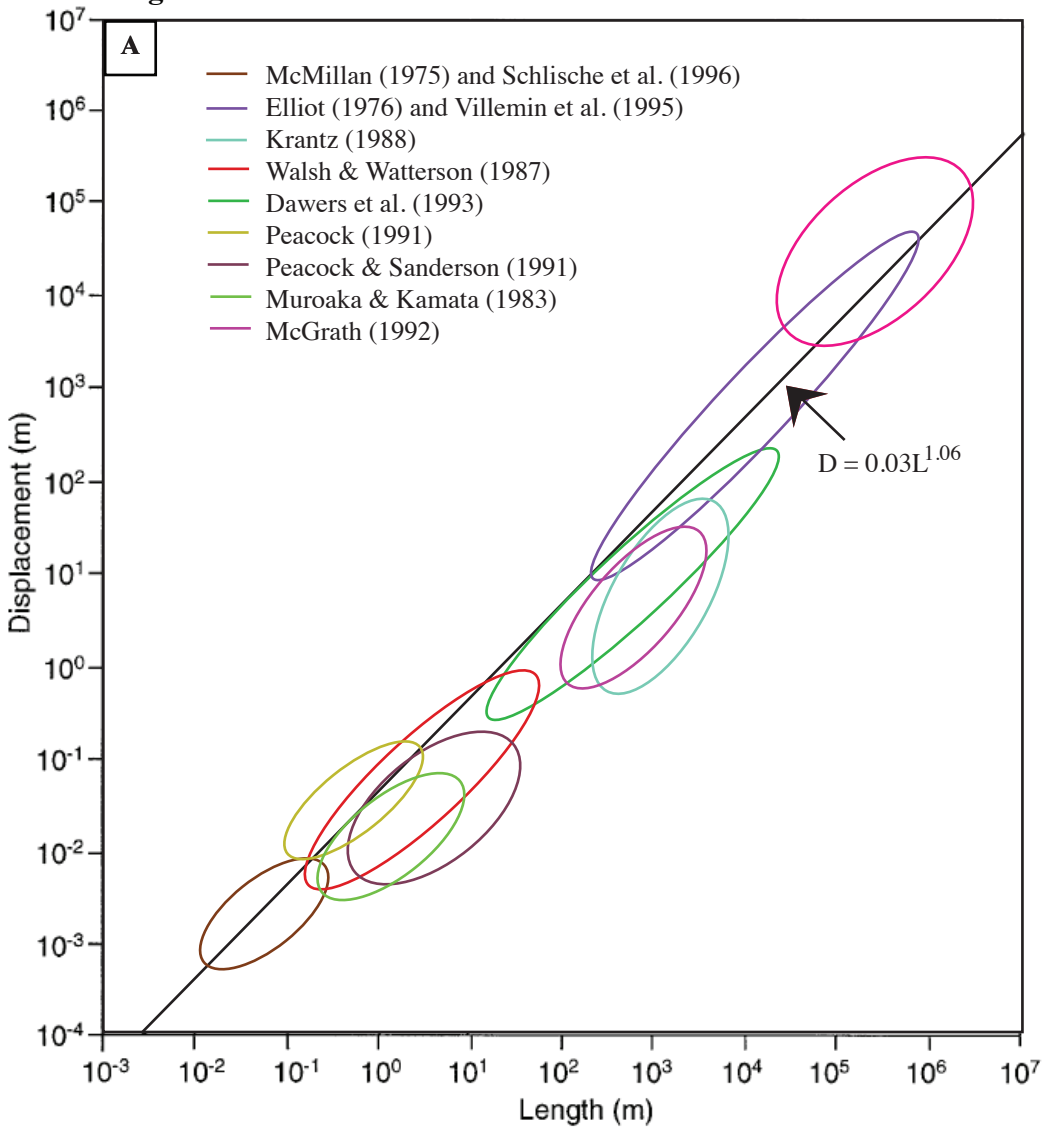

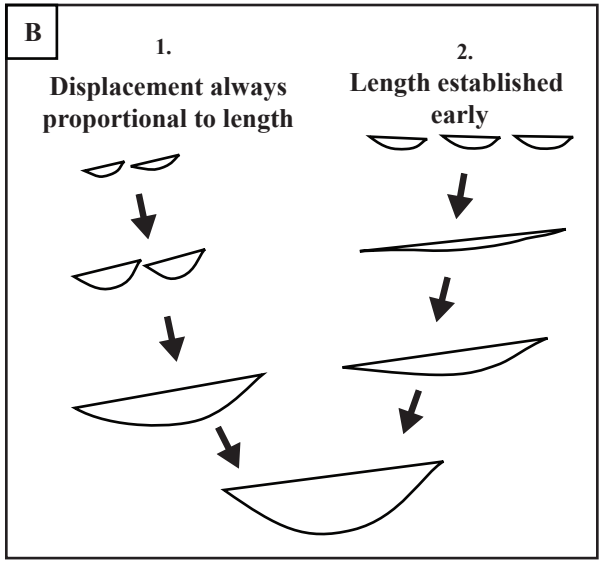

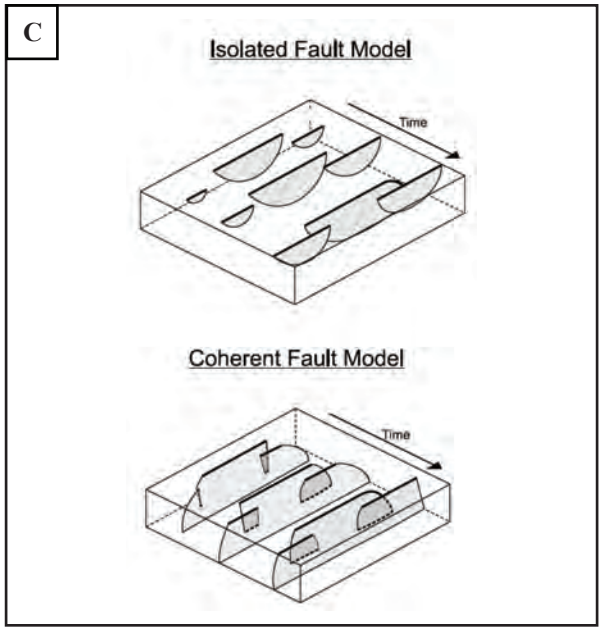

Figure 4. The Precambrian-Paleozoic unconformity is domed and visible throughout the Teton Range.

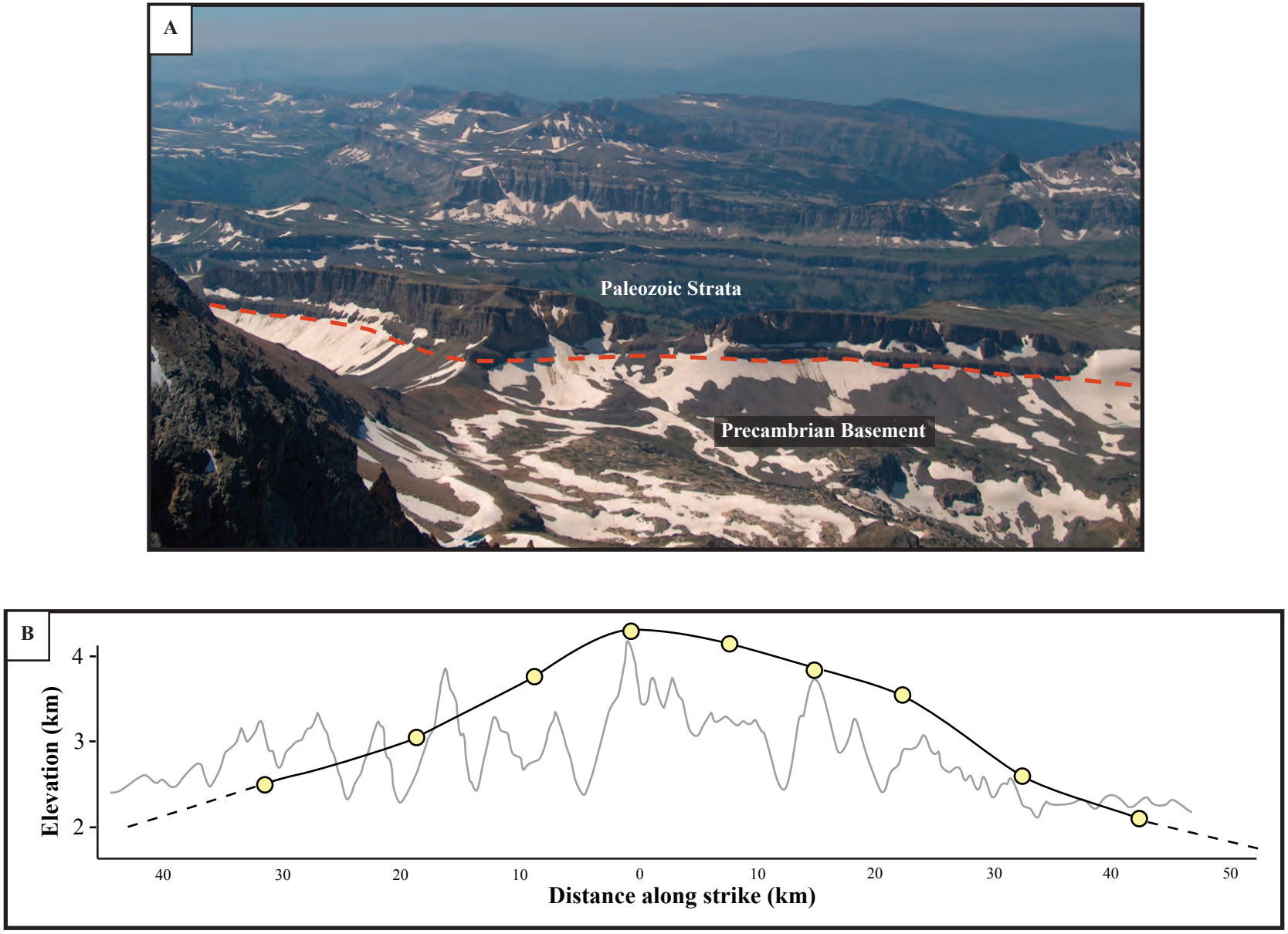

Figure 5. Modified regional tectonic map of Love et al. (2003).

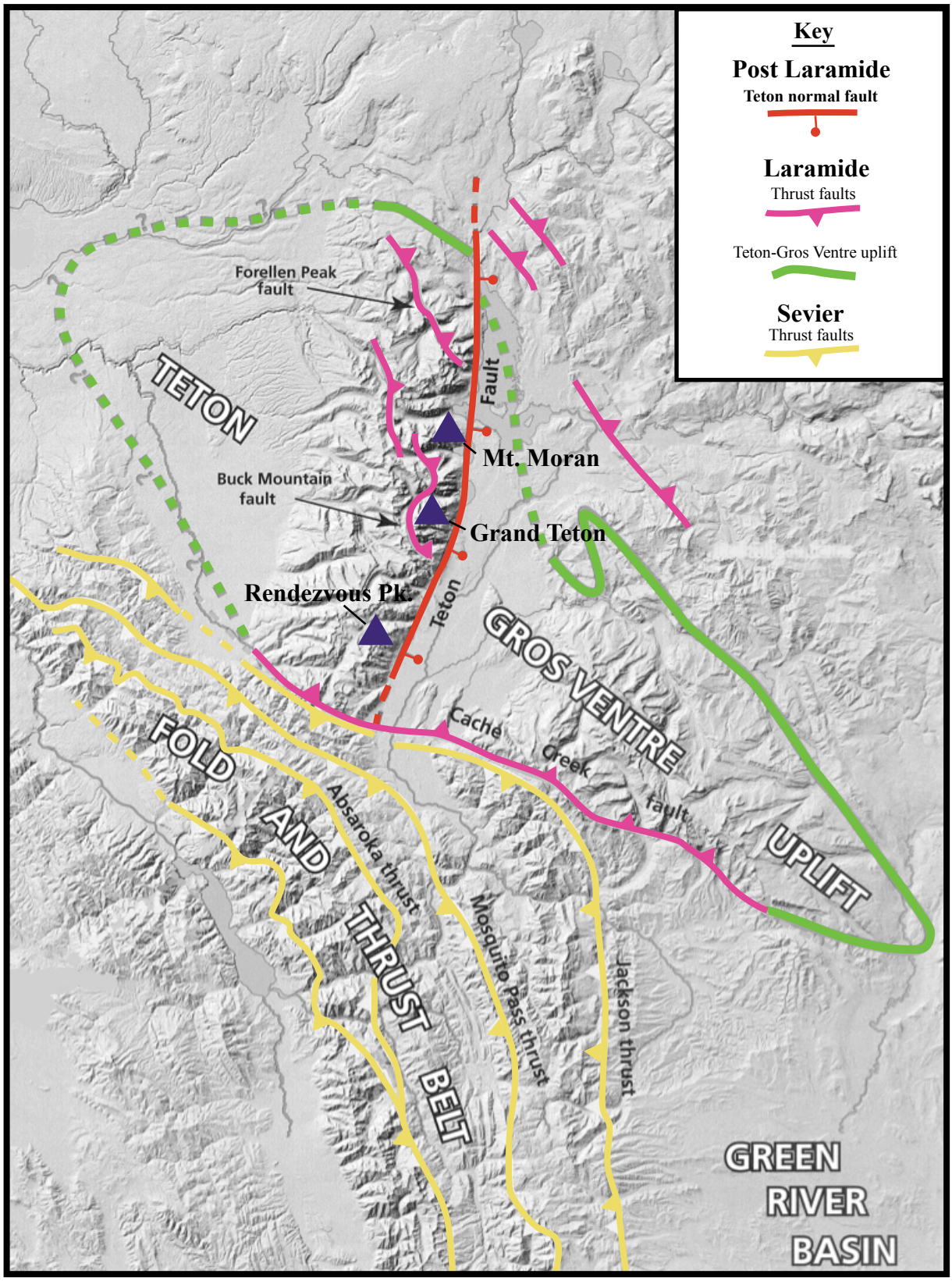

Figure 6. Intra-range faults are noted throughout the Teton Range.

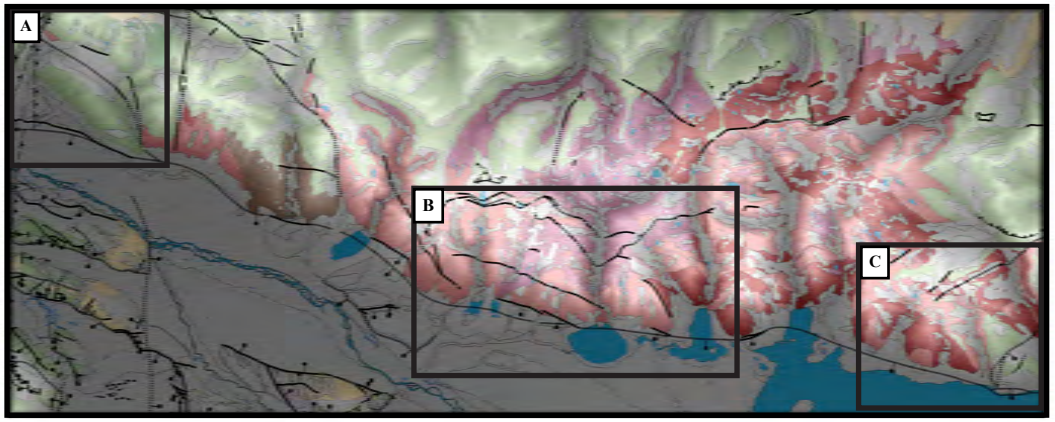

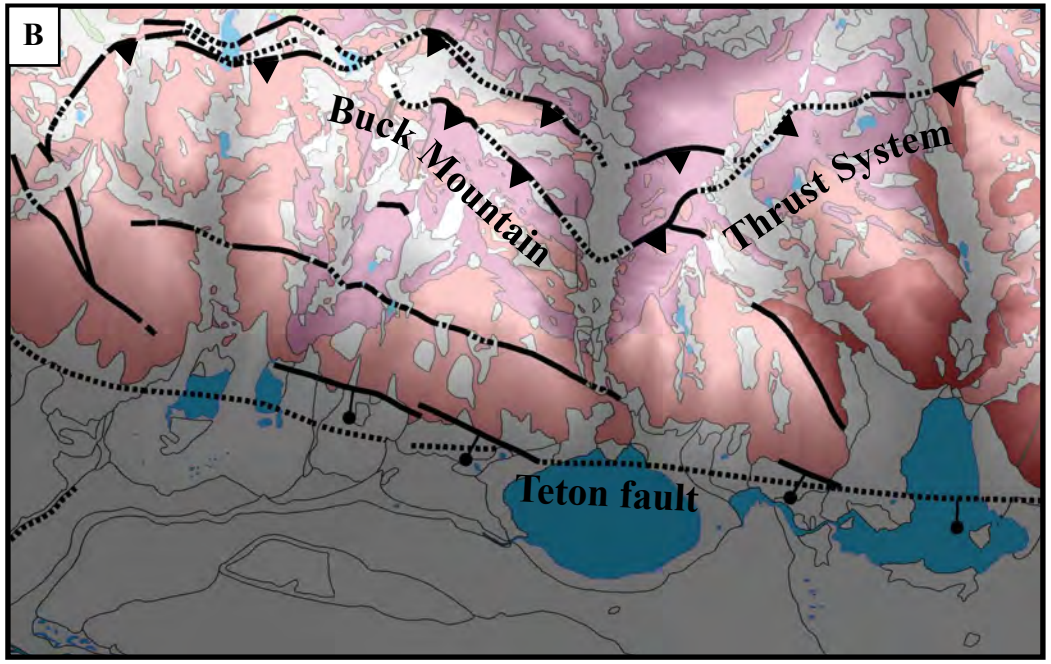

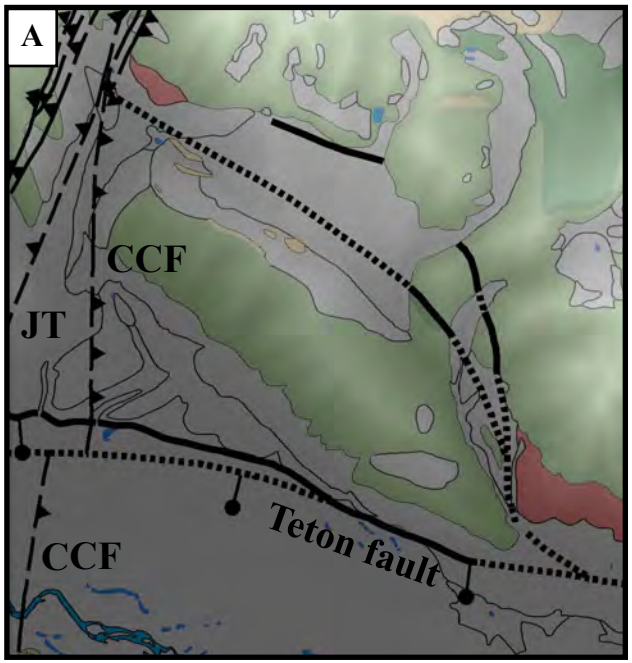

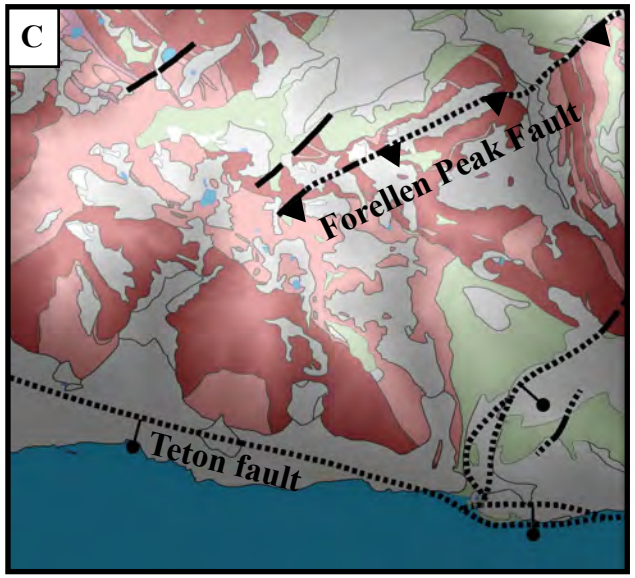

Figure 7. Orientation of Jackson Hole sediments and proposed Teton fault dip.

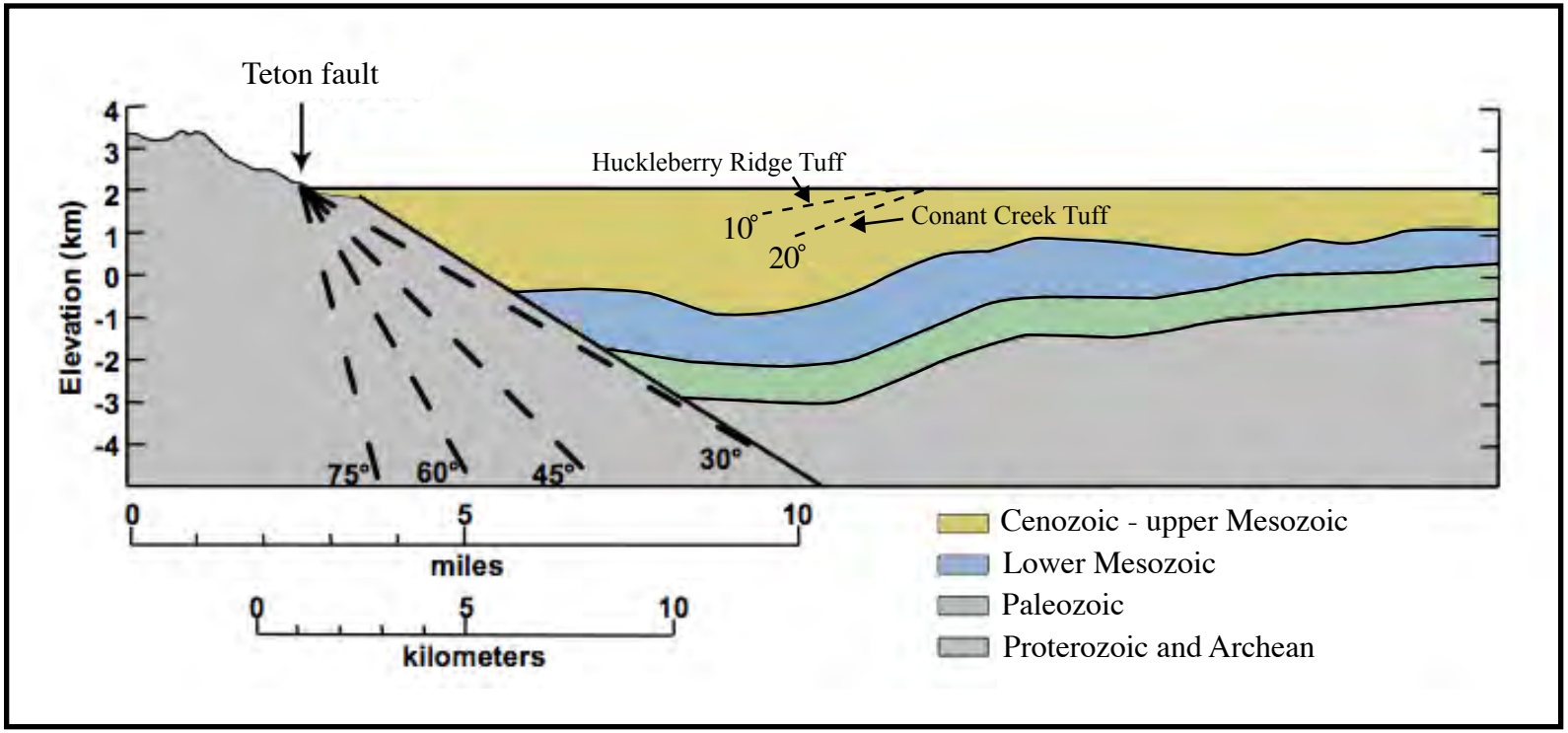

Figure 8. Correlation between age of faults and proximity to Yellowstone following Pierce and Morgan (2009).

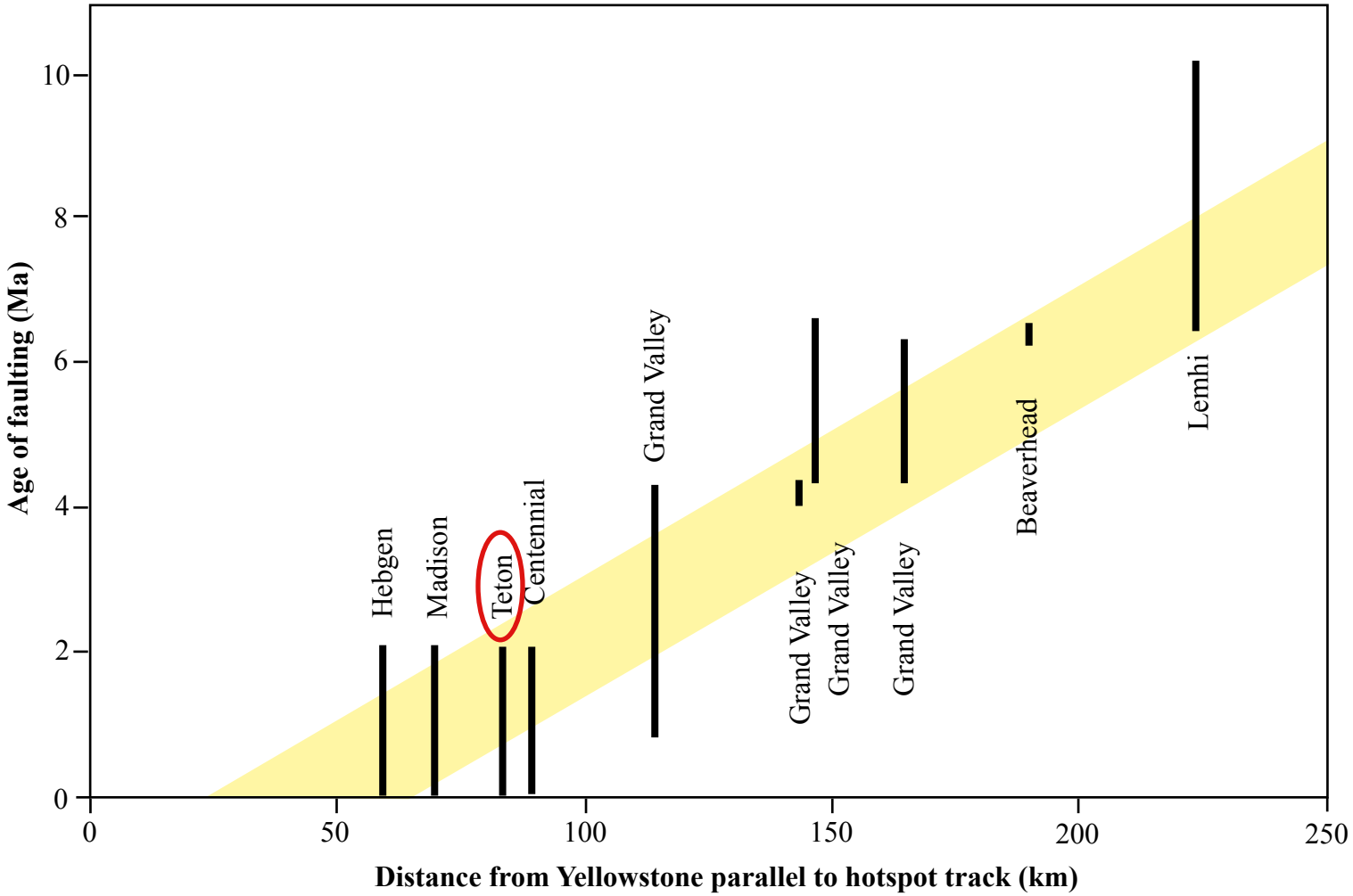

3. METHODS

3.1 Low-Temperature Thermochronology

Recent efforts at quantifying the history of fault controlled mountain belts have utilized low-temperature closure systems to document the latest stages of uplift (e.g. Armstrong et al., 2003). As an increasing amount of research examines the interaction between climate and tectonics, it is important to note these final episodes of exhumation and denudation. Apatite, a common phosphate mineral, is appropriate for several different isotopic techniques as it generally contains a few tens of ppm of both U and Th (e.g. Strutt, 1908). Two common methods involve: (1) analyzing the accumulation of alpha particles produced during U and Th series decay, or (U-Th)/He dating, and (2) examination of track damage produced during spontaneous fission of ^{238}U, or fission track dating.

The decay of ^{238}U, ^{235}U, and ^{232}Th produces ^{4}He (alpha particles), which accumulate at a known rate. ^{147}Sm decay also contributes ^{4}He, although generally a negligible amount (Farley et al., 2001). By measuring present day amounts of U, Th, and He (and disregarding Sm), the He apparent age can be calculated as:

$$^{4}He = 8^{238}\mathrm{U}(e^{\lambda 238t} - 1) + 7(^{238}\mathrm{U}/137.88)(e^{\lambda 235t} - 1) + 6^{232}\mathrm{Th}(e^{\lambda 232t} - 1)$$

where λ is defined as the decay constant for each isotope, the constants represent the number of alpha particles emitted in each decay chain, t is the apatite cooling age (AHe), and 1/137.88 is the present day ^{235}U/^{238}U ratio (Farley, 2002). Based on similar systems involving the decay of U and Th, early AHe attempts aimed to calculate time elapsed since crystallization; however, (U-Th)/He consistently seemed to produce younger ages than calculated by other techniques (Reiners et al., 2005). It was later suggested that perhaps the young ages actually represented the time since the mineral cooled from a temperature lower than that associated with crystallization (Zeitler et al., 1987). Further laboratory experiments involving controlled heating intervals determined that apatite helium diffusion is a demonstrable and predictable thermally activated process (e.g. Zeitler et al., 1987, Wolf et al., 1996). These studies eventually led to the derivation of a closure temperature (T_c), as the temperature corresponding to the calculated AHe age (Dodson, 1973). The revival of apatite (U-Th)/He techniques evolved into the establishment of the AHe T_c as 63-73°C, based on an average crustal cooling rate of 10°C/Myr and apatite

grain radii of 50-150 μm (Farley, 2000). Assuming a typical continental geothermal gradient of 25°C, the range of AHe corresponds to crustal depths of ~1.5-3 km, allowing a unique view into the very latest stages of exhumation (Figure 9A).

Samples are collected in vertical transects to define an age-elevation gradient (Figure 9B). Any inflection point could indicate a change in rate of uplift or even onset of faulting. However, complications arise when samples experience extended residence times at temperatures below T_c. If two samples cooled through the T_c simultaneously, but one sample resided just below the T_c for an extended period of time, it would produce a different age than the sample that experienced rapid exhumation or denudation. This is because He diffusion still occurs at temperatures above ~35°C. The zone that extends from ~35° to ~75°C is the He partial retention zone (HePRZ; Figure 9C) (e.g. Farley and Stockli, 2002). It is referred to as the "partial" retention zone because diffusion is not rapid enough to sustain a zero concentration of helium, nor is it slow enough to allow complete retention of helium (Ehlers and Farley, 2003). Within the HePRZ, He ages decrease rapidly with temperature, and thus HePRZ residence time must be taken into consideration when interpreting AHe age data.

Fission track dating relies on the spontaneous fission of ^{238}U into two unequal product nuclides. The kinetic energy produced by the fission is transferred to the nuclides, sending them in opposite directions and leaving a measurable linear trail (a fission track) of radiation damage. Previous fission track studies have interpreted certain patterns of track-length changes as a function of the exposure time to annealing temperatures (Laslett et al., 1984; Gleadow et al., 1986). Depending on the cooling rate and kinetics of the crystal, fission tracks in apatite begin to be retained below ~150°-120°C (e.g. Ketcham et al., 1999). Ages are derived from the density of fission tracks and the concentration of ^{238}U (e.g. Naeser, 1976). Over time, fission tracks tend to anneal, with significant length reduction occurring within the partial annealing zone (PAZ; conceptually similar to the HePRZ) between 60° and 110°C (Gleadow & Duddy, 1981; Green et al., 1986). At lower temperatures within and below the PAZ, all tracks are retained. However, at higher temperatures within the PAZ, new tracks are long and the older tracks are progressively annealed. Therefore, by studying track-length distributions, conclusions can be drawn regarding the amount of time spent within and below the PAZ.

Apatite fission track analyses were conducted at the University of Wyoming by W.C. Krugh, utilizing the external detector method (Hurford and Green, 1983). Spontaneous fission

tracks were revealed by etching in 5.5M HNO_3 at a water bath-controlled temperature of 21° ± 1°C for 20 seconds. Samples were sent to the Oregon State University TRIGA research reactor and exposed to a thermal neutron fluence of ~ $1x10^{16}$ neutrons/cm^2. Following irradiation, induced tracks were revealed by etching muscovite external detectors in 48% HF_{aq} at room temperature for 12 minutes. Fission track densities and track length distributions were measured on an Olympus BH28 optical microscope with a computer-controlled stage, drawing tube, and digitizing tablet. All measurements were conducted at a magnification of 1875x (air objective).

Apparent cooling ages were calculated using a zeta calibration factor ζ_{CN5} (Ma ± 1σ) of 315.4 ± 13.2. When possible, a minimum of 20 crystals was used to calculate apparent cooling ages for each sample. All ages are reported as central ages ± 1σ (Galbraith and Laslett, 1993). Horizontal confined track length distributions were obtained from a combination of track in track and carefully chosen track in crack/cleavage measurements. When possible, 100 track lengths were measured for each sample. The angle of each track length was measured, with respect to the crystallographic c-axis, to incorporate orientation-dependent annealing kinetics in track length modeling (Donelick et al., 1999). The length and width of etch pits (D_{par} and D_{perp} respectively) were measured to constrain variations in annealing kinetics related to crystal composition (Ketcham et al., 1999). The fission track datasets were compared to model time-temperature histories using the inverse modeling program HeFTy (Ketcham, 2005).

HeFTy is operated on the assumption that if the parent isotope, daughter products, and time-temperature sensitive processes are well-constrained for a thermochronometric system, then it is possible to construct a forward model (Ketcham, 2005). This forward model is then used in the inverse sense to predict how a sample would evolve with a given starting arrangement and time-temperature history. HeFTy can be used for both fission-track and (U-Th)/He systems, and can simultaneously model these systems when applicable. When AFT data is analyzed, statistics test the goodness of fit for the length distribution and age. Likewise, for AHe datasets, the goodness of fit for a history is subject to corrections based on grain size and ejection kinetics. Modeling of time-temperature paths uses a constrained Monte Carlo scheme. Alternate datasets and geological information are taken into consideration and used to specify constraints through which the paths must path. Additionally, between these constraints, the general character of cooling can be specified (e.g. slow, interval, etc.). By integrating multiple datasets, HeFTy can

be used to produce reasonable time-temperature histories for a given sample.

3.2 Sampling Procedure

Because the intent of this study was to determine if any temporal or spatial variations exist in uplift rate throughout the Teton Range, samples were collected both along and across strike. Three vertical transects were sampled to establish an age-elevation gradient in the northern, central, and southern parts of the Tetons (Figure 10). Ideally, samples in the vertical transects would be within ~150-250 m of each other, to better pinpoint any inflections in the uplift history. Additionally, a series of samples were taken at low elevations along the Teton fault to infer any differences in onset of faulting along strike. When possible, lithologies were chosen that indicated a high fraction of apatite (e.g. granitic gneiss) and areas of intense hydrothermal alteration or weathering were avoided.

The northern section included the summit of Mount Moran, as this is the highest exposed peak north of the Grand Teton. Starting near the summit (3,842 m) bedrock was collected roughly every 200 to 250 meters, resulting in a total of 10 samples. This transect was the most thorough, as it contained the best exposure. The central section included the Grand Teton, accessed by Garnet Canyon. As AHe ages existed for elevations lower than ~3530 meters (Tranel and Spotila, 2007), sampling strategies aimed to collect high elevation samples. The highest sample was collected at ~4040 m, roughly ~150 m short of the summit. A second sample was collected at ~3495 m. Because the southern Tetons are capped by thick carbonate units, the elevation of the transect peak was not an important factor when choosing the southern sample locations. A transect near Jackson Hole Ski Resort on Rendezvous Mountain was chosen for this reason, as samples were more easily accessible due to slope clearing. The highest non-sedimentary bedrock sample was collected at ~2728 m and every 200 to 300 meters below, resulting in 7 samples. Low elevation samples were collected at roughly 3-4 km intervals along the Teton fault. Because of the recent uplift and continuing erosion, the eastern escarpment is marked by numerous alluvial fans and landslide deposits, especially in the central portion. The first instance of exposed bedrock often occurs 100 to 200 meters above the valley floor, thus along-strike samples range in elevation between 2060 and 2230 meters. Including the base samples for the three vertical transects, a total of 15 samples were taken at low elevation.

3.3 Analytical Procedures

Bedrock samples (3-6 kg) were initially processed using both standard jaw and rotary mechanical crushers to attain a grain size below 250 μ. The samples were then density sorted using a Wilfley table and heavy liquids (LST). The densest portions were magnetically separated resulting in a predominantly apatite fraction. Although many samples contained a large amount of zircon, pyrite, or other minerals of little interest, those with a high (>80%) fraction of apatite were divided and a portion sent to Barbara Carrapa's lab at University of Wyoming for AFT analysis. Next, to avoid anomalous He values, apatite grains were carefully screened to detect the presence of fluid or mineral inclusions. Individual grains were examined under cross polars at 110X to identify birefringent inclusions containing high U and Th concentrations. Zircon is especially important to avoid, as the methods used to prepare samples for ICP-MS do not dissolve zircon, yet diffusion of He still occurs. The U and Th concentrations are not measured, but erroneously high He values are still recorded, resulting in old AHe ages (Farley and Stockli, 2002). Ideally, chosen grains have no birefringence or obvious zoning; however, in some lower quality samples grains with minimal birefringence were unavoidable. SEM screening of samples from Garnet Canyon (Tranel et al., in review) showed that a high percentage of grains contained inclusions and/or strong zoning, which is common in apatite derived from older rock and could further cause issues with He diffusion (Farley and Stockli, 2002). For this reason, many samples that contained particularly poor apatite were loaded as single grains, as opposed to aliquots, to avoid the chance of an inclusion contaminating multiple grains.

It is well documented that apatite grain size affects both the closure temperature and the AHe age (Figure 11) (e.g. Farley, 2000; Reiners and Farley, 2001). In many of the Tetons samples, only small grains (<50 μm) were available, and corrections must be made. Thus, the dimensions and geometry of each grain are noted prior to loading in order to calculate the mass weighted average radius (MWAR) for aliquot samples. To calculate the closure temperature, the following equation was used, which is based on thermally activated diffusion (McDougall and Harrison, 1999):

$$T_c = \frac{E/R}{\ln\left[\frac{ART_c^2 D_0/a^2}{EdT/dt}\right]}$$

where T_c is the closure temperature, E is the activation energy (33 kcal/mol) (Farley, 2000), R is the gas constant, A is the shape factor (55 for an infinite cylinder) (Dodson, 1973), D_0 is the He diffusitivity at infinite temperature (50 cm^2/s) (Farley, 2000), dT/dt is the cooling rate, and a is the diffusion domain radius. Single grains analyzed were given the measured radius as *a* and the MWAR was utilized for aliquots.

Depending on the availability and quality of the apatite, grains were selected individually or as aliquots and sealed into 0.7 x 1 mm platinum tubes. The tubes were then places inside larger 1.5 x 2 mm Platinum tubes, which were then sealed and hand engraved for later identification. To derive the He content of samples, the individual tubes were dropped into a boron nitride cup within a resistively-heated ultra high vacuum furnace. The furnace was heated to >940ºC for 20 minutes to release all accumulated helium within the apatite grains. From the released gas, helium was then purified in a cryogenic trap cycling between 16-37 K. The remaining helium fraction was then combined with a ^{3}He spike and sent through a quadrupole mass spectrometer. The ^{4}He/^{3}He ratio was measured and used to determine the amount of released helium from the apatite grains. After extraction from the furnace, the large platinum tubes were opened and the smaller tubes removed and opened under ~150 μL of ultra-pure distilled water in Teflon vials. Small amounts of HNO_3 were added to the vials to dissolve the apatite, which were then spiked with known amounts of ^{235}U and ^{230}Th. The resulting solution was then shipped to Julia Goreva's lab at the University of Arizona where U and Th concentrations were measured by isotope dilution using inductively coupled plasma mass spectrometry (ICP-MS).

The aforementioned effects of grain size on diffusion are of particular concern. Diffusitivity in apatite scales with the inverse square of the grain radius, thus if two grains have the same cooling rate and age, a ~30 μm apatite grain would produce a closure temperature of 50°C, whereas a ~90 μm grain would produce 65°C. Also of significant importance, are the effects caused by sample residence within the HePRZ. He ages are very sensitive to small variations in temperature or diffusitivity, as noted by Farley and Stockli (2002): “an apatite held

at 48°C for 100 Myr will have a He age ~15 Myr (40%) older than one held at 52°C". Software programs such as TERRA (Ehlers et al, 2005), AFTSolve (Ketcham et al., 2000), and HeFTy (Ketcham, 2005) aim to accurately interpret low-temperature data by incorporating various diffusion and annealing models. Because the Teton samples showed evidence for residence time within the HePRZ, and because both AHe and AFT have different temperature sensitivities, HeFTy (Ketcham, 2005) was utilized to produce a simple cooling model for each transect. AHe data was entered as single grains, or in the case of aliquots, as averaged MWAR and FT values.

A reasonable modern geothermal gradient (~25°C/km) was assumed and each model was designed to fit the ages and vertical separation within each transect. HeFTy was used to account for the effects of variations in He production and diffusion for each sample, as opposed to using only the closure temperature. An apparent rate was previously calculated by projecting the zero age, but a more thorough method of modeling the cooling and exhumation history was necessary since an actual inflection point was not observed. After the appropriate details influencing the kinetics of He diffusion were entered, different simple cooling histories were tested in an attempt to produce the observed results. This was iteratively switched for each marker sample within each transect (highest and lowest elevation) and also tested for different geothermal gradients. By using HeFTy, viable models of cooling and exhumation can be produced that agree with multiple samples within each transect.

3.4 Structural Analysis

The Precambrian-Paleozoic unconformity provides a well-preserved and easily identifiable marker horizon for structural reconstruction. Doming of the unconformity, whether a result of displacement on the Teton fault or an older event, can be used to study the mechanics of deformation within the Teton Range. If indeed due to motion on the Teton fault, then it is possible to use the tapered unconformity as a basis for strain calculations or to estimate the total throw. Alternatively, if the unconformity is a result of an older compressional event, then observations could be made detailing the active stresses during that event. In order to accurately record the current and eroded position of the unconformity, a series of nine east-west cross sections were constructed across the Teton Range. The unconformity is exposed in at least the western portion of each section, and in some cases at high elevations in the central or eastern range (e.g. Mount Moran). Offset data across intra-range faults is limited (Smith, 1991) and

difficult to estimate as it generally involves deformed basement.

Some preexisting cross-sections were examined prior to this project (Behrendt et al., 1968; Smith, 1991; Byrd et al., 1994; Love et al., 2003) and when overlapping or adjacent to the new section lines, they were used as a guide. New sections were drawn by combining bedrock geology maps (Love et al., 1992), aerial photos (Love et al., 2003), and seismic refraction and gravity modeling results (Behrendt et al., 1968; Byrd et al, 1994). While the footwall contents are easily reproduced because of the extensive data available pertaining to lithology and orientation, the geometry of sediments of Jackson Hole are loosely based on aforementioned geophysical investigations. Also, because the layers are identified by density, the subsurface geology is often defined only by general lithology (e.g. basement, Paleozoic sediments), so thicknesses of individual units within the section hanging wall are based on measured thicknesses in the footwall.

The new sections were used to build a model of the Teton Range with the 3DMove software, donated by Midland Valley for academic use. Although the Move software was primarily developed for subsurface examination in industry, it provides an excellent opportunity for visualization of the Tetons and, to some degree, quantitative analysis. The cross-sections were imported into 2D Move, digitized, geo-referenced and then assembled in 3D Move. The unconformity was reconstructed and this was used to generate a structure contour map of the height of the unconformity above sea level, clearly displaying its domed structure. From this we can begin to analyze strain and the geometry of the unconformity in relation to other structures (Teton fault, Buck Mountain fault, etc.). Additionally, digital elevation models (DEM's) can be added to the model to analyze the relationship between topography and geology. Volume calculations were performed for the space between the unconformity and the DEM as an estimate of eroded sediment. The volume estimate is ideal for further examining the geomorphology and history of erosion within the Teton Range.

Figure Captions

Figure 9: Closure temperature and sampling strategies of low-temperature dating methods. A) Schematic diagram showing typical depth for AHe and AFT closure temperatures. B) Vertical sample transects translate to an age-elevation gradient. C) Age-temperature sensitivity of samples within the helium partial retention zone (HePRZ).

Figure 10: Vertical transect locations. The southern transect was sampled at Rendezvous Mountain, central transect at the Grand Teton, and the northern transect at Mount Moran. Photo by Summer Brown, 2008.

Figure 11: Relationship between grain size (μm) and AHe age. Grain size-AHe age relationship data is from the diffusion measurements of Farley (2000). Seive size ranges (in μm) are indicated. Shows that diffusitivity decreases as grain size increases.

Figure 9. Closure temperature and sampling strategies of low-temperature dating methods.

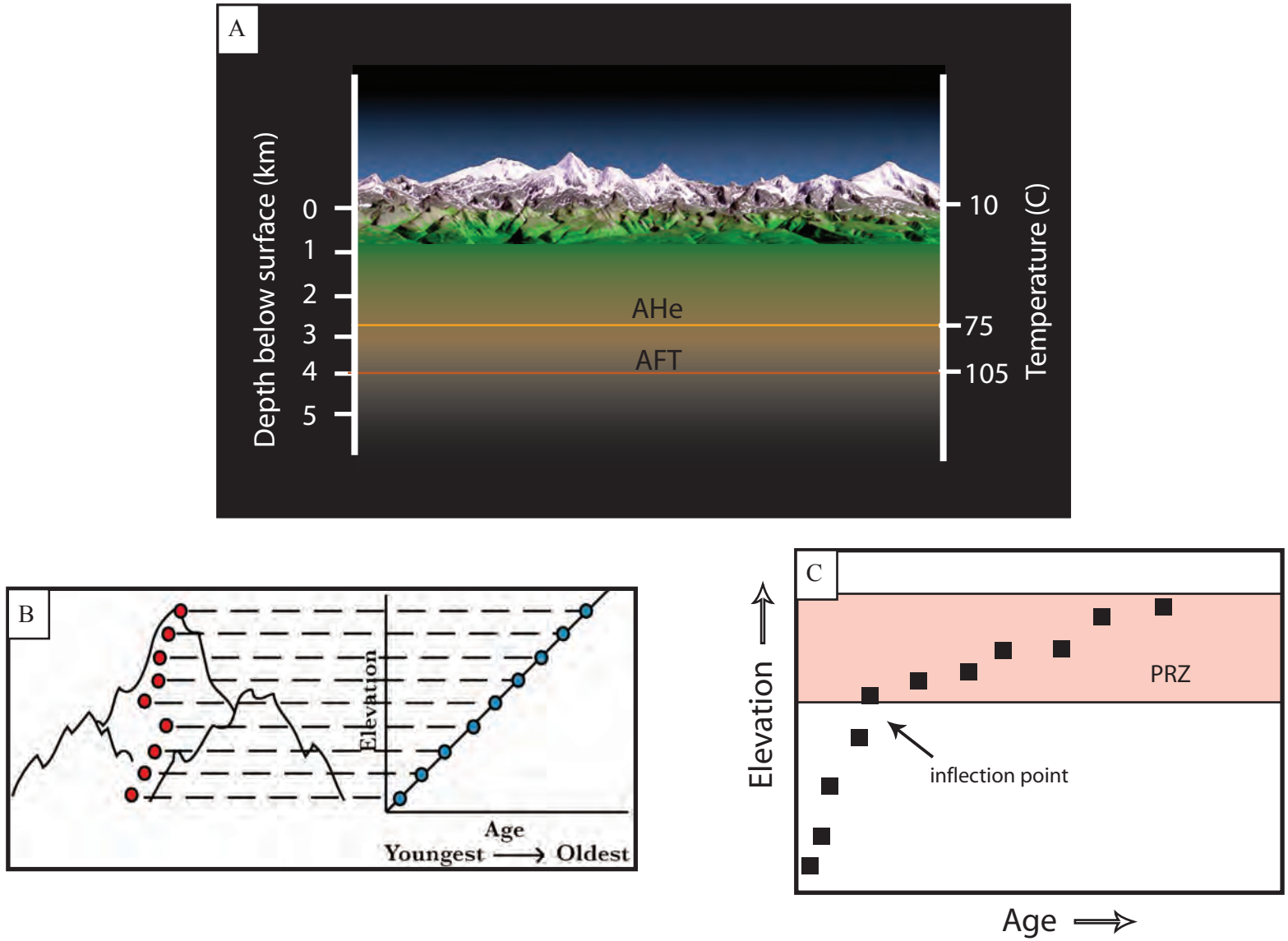

Figure 10. Vertical transect locations.

Figure 11. Relationship between grain size (μm) and AHe age.

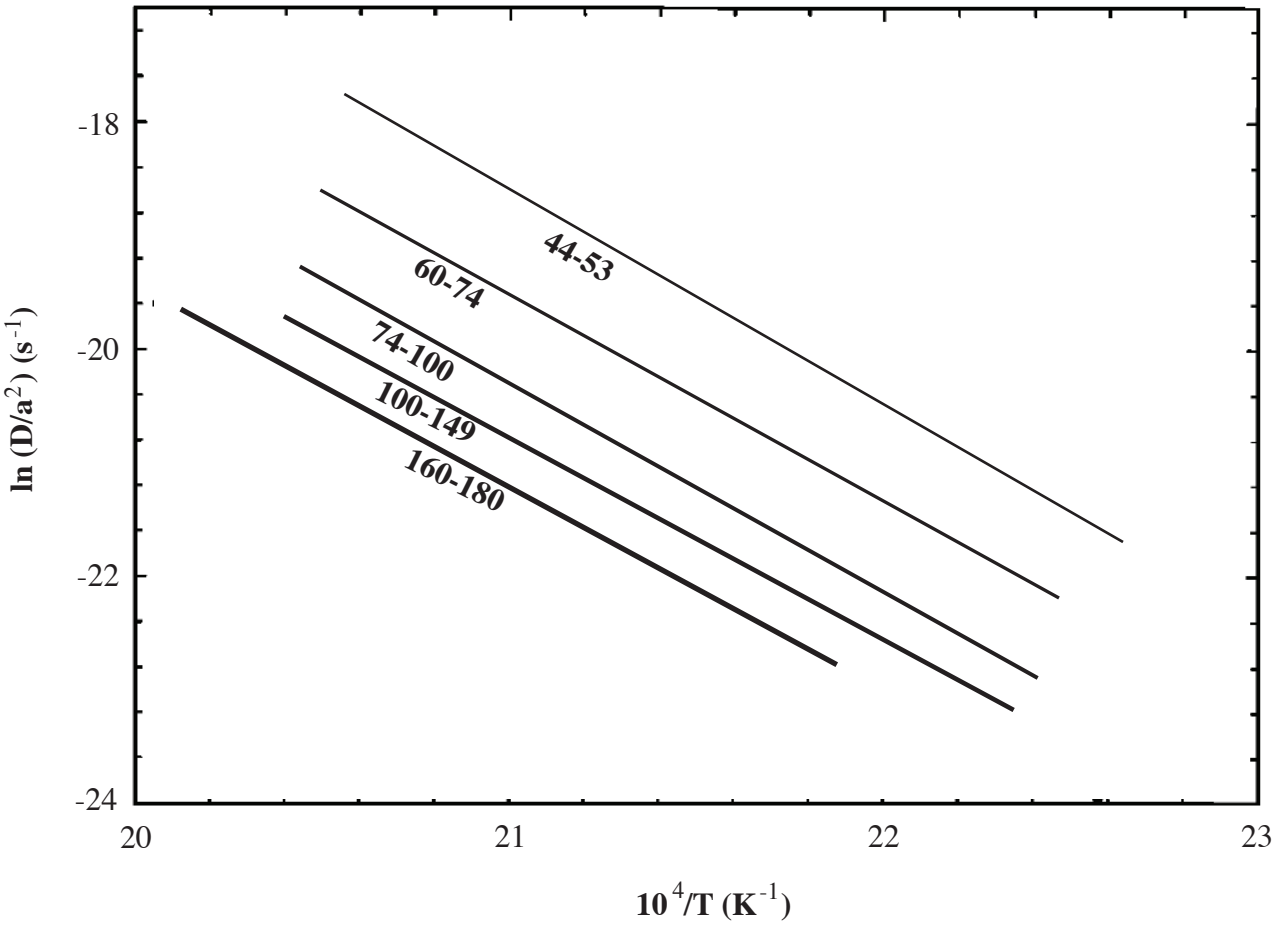

4. RESULTS

4.1 Data Quality and Reproducibility

Reproducibility of samples from the Teton Range is relatively poor, consistent with the findings of Tranel et al. (in review). The average 1σ reproducibility is ~21% (this study) and ~22% (Tranel et al., in review), whereas it is often expected to be closer to ~5-10%. Although 35 samples were collected, only 25 contained a sufficient amount of quality apatite to proceed with (U-Th)/He techniques, and 20 samples returned ages. Many samples yielded anomalous ages, most likely from the presence of inclusions or zonation within the apatite, which were culled prior to averaging. Many samples that were particularly poor or limited in apatite were processed as single grains, to avoid contamination of the few high quality grains present. For 106 tubes processed (containing either a single grain or an aliquot of multiple grains), 16 produced errors, either during He extraction or U and Th detection. Of the 90 tubes producing ages, 24 were identified as outliers and culled (27%), which is a higher percentage of outliers than in recent published work. Typically, the lowest elevation samples contained the least amount of and poorest quality apatite, although this was also an issue for some higher elevation samples, particularly from Rendezvous Mountain where 7 samples were collected, but only three resulted in meaningful ages.

SEM examination of apatite from two lithologies within Garnet Canyon showed a high occurrence of compositional zonation, particularly in apatite from layered gneiss samples (Tranel et al., in review). Even so, there does not seem to be a correlation between outliers and rock type, which is a possibility given research studying outside contributions of He (from adjacent U and Th rich minerals) (e.g. Farley and Stockli, 2002). Additionally, extremely low He values are problematic for the youngest samples. For example, the youngest age (5.82 Ma) was recorded adjacent to String Lake between the Grand Teton and Mount Moran, but contained small quantities of low-quality apatite and thus only one of the six grains analyzed produced a meaningful age. The northernmost sample was a low elevation sample from Colter Canyon, and produced an age significantly older than the rest of the along strike samples. This sample was extracted from an isolated outcrop within ~1 km of an active hot spring, Jackson Lake Hot Springs. This particular hot spring has been documented to reach temperatures in excess of 70°C and might play a role in the anomalously old along-strike age (Love et al., 2003).

4.2 Thermochronometry

AHe Results

AHe ages from the Teton Range are between 5.82 and 66.8 Ma (Table 1). High elevation AHe ages increase from north to south, while lower elevation ages are fairly consistent along strike (Figure 12). Rendezvous Mountain samples range from 66.8 ± 5.2 Ma (1σ) adjacent to the unconformity to 7.41 ± 1.8 Ma at the base. Samples from Grand Teton transect range from 50.7 ± 2.7 Ma at the Upper Saddle to 8.26 ± 0.6 Ma at the base. Mount Moran samples range from 26.5 ± 4.1 Ma adjacent to the unconformity to 6.17 ± 3.2 Ma at the base. Whereas samples from the Grand Teton and Rendezvous Mountain range from ~8-70 Ma, ages at Mount Moran are younger, between ~6 and 26 Ma. This is apparent when each transect is plotted as an age-elevation gradient, and the slope of the Mount Moran section is 0.08 mm/yr (Figure 13), followed by the Grand Teton at 0.04 mm/yr (Figure 14), and Rendezvous Mountain at less than 0.01 mm/yr (Figure 15). Although the value for the Grand Teton transect differs slightly from previous estimates (0.03 mm/yr; Tranel et al., in review), it is not significant enough to require revisions of any work based on that value, but justifies the need for dense sampling within future vertical transects. Within each transect there is a strong age-elevation correlation. If interpreted as cooling rates, they would be notably slow; instead, they most likely reflect He loss due to time spent near and within the HePRZ, and as such, cannot be considered to represent the cooling rate. This is consistent with the findings of Roberts and Burbank (1993). Within the individual transects, cooling rates are consistent and correlate strongly with elevation, although because the samples are from a tilted fault block, a better correlation with structural depth below the unconformity is expected (Figure 16). For example, the oldest recorded AHe age was documented on Rendezvous Mountain and at Teton Pass (66.8 Ma). Although differing in distance along strike, both samples were collected roughly 20 meters below the unconformity.

When each of the vertical transects is plotted as age-elevation gradients, all lack inflections representing an increase in cooling rate. This indicates that rapid cooling occurred after the youngest age (or slightly after the second youngest age, as a change in trend still would not be noticeable). Modified plots show extrapolation of the data to indicate where the expected zero age would occur (Figure 17, 18, 19); however, it is possible that these could produce an underestimation of rate, since they are forced to assume the inflection at the youngest age. Therefore, the values obtained through this method are minimum apparent exhumation rates.

The post-cooling exhumation rates are 0.28 mm/yr at Mount Moran, 0.24 mm/yr at the Grand Teton, and 0.23 mm/yr at Rendezvous Mountain. The extrapolation also indicates that exhumation has been fairly consistent throughout the range since ~6-8 Ma, calculating between 1.7 and 2 km of footwall rock uplift for the base of all three transects.

In addition to the lowest elevation samples from the vertical transects, 6 other ages define the uplift history along the Teton fault. There is no obvious trend from north to south, as within error, all ages are about the same (Figure 20). The mean for the low elevation samples is 8.5 ± 1.9 Ma. This excludes the northernmost sample that produced an age of 14.3 ± 3.1 Ma. Because bedrock is not readily available along the Teton fault, variability in the ages is expected, as it was impossible to sample from the same elevation everywhere along strike. Thus, we might not expect all of the samples to occur at the aforementioned inflection point. However, based on the similarity of the ages, we interpret that this is the minimum age of onset of rapid Neogene exhumation from uplift on the Teton fault.

AFT Results

Apatite fission track ages range from 11.7 to 54.1 Ma (Table 2). Because of apatite quality, only two samples resulted in AFT ages from Rendezvous Mountain. The highest elevation produced an age of 54.1 ± 4.4 Ma. The lowest sample, only ~320 m below, is 45.7 ± 3.6 Ma. Ages from the Grand Teton ranged from 14.1 ± 2.1 Ma ~400 m above the valley floor to 43.2 ± 3.4 Ma at the Upper Saddle. Mount Moran ages range from 11.7 ± 1.7 Ma at the base to 38.0 ± 3.1 Ma at the summit. Of the nine samples analyzed, AFT results for most of the localities are generally consistent with the AHe ages, documenting similar age-elevation relationships and ranges for each transect. However, in some cases the AFT ages are younger than the AHe age for the sample (Figure 21), straying from the expected AHe-AFT relationship (e.g. Wolf et al., 1998).

Similar age discrepancies have been observed in other studies, and generally the AHe age is considered to be "too old", regardless of the repeatability. Green and Duddy (2006) documented AHe ages that were older than the corresponding AFT ages where the AHe ages exceeded 50 Ma, although the effect is more pronounced at ages over 100 Ma. Although some of the Teton ages are over 50 Ma, they are few in number, and thus do not explain discrepancies with younger, lower elevation samples. Alternatively, excess ^{4}He from adjacent grains could

potentially explain the old AHe ages, but extensive petrographic analysis would be required to determine if this accounts for the observed anomaly. Soderlund et al. (2005) and Hendriks and Redfield (2005) proposed that samples anomalously high in U with a slow cooling history could experience radiation-enhanced track annealing, thus producing an AFT age that is "too young". This is potentially applicable in only one of the samples where the U content is exceptionally higher than the average for the entire suite (~40 ppm). Sample TR08-19 produced an AHe age of 66.8, but an AFT age of 54.1. The U content for this sample, however, was ~125 ppm, far above the average for the Tetons, and well exceeding the average for most other studies (~10-20 ppm). Two other samples, TR08-03 and TT2 also have AHe ages greater than the AFT ages, but with acceptable U concentrations. TR08-03 is from the Rendezvous Metagabbro, and it has been suggested that annealing behavior is systematically different within gabbroic rocks due to high chlorine content (Green et al., 1986; Lorencak, 2003). This could result in an underestimation of fission track annealing for sample TR08-03.

Hauessler et al. (2008) suggested that U and Th zonation could be problematic for diffusion, as He diffusing from a high U or Th core might not make it past the rim of the grain, thus ensuring overcorrection during post processing. Given the strong zoning observed within the apatite from Garnet Canyon (Tranel et al., in review), this could certainly explain some of the "too old" ages. Unfortunately, there is no way to examine the processed grains for zoning, as they are dissolved in acid before U-Th analysis. Due to the high percentage of zoning within layered gneisses from the Tetons (73%), it is likely that this contributed to the old age of TT2. When the uncorrected AHe ages are plotted against the AFT ages, all of the AHe ages are younger than the AFT values, as expected given the lower closure temperature for (U-TH)/He dating (Figure 22). Thus, it is possible that zoning likely affects the majority of the samples, producing a "too old" AHe age. Because of the relative range of ages, it probably would not drastically alter the interpretations of the dataset as a whole, and because the AHe dataset is significantly larger, the AHe ages will be primarily used for this analysis.

Old vs. New AFT

One prominent feature of the new fission track ages is the discrepancy with the older AFT data of Roberts and Burbank (1993). Based on the distribution of the AFT values throughout the Tetons, Roberts and Burbank (1993) devised a comprehensive uplift model

involving doming of the unconformity prior to the onset of the Teton fault. Additionally, they proposed that recent, rapid uplift of the Mount Moran section was necessary to bring it to its current position. This is evidenced by the differences in age and track lengths for Mount Moran, both indicating that the section spent more time in the PAZ and uplifted out of the PAZ later than the Buck Mountain and Rendezvous Peak samples. The new transects coincide well with the Roberts and Burbank (1993) sections, although the nearby and higher-elevation Grand Teton was sampled instead of Buck Mountain for the central section. The new ages are consistently younger than the Roberts and Burbank ages, and in some cases are younger than half the previous estimates (e.g 13.6 Ma compared to 41.4 Ma at ~2970 m on Mount Moran) (Figure 23).

4.3 Cooling History

For all samples, the recent geothermal gradient was assumed to be 25°C/km. The resulting profile then determined if and by how much the geothermal gradient varies over time. In each of the three profiles, it appears to increase by 2-3°C since the Cretaceous, which is reasonable considering the transition from the Laramide orogeny to Basin and Range extension. Typically, the HeFTy corrected ages for the AHe samples are slightly older than our corrected ages, but this is because HeFTy assumes a spherical grain shape for diffusion corrections. Modeling results of all three transects indicate an extended amount of time within the HePRZ (Figure 24, 25, 26). The onset of Neogene uplift is recorded earlier on the Grand Teton and Mount Moran profiles (~11 Ma) compared to Rendezvous Mountain which records an onset of ~9 Ma. The Grand Teton profile suggests greater uplift of the basal samples since the onset of faulting, ~2.5 km, whereas the Mount Moran profile implies ~2 km of uplift, and the Rendezvous Mountain profile suggests only ~1.6 km. The Mount Moran samples appear to have resided lower down within the HePRZ prior to ~30 Ma, thus explaining the overall younger ages observed in the Moran section. Modeling of the northern section also reveals a period of increased exhumation after ~30 Ma.

4.4 Structural Analysis

By incorporating the nine cross sections into 3DMove (Figure 27) we were able to reconstruct the position of the unconformity. The surface is most accurate positioned where the unconformity is exposed or noted in the subsurface, and is less accurate where it was projected

great distances above the sections. One of the largest uncertainties comes from projecting the unconformity eastward to intersect with the projection of the Teton fault. Ideally, the unconformity surface would reflect drag along the fault; however, as we have no way to constrain the amount or extent of this deformation, and because it would severely complicate volume calculations, the unconformity is modeled maintaining its dip as it approaches the fault. Likewise, although the surface expression is segmented, the Teton fault was treated as a single planar surface to aid in calculations. Nonetheless, the resulting model of the Teton Range suitably portrays the extent and domed shape of the unconformity (Figure 28).

A structure contour map of the unconformity (Figure 29) was produced based on the unconformity surface in 3DMove. Because it was imported into ArcMap to produce the contours, any areas near faults were inaccurate, and needed to be contoured by hand. In order to calculate an estimate of the total volume of eroded basement, the space between the unconformity and the topography was analyzed in 3DMove producing a volume of ~276 cubic kilometers. This is a reasonable estimate, as calculations for an area surrounding Mount Moran produced ~35 cubic kilometers (Brown et al, 2008). The area around Mount Moran is important as it represents the most accurate and extensive structural section below the unconformity. Approximately ~1700 m of basement exists between the unconformity at the summit of Mount Moran and the mouth of Moran Canyon. While the unconformity is higher at the Grand, intra-range faulting (i.e. displacement across the Buck Mountain fault) prevents a precise estimate of structural depth. For the Mount Moran area, an average depth to incision was calculated, resulting in ~0.6 km. Recalculated for the entire Teton Range (~471 sq. km) based on the new volume estimate, this results in an average depth to incision of ~0.3 km. Although the Phanerozoic section was not included in the volume calculation, it is about ~1.5 km thick. Added to the average depth of incision (assuming that if an area was eroded through the unconformity, the Phanerozoic units were also removed), this results in an average depth to incision of ~1.8 km. This can be used to calculate long-term spatially averaged erosion rates for the Teton Range. Assuming that the majority of erosion occurred after the onset of Teton uplift, a ~10 Ma onset of faulting produces a rate of ~0.18 mm/yr.

Figure Captions

Table 1: AHe data. AHe ages for the Teton Range. See footnote in table for description of errors.

Table 2 : AFT data. AFT ages for the Teton Range analyzed at University of Wyoming.

Figure 12: AHe data. Elevation versus distance along the Teton fault with annotated AHe ages. Low-elevation samples are consistently <10 Ma, while higher elevation samples vary along strike. Errors listed are 1-σ uncertainty.

Figure 13: Mount Moran AHe data. Age versus elevation plot for AHe samples from the Mount Moran transect. Samples show a strong correlation between age and elevation and $R^2 = 0.88$. Errors bars are plotted as 1-σ uncertainty.

Figure 14: Grand Teton AHe data. Age versus elevation plot for AHe samples from the Grand Teton transect. Samples show a strong correlation between age and elevation and $R^2 = 0.88$. Errors bars are plotted as 1-σ uncertainty.

Figure 15: Rendezvous Mountain AHe data. Age versus elevation plot for AHe samples from the Rendezous Mountain transect. Samples show a strong correlation between age and elevation and $R^2 = 0.96$. Errors bars are plotted as 1-σ uncertainty.

Figure 16: AHe age plotted versus structural depth below unconformity. Samples within each transect correlate well with structural depth, as it is a function of elevation.

Figure 17: Mount Moran exhumation rate extrapolation of AHe data. The plot implies an additional 1.7 km of exhumation since 6 Ma, resulting in a higher post-cooling exhumation rate of .28 mm/yr.

Figure 18: Grand Teton exhumation rate extrapolation of AHe data. The plot implies an additional 2 km exhumation since 8.3 Ma, resulting in a higher post-cooling exhumation rate of .24 mm/yr.

Figure 19: Rendezvous Mountain exhumation rate extrapolation of AHe data. The plot implies an additional 1.7 km exhumation since 7.4 Ma, resulting in a higher post-cooling exhumation rate of .23 mm/yr.

Figure 20: Age-elevation trends along strike. Annotated values represent sample elevation. AHe ages are consistent along strike and the average (not including northernmost sample) is 8.5 ± 1.9 Ma.

Figure 21: AHe vs. AFT. AHe age plotted against the corresponding AFT age for the same sample. Three samples have an AHe age > AFT age.

Figure 22: AFT vs. AHe with Uncorrected Sample Ages. AFT age plotted against AHe age, using the uncorrected AHe age for samples where AHe was originally older than AFT. Indicates that the apatite was most likely strongly zoned.

Figure 23: New AFT vs. Old AFT. The newer AFT ages are plotted against the previous AFT data of Roberts and Burbank (1993). Plotted as the sampled elevation with annotated AHe and AFT ages. The Rendezvous Mountain transect is proximal to the previous Rendezvous Peak transect. The Grand Teton transect is slightly north of the Buck Mountain transect. The Mount Moran transects begin at different base locations, but intersect at the summit. New AFT ages are consistently younger than the previous AFT ages.

Figure 24: HeFTy modeling results for the Mount Moran transect. Modeled ages are slightly older than the actual ages in Table 1, due to the spherical diffusion corrections used by HeFTy. Recent geothermal gradient was assumed to be 25°C/km. Indicates a ~11 Ma onset of faulting and ~2 km of footwall uplift since onset. A period increased exhumation is observed after ~30 Ma.

Figure 25: HeFTy modeling results for the Grand Teton transect. Modeled ages are slightly older than the actual ages in Table 1, due to spherical corrections used by HeFTy. Recent geothermal gradient was assumed to be 25°C/km. Indicates a ~11 Ma onset of uplift and ~2.5 km exhumation since onset.

Figure 26: HeFTy modeling results for the Rendezvous Mountain transect. Modeled ages are slightly older than the actual ages in Table 1, due to the spherical diffusion corrections used by HeFTy. Recent geothermal gradient was assumed to be 25°C/km. Indicates a ~9 Ma onset of uplift and ~1.6 km exhumation since onset.

Figure 27: Cross sections in 3DMove. Nine east-west cross sections were incorporated in Midland Valley's 3DMove.

Figure 28: Domed character of the unconformity in 3DMove. A) Model with translucent unconformity and oblique view, looking south. B) Model with opaque unconformity and oblique view, looking south. C) View looking west of model unconformity from "Jackson Hole" showing slight doming and intersection with topography in the northern Tetons.

Figure 29: Structure contour map of the Precambrian-Paleozoic unconformity. Mount Moran (M) and the Grand Teton (G) are noted. Contours represent 100 m intervals.

TABLE 1: AHe data.														
Sample	**Elevation (m)**	**Latitude**	**Longitude**	**Rock type**	**Mass (mg)**	**mwar (µm)**	**He (pmol)**	**U (ppm)**	**Th (ppm)**	**# grains**	**F_T**	**Corr. Age (Ma)**	**Average Age (Ma)**	**Standard Deviation (1σ)**
TR08-02-1	2066	43.6156	-110.8161	Metagabbro	0.0059	55.2	0.0109	37.5	4.2	1	0.77	11.94	**9.63**	**2.4**
TR08-02-2					0.0038	50.6	0.0038	35.5	3.6	1	0.75	7.14		
TR08-02-3					*0.0016*	*43.7*	*0.0046*	*45.0*	*5.5*	*1*	*0.68*	*18.21*		
TR08-02-4					0.0037	57.5	*			1	0.79			
TR08-02-5					*0.0019*	*52.9*	*0.0077*	*25.3*	*2.4*	*1*	*0.75*	*40.84*		
TR08-02-6					*0.0040*	*50.6*	*0.0181*	*38.4*	*7.6*	*1*	*0.75*	*28.97*		
TR08-02-7					*0.0024*	*46.0*	*0.0131*	*46.5*	*9.8*	*1*	*0.71*	*30.70*		
TR08-02-8					0.0011	41.4	0.0038	93.3	23.8	1	0.69	9.81		
TR08-03A	2975	43.8265	-110.7661	Layered Gneiss	0.0039	31.7	0.0046	21.0	7.7	5	0.65	15.41	**16.52**	**1.6**
TR08-03B					0.0037	32.5	0.0037	15.0	6.1	5	0.65	17.63		
TR08-03C					*0.0048*	*34.6*	*0.0216*	*25.8*	*12.7*	*4*	*0.65*	*45.83*		
TR08-03D					*0.0080*	*44.5*	*0.0251*	*20.7*	*7.0*	*5*	*0.70*	*38.17*		
TR08-05-2	2636	43.8244	-110.7593	Layered Gneiss	0.0038	39.5	0.0084	51.0	1.4	3	0.69	12.03	**12.03**	
TR08-05-3					*0.0068*	*47.5*	*0.0357*	*34.3*	*7.1*	*4*	*0.71*	*39.38*		
TR08-06-1	2450	43.8222	-110.7563	Layered Gneiss	0.0008	32.2	0.0006	23.8	35.3	1	0.64	7.20	**8.87**	**4.1**
TR08-06-2					0.0029	55.2	*			1	0.77			
TR08-06-3					0.0013	46.0	0.0003	~	3.1	1	0.71			
TR08-06-4					0.0011	32.2	0.0039	62.1	95.6	1	0.62	13.34		
TR08-06-5					0.0007	27.6	0.0004	18.8	4.0	1	0.56	10.93		
TR08-06-6					0.0044	69.0	0.0017	20.1	5.5	1	0.85	4.00		
TR08-06-7					0.0084	78.2	0.0010	~	0.8	1	0.84			
TR08-06-8					0.0046	80.5	0.0001	~	-	1	0.82			
TR08-07A	2185	43.8192	-110.7526	Layered Gneiss	0.0068	40.8	0.0195	70.2	42.6	5	0.66	10.35	**10.51**	**1.5**
TR08-07B					*0.0092*	*53.6*	*0.1020*	*122.2*	*55.3*	*4*	*0.74*	*21.21*		
TR08-07C					0.0067	43.4	0.0153	63.3	33.3	4	0.67	9.11		
TR08-07D					0.0052	42.2	0.0211	83.3	56.8	4	0.66	12.07		
TR08-09-1	2481	43.4999	-110.9387	Layered Gneiss	0.0055	46.2	0.0448	26.5	16.4	3	0.73	70.40	**66.77**	**13.7**
TR08-09-2					*0.0142*	*68.1*	*0.2857*	*43.7*	*11.7*	*3*	*0.78*	*105.78*		
TR08-09-3					0.0081	53.4	0.0444	23.5	20.7	3	0.71	51.62		
TR08-09-4					0.0067	58.6	0.1405	56.2	62.9	3	0.72	78.30		
TR08-11A	2060	43.6479	-110.8074	Layered Gneiss	*0.0030*	*50.6*	*0.0394*	*86.3*	*19.5*	*1*	*0.76*	*35.78*	**9.66**	**2.5**
TR08-11B					*0.0124*	*96.6*	*0.0127*	*2.9*	*2.2*	*1*	*0.89*	*64.19*		
TR08-11C					0.0056	55.2	0.0011	3.5	8.4	1	0.81	8.48		
TR08-11D					0.0124	96.6	0.0017	1.5	3.6	1	0.89	12.48		
TR08-11E					*0.0096*	*87.4*	*0.0096*	*8.0*	*3.3*	*1*	*0.88*	*24.70*		
TR08-11F					*0.0071*	*69.0*	*0.0036*	*2.9*	*8.6*	*1*	*0.85*	*22.94*		
TR08-11G					*0.0074*	*69.0*	*0.0162*	*31.4*	*7.3*	*1*	*0.85*	*14.96*		
TR08-11H					0.0109	78.2	0.0500	124.7	11.1	1	0.86	8.01		

Sample	Elevation (m)	Latitude	Longitude	Rock type	Mass (mg)	mwar (µm)	He (pmol)	U (ppm)	Th (ppm)	# grains	F_T	Corr. Age (Ma)	Average Age (Ma)	Standard Deviation
TR08-12-1	2230	43.7898	-110.7413	Layered Gneiss	0.0018	39.0	*			1	0.71		**5.82**	
TR08-12-2					0.0009	34.5	*	16.2	10.7	1	0.66			
TR08-12-3					0.0017	46.0	*			1	0.69			
TR08-12-4					0.0036	55.2	0.0006	5.6	7.5	1	0.78	5.82		
TR08-12-5					0.0015	43.7	*	4.2	2.9	1	0.72			
TR08-12-6					*0.0007*	*29.9*	*0.0011*	~	*51.9*	*1*	*0.66*	*35.55*		
TR08-13A	2088	43.7659	-110.7456	Layered Gneiss	0.0035	31.3	0.0046	40.7	10.4	4	0.67	8.79	**10.48**	
TR08-13B					0.0033	29.1	0.0229	169.8	52.2	5	0.65	11.27		
TR08-13C					0.0063	37.3	0.0116	43.1	10.3	6	0.68	11.38		
TR08-13D					*0.0134*	*55.2*	*0.0606*	*71.5*	*12.2*	*4*	*0.73*	*15.88*		
TR08-15-1	3835	43.8339	-110.7764	Layered Gneiss	0.0007	27.6	0.0019	37.2	21.0	1	0.63	20.79	**26.45**	
TR08-15-2					0.0009	29.0	0.0020	34.1	7.4	1	0.62	19.77		
TR08-15-3					*0.0007*	*31.3*	*0.0190*	*158.4*	*21.6*	*1*	*0.62*	*51.63*		
TR08-15-4					0.0008	27.6	0.0017	25.2	0.0	1	0.60	26.54		
TR08-15-6					0.0016	36.8	0.0059	24.8	3.3	1	0.69	41.35		
TR08-15-7					*0.0013*	*32.2*	*0.0313*	*113.5*	*18.0*	*1*	*0.65*	*61.29*		
TR08-15-8					0.0010	34.5	0.0022	26.5	2.0	1	0.66	23.80		
TR08-19A	2728	43.5983	-110.8603	Metagabbro	0.0078	42.8	0.2815	122.3	143.2	5	0.74	59.35	**66.77**	**5.2**
TR08-19B					0.0077	50.0	0.2224	83.9	131.9	4	0.71	67.26		
TR08-19C					0.0109	49.4	0.6768	179.1	235.5	5	0.72	69.46		
TR08-19D					0.0126	56.8	0.5393	113.3	139.9	4	0.78	71.01		
TR08-22A	2188	43.8603	-110.7707	Layered Gneiss	0.0042	32.6	0.0073	48.5	13.7	5	0.64	10.06	**10.51**	**1.5**
TR02-22B					0.0037	28.4	0.0106	70.2	18.0	4	0.59	12.57		
TR08-22C					0.0037	36.1	0.0105	79.4	25.2	4	0.62	10.24		
TR08-22D					0.0068	44.5	0.0143	61.3	18.6	5	0.67	9.16		
TR08-23A	2130	43.7388	-110.7484	Layered Gneiss	0.0111	40.4	0.0219	58.3	13.4	6	0.72	8.58	**8.26**	**0.6**
TR08-23B					0.0109	46.4	0.0133	41.8	6.9	5	0.73	7.38		
TR08-23C					0.0053	34.0	0.0060	37.1	5.9	5	0.64	8.85		
TR08-23D					0.0240	60.8	0.0235	29.4	3.1	5	0.76	8.23		
TR08-24-1	4040	43.7409	-110.8046	Quartz Monzonite	0.0007	32.2	0.0027	19.7	8.4	1	0.63	51.30	**50.70**	**2.7**
TR08-24-2					*0.0005*	*23.0*	*0.0050*	*22.2*	*9.6*	*1*	*0.53*	*138.78*		
TR08-24-3					*0.0006*	*23.0*	*0.0020*	*31.0*	*5.1*	*1*	*0.51*	*39.90*		
TR08-24-4					0.0007	27.6	0.0018	15.6	4.7	1	0.56	52.84		
TR08-24-5					0.0006	25.3	0.0020	23.3	7.8	1	0.56	45.51		
TR08-24-6					0.0006	25.3	0.0024	23.8	14.3	1	0.56	50.27		
TR08-24-7					0.0004	23.0	0.0010	17.6	4.4	1	0.48	52.06		
TR08-24-8					0.0007	27.6	0.0030	23.5	16.8	1	0.59	51.99		
TR08-27A	2400	43.5900	-110.8489	Layered Gneiss	0.0071	46.2	0.0638	88.5	49.5	4	0.73	23.56	**40.70**	**12.2**
TR08-27B					0.0195	62.3	0.0977	24.3	17.2	4	0.80	41.88		
TR08-27C					0.0165	58.9	0.1296	32.0	40.8	4	0.79	45.24		
TR08-27D					0.0121	46.1	0.0619	21.6	17.8	5	0.72	52.12		

Sample	Elevation (m)	Latitude	Longitude	Rock type	Mass (mg)	mwar (µm)	He (pmol)	U (ppm)	Th (ppm)	# grains	F_T	Corr. Age (Ma)	Average Age (Ma)	Standard Deviation
TR08-28-1	2201	43.5873	-110.8468	Layered Gneiss	0.0057	45.9	*	38.7	10.7	3	0.76		**7.41**	**1.8**
TR08-28-2					0.0053	50.1	0.0054	34.6	3.6	3	0.74	7.46		
TR08-28-3					0.0076	55.9	0.0160	49.4	11.9	2	0.78	9.96		
TR08-28-4					0.0053	46.9	0.0030	23.9	1.6	3	0.76	5.82		
TR08-28-5					0.0012	31.8	0.0012	43.8	11.2	2	0.64	6.39		
TR08-30-1	3505	43.8318	-110.7723	Layered Gneiss	*0.0055*	*41.7*	*0.0080*	*8.3*	*2.6*	*4*	*0.69*	*45.56*	**21.17**	**3.4**
TR08-30-2					0.0065	42.6	0.0021	6.2	4.7	4	0.69	17.31		
TR08-30-3					0.0086	44.1	0.0106	12.5	8.5	4	0.69	23.39		
TR08-30-4					0.0059	43.5	0.0049	9.7	2.8	5	0.67	22.82		
TR08-31A	3304	43.8300	-110.7694	Layered Gneiss	0.0050	37.3	0.0058	14.7	17.2	4	0.67	17.48	**14.26**	**4.6**
TR08-31B					*0.0039*	*34.8*	*0.0093*	*17.5*	*19.8*	*4*	*0.67*	*30.61*		
TR08-31C					*0.0026*	*31.4*	*0.0189*	*18.3*	*24.2*	*4*	*0.63*	*91.40*		
TR08-31D					0.0060	45.1	0.0074	26.8	16.5	4	0.69	11.04		
TR08-32A	2116	43.8173	-110.7531	Layered Gneiss	0.0033	31.7	0.0029	86.5	34.3	4	0.64	2.77	**6.17**	**3.2**
TR08-32B					0.0047	32.0	0.0074	66.5	28.2	4	0.63	6.55		
TR08-32C					*0.0048*	*48.3*	*0.0104*	*45.2*	*4.4*	*3*	*0.65*	*13.92*		
TR08-32D					0.0050	35.6	0.0058	34.8	9.4	5	0.65	9.20		
TR08-36-1	2108	43.9487	-110.7055	Layered Gneiss	0.0005	32.2	0.0001	~	-	1	0.62		**14.32**	**3.1**
TR08-36-2					0.0089	41.4	0.0001	~	-	1	0.68			
TR08-36-3					0.0005	32.2	*	~	1.2	1	0.55			
TR08-36-4					0.0006	34.5	0.0002	4.3	4.7	1	0.64	15.36		
TR08-36-5					0.0063	62.1	0.0213	73.5	12.3	1	0.79	10.80		
TR08-36-6					*0.0003*	*27.6*	*0.0064*	*5.9*	*44.0*	*1*	*0.56*	*39.21*		
TR08-36-7					0.0006	29.9	0.0001	2.7	1.1	1	0.62	16.79		
TR08-36-8					0.0005	27.6	*	4.4	8.0	1	0.63			
TR08-36-9					0.0004	32.2	0.0004	*420.0*	*255.9*	1	0.52			
TT-2	3385	43.7346	-110.8074	Layered Gneiss	0.0019	41.4	0.0360	70.6	48.6	1	0.72	61.0	**54.0**	**15.9**
TT-4	2985	43.7288	-110.7926	Quartz Monzonite	0.0036	28.6	0.0243	99.8	52.6	7	0.59	19.4	**21.4**	**2.11**
TT-5	2853	43.7260	-110.7910	Layered Gneiss	0.0024	69.0	0.0050	15.5	2.8	1	0.74	34.3	**25.8**	**5.42**
TT-8	2461	43.7237	-110.7639	Quartz Monzonite	0.0042	42.8	0.0036	28.2	11.3	4	0.70	7.62	**11.3**	**5.22**

Grains or aliquots listed in *italics* were considered anomalous for the given sample based on replicates and were not included in the age calculation.
* indicates samples where there was a He detection error
~ indicates samples where there was a U detection error
- indicates samples where there was a Th detection error
TR08 samples collected by Brown (2008); TT samples collected by Tranel (2007), for replicate details see Tranel et al. (in review)

Table 2. AFT Data

Sample	Elevation (m)	# of Crystals Counted	ρ_s	N_s	ρ_i	N_i	ρ_d	N_d	$P\chi^2$ (%)	Age ± 2σ (Ma)	Mean Dpar on Age ± stdev (µm)	Track Lengths Measured	Mean Track Length ± stdev (µm)	Mean Dpar on Length ± stdev (µm)
TR-08-03	2975	21	0.581	56	10.081	971	14.995	4262	90.4	**13.6 ± 4.0**	1.4 ± 0.2	29	12.5 ± 2.1	1.5 ± 0.3
TR-08-11	2060	19	0.710	53	22.030	1644	14.870	4262	29.9	**7.6 ± 2.2**	1.4 ± 0.2	-	-	-
TR-08-15	3835	20	3.599	258	21.596	1548	14.498	4262	42.6	**38.0 ± 6.2**	1.6 ± 0.2	99	11.7 ± 1.9	1.7 ± 0.2
TR-08-19	2728	19	9.839	420	40.246	1718	14.374	4262	30.6	**55.4 ± 8.0**	2.0 ± 0.3	100	12.8 ± 1.5	2.1 ± 0.3
TR-08-22	2188	20	0.851	53	20.009	1246	14.126	4262	77.7	**9.5 ± 2.8**	1.7 ± 0.2	57	13.2 ± 1.3	1.9 ± 0.3
TR-08-24	4040	20	2.142	146	15.038	1025	13.753	4262	29.0	**30.8 ± 6.4**	1.3 ± 0.3	46	12.7 ± 1.3	1.4 ± 0.3
TR-08-27	2400	20	4.141	340	19.620	1611	13.629	4262	16.8	**45.7 ± 7.2**	1.4 ± 0.2	29	12.5 ± 1.2	1.6 ± 0.1
TR-08-32	2116	20	0.841	56	15.159	1009	13.381	4262	61.7	**11.7 ± 3.4**	1.5 ± 0.2	-	-	-
TT2	3495	20	7.946	297	37.966	1419	13.133	4262	56.3	**43.2 ± 3.4**	1.7 ± 0.2	100	12.1 ± 1.5	1.7 ± 0.3
TT5	2820	24	4.443	397	22.475	2008	12.884	4262	11.0	**40.1 ± 6.6**	1.8 ± 0.3	100	11.4 ± 2.2	1.9 ± 0.2
TT10	2280	22	0.614	49	9.317	743	12.760	4262	99.0	**13.3 ± 4.0**	1.5 ± 0.2	-	-	-

Figure 12. AHe Data.

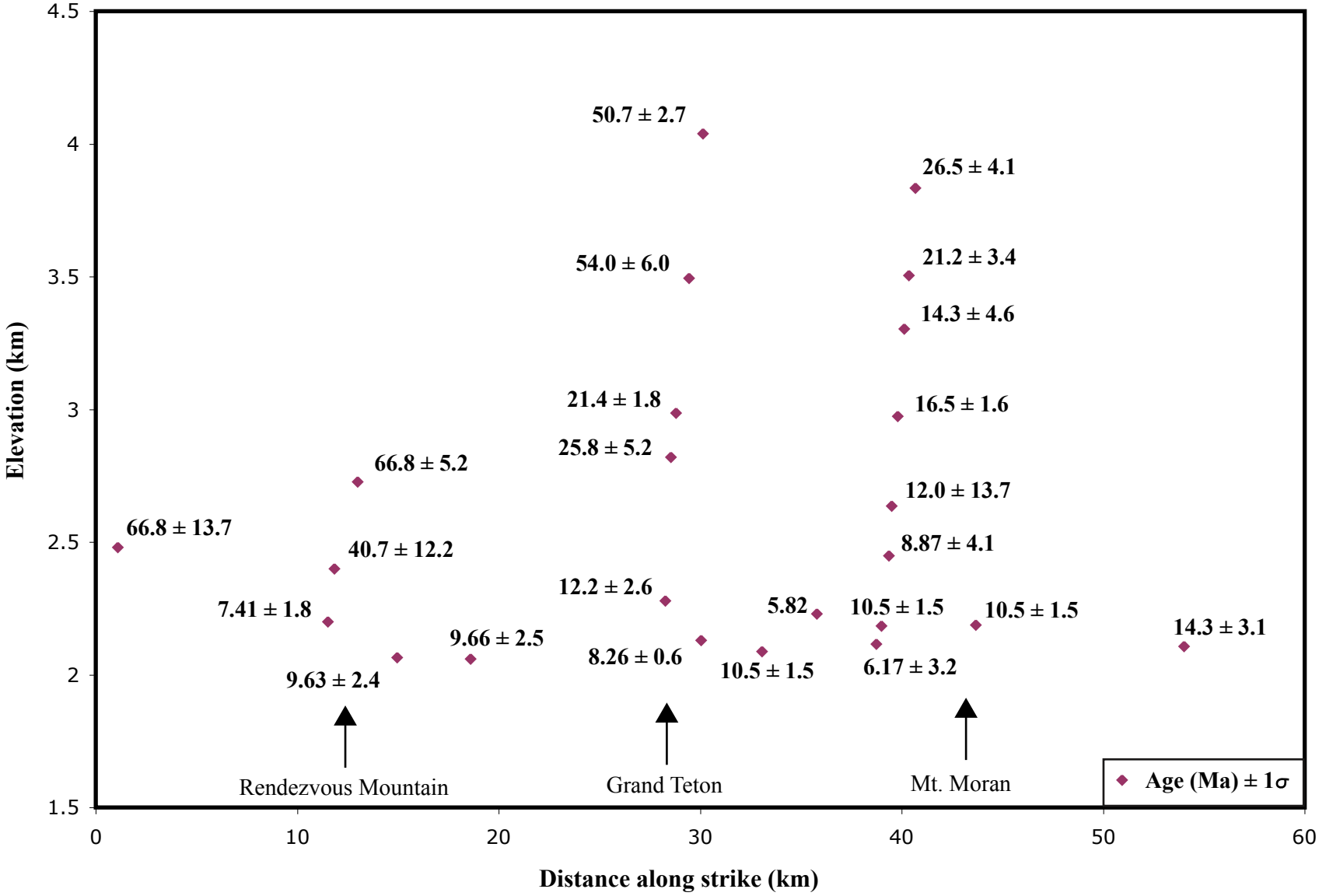

Figure 13. Mount Moran AHe data.

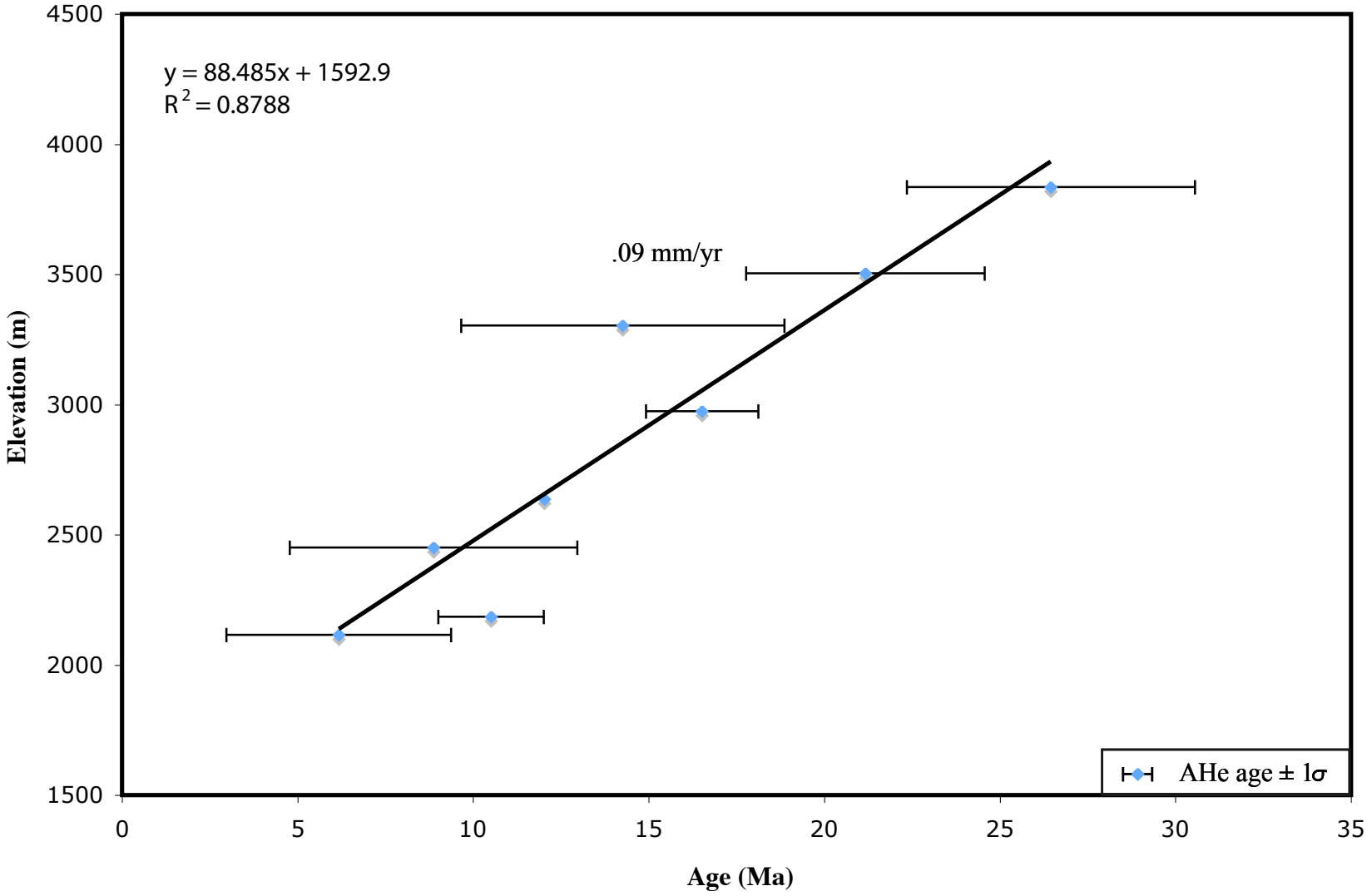

Figure 14. Grand Teton AHe data.

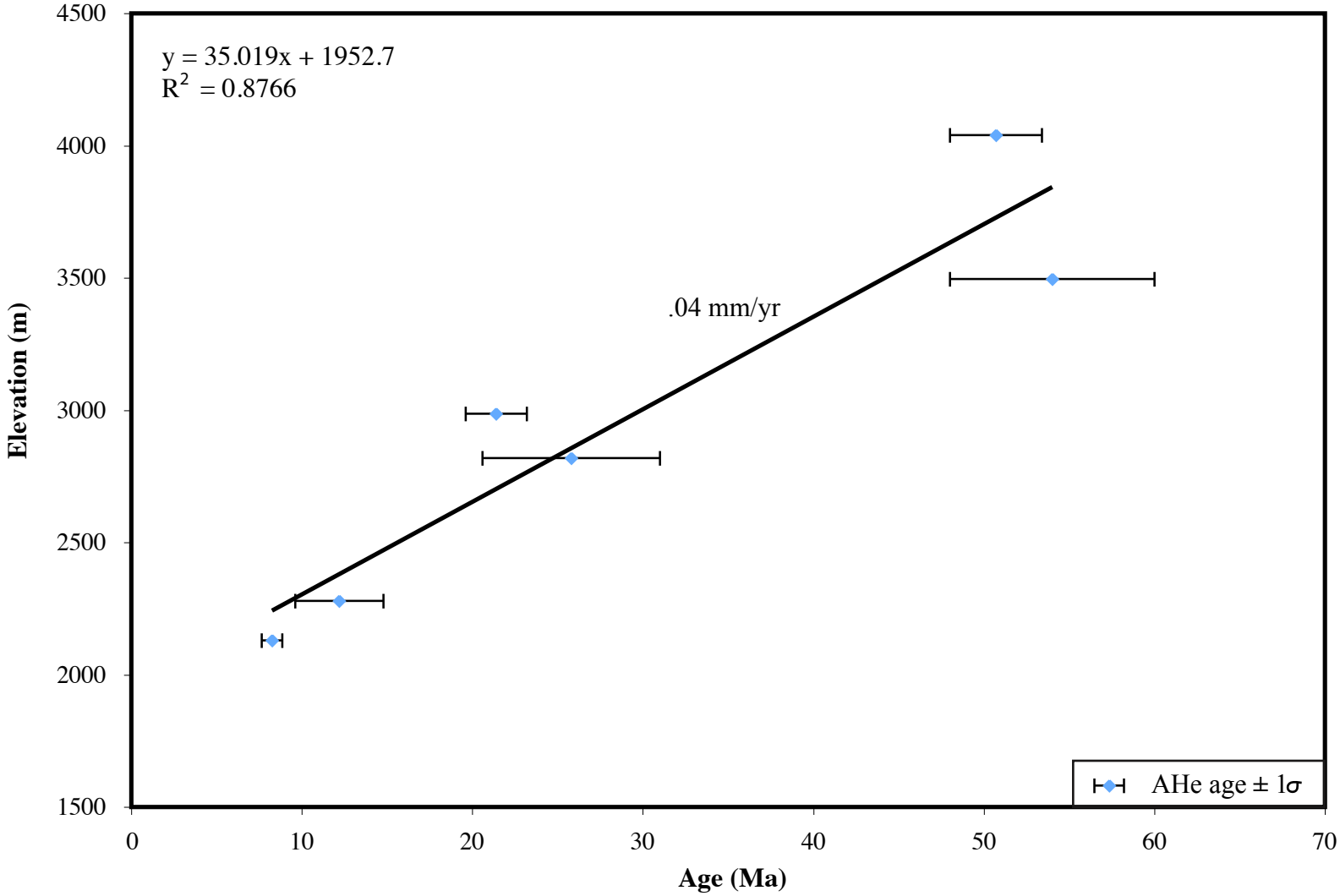

Figure 15. Rendezvous Mountain AHe data.

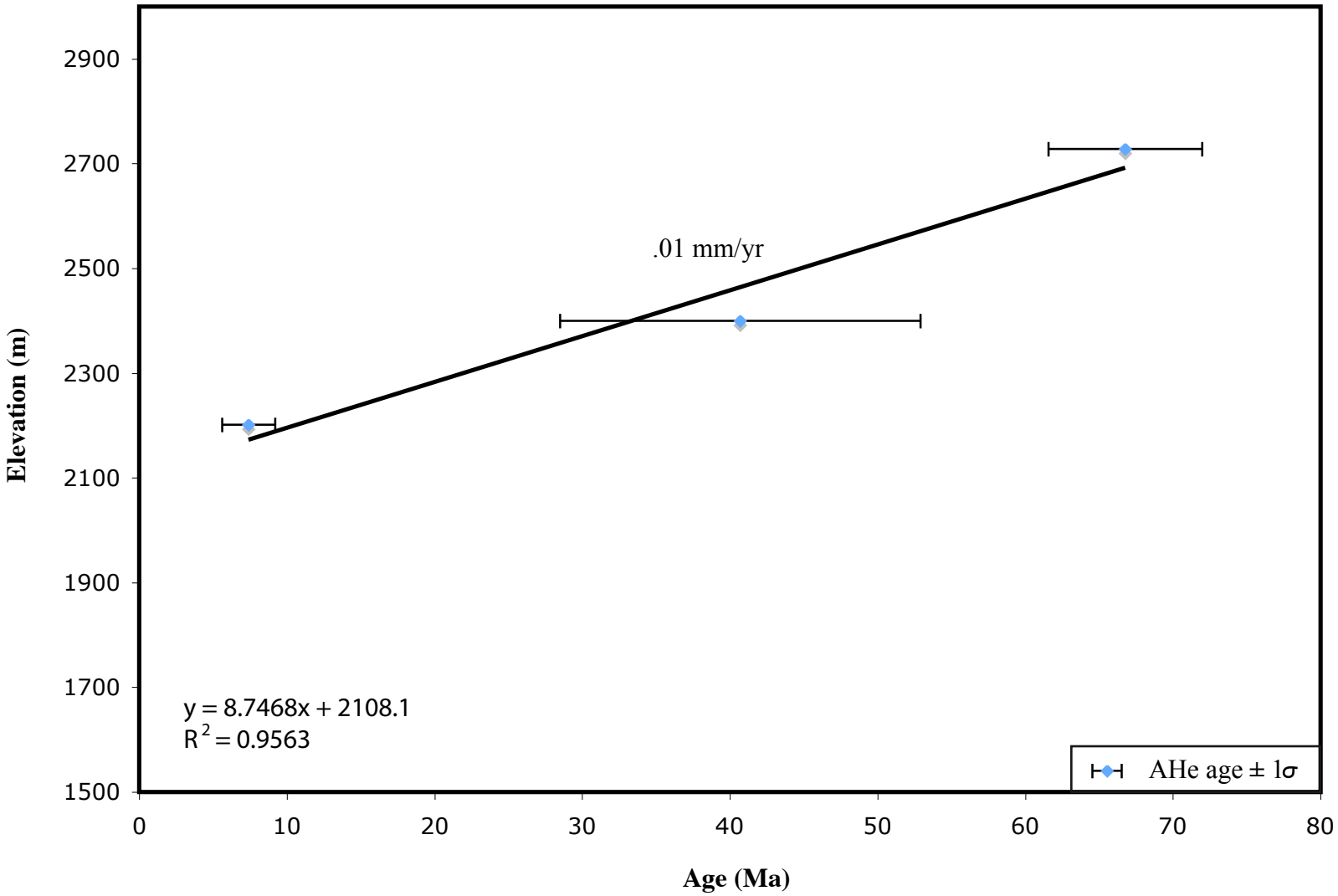

Figure 16. AHe Age vs. Structural Depth Below Unconformity.

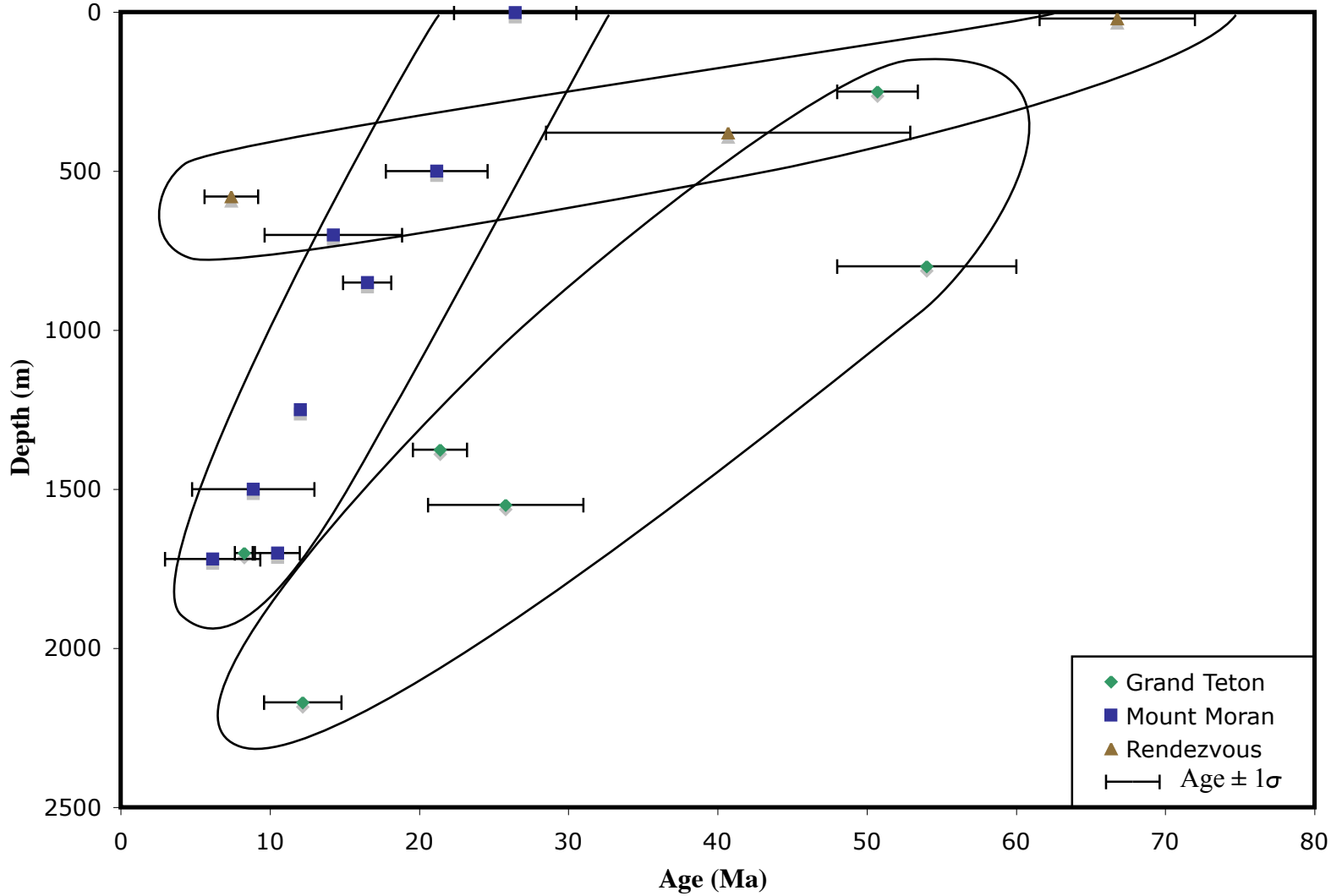

Figure 17. Mount Moran exhumation rate extrapolation of AHe data.

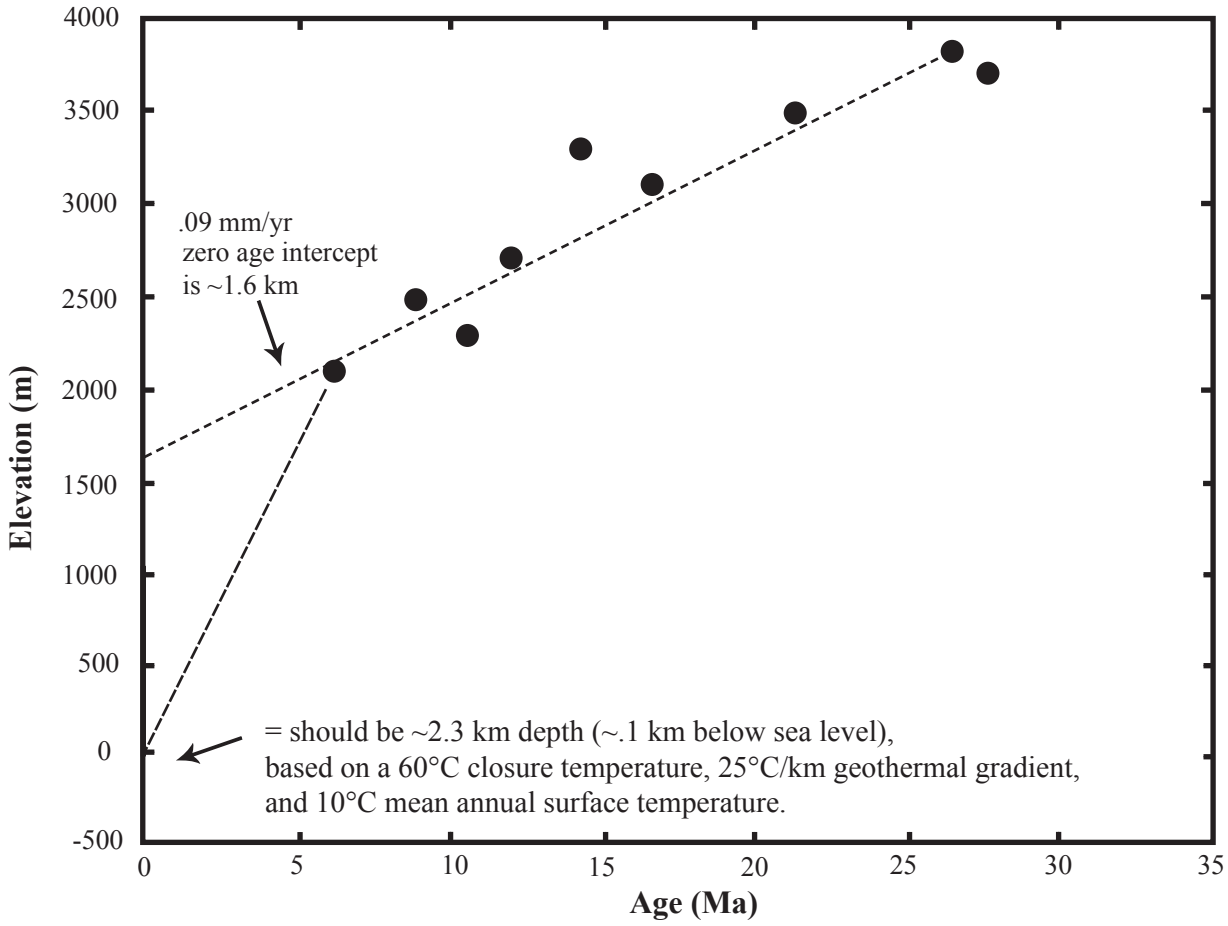

Implies an additional 1.7 km exhumation since 6 Ma, resulting in a higher post-cooling exhumation rate of .28 mm/yr.

Figure 18. Grand Teton exhumation rate extrapolation of AHe data.

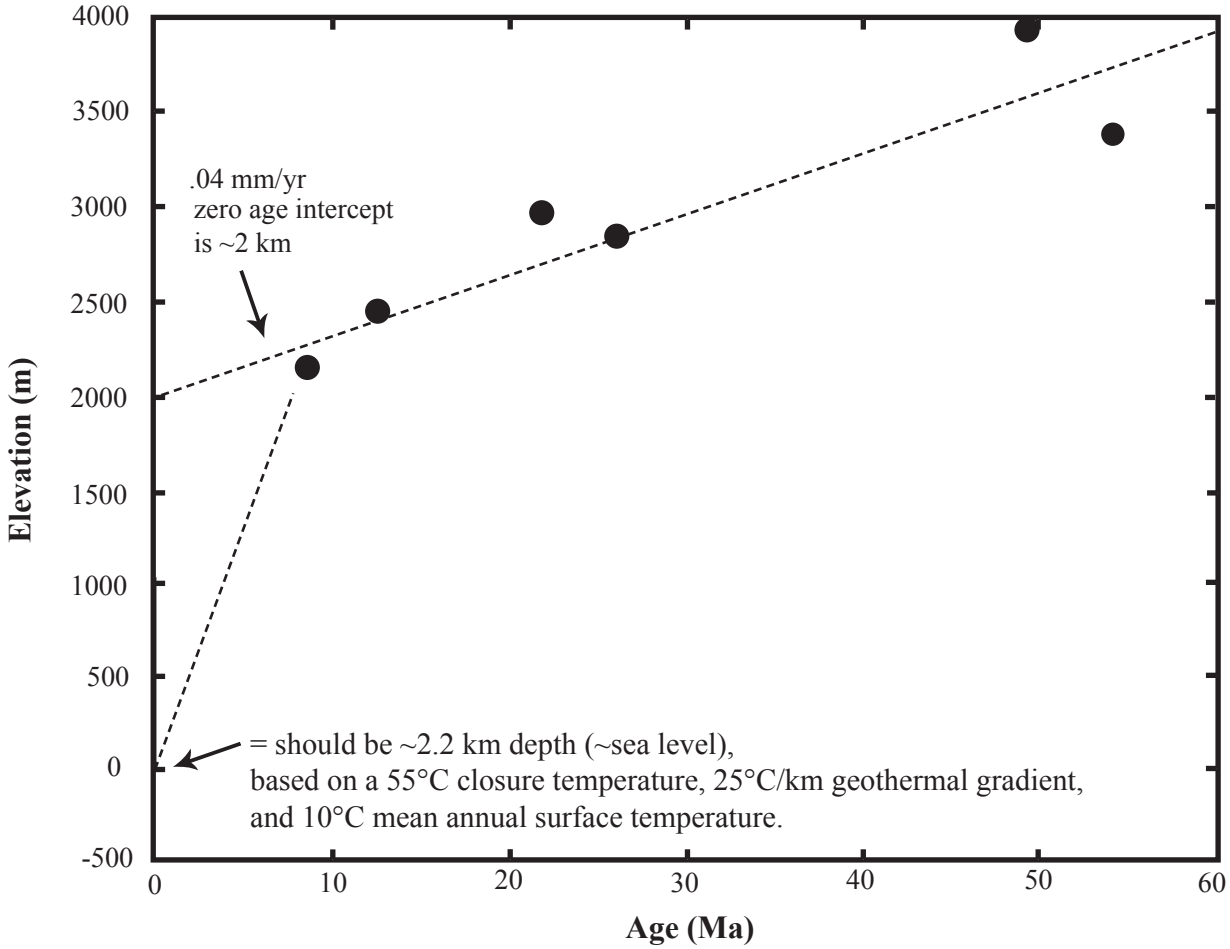

Implies an additional 2 km exhumation since 8.3 Ma, resulting in a higher post-cooling exhumation rate of .24 mm/yr.

Figure 19. Rendezvous Mountain exhumation rate extrapolation of AHe data.

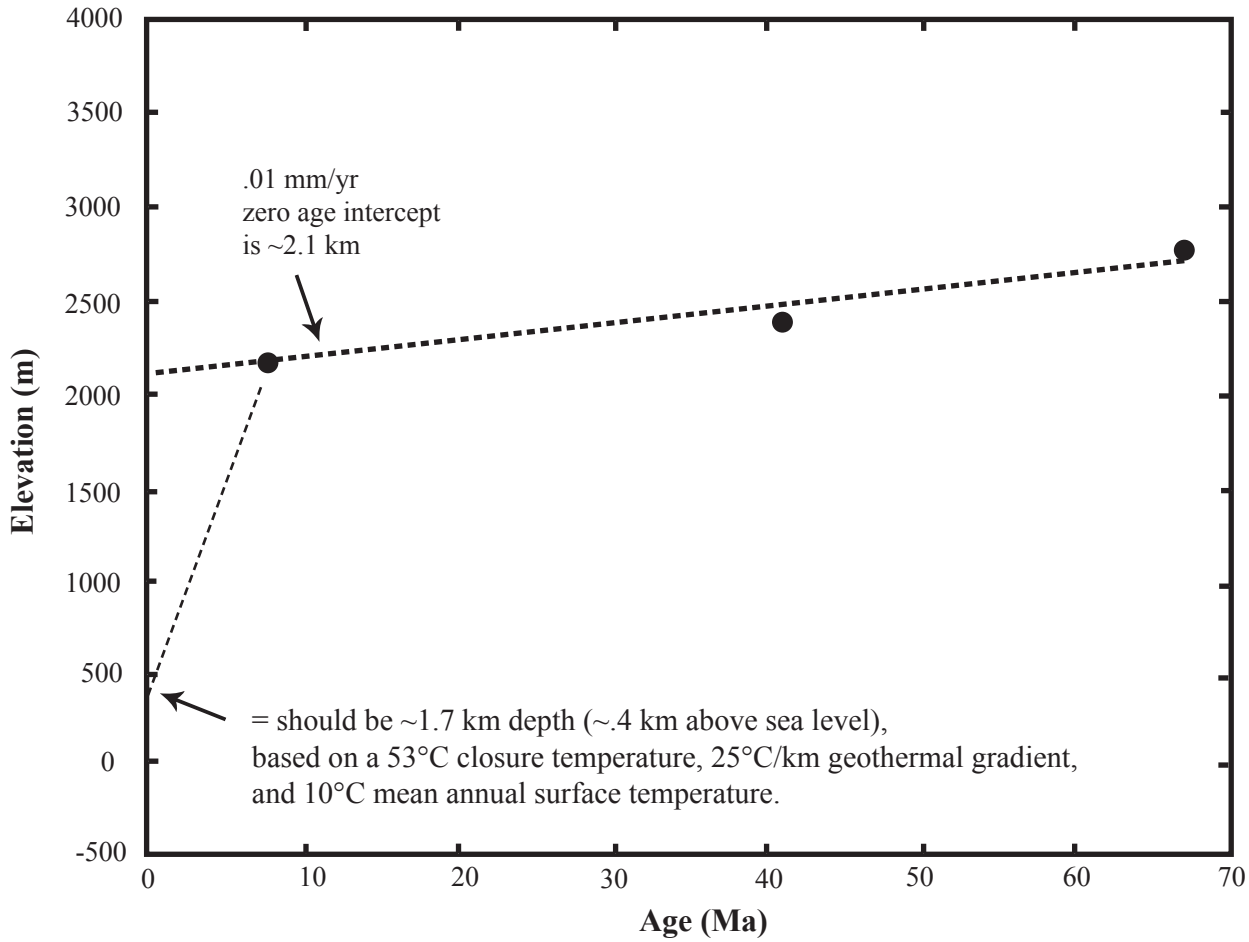

Implies an additional 1.7 km exhumation since 7.4 Ma, resulting in a higher post-cooling exhumation rate of .23 mm/yr.

Figure 20. Age-elevation trends along strike.

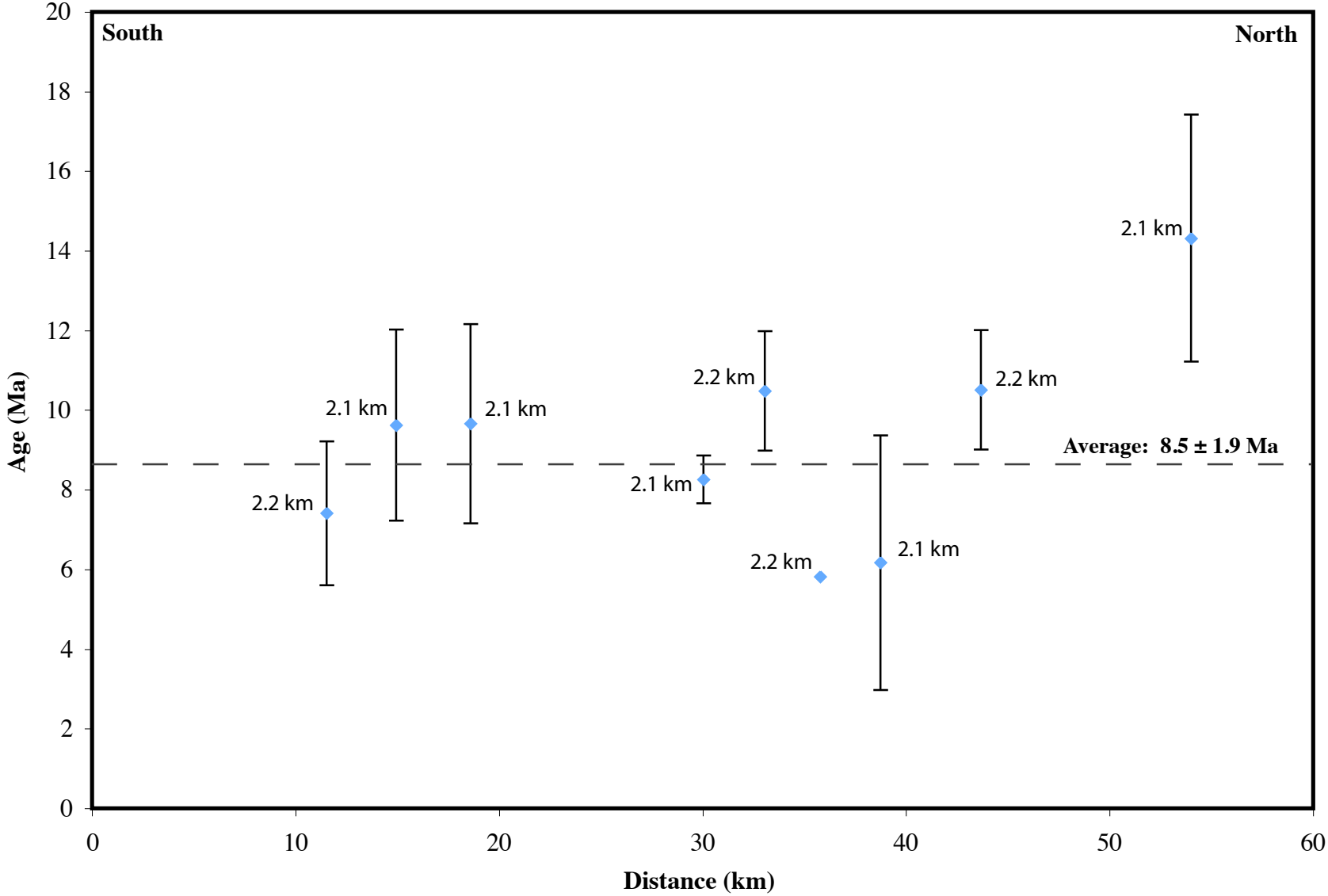

Figure 21. AFT vs. AHe

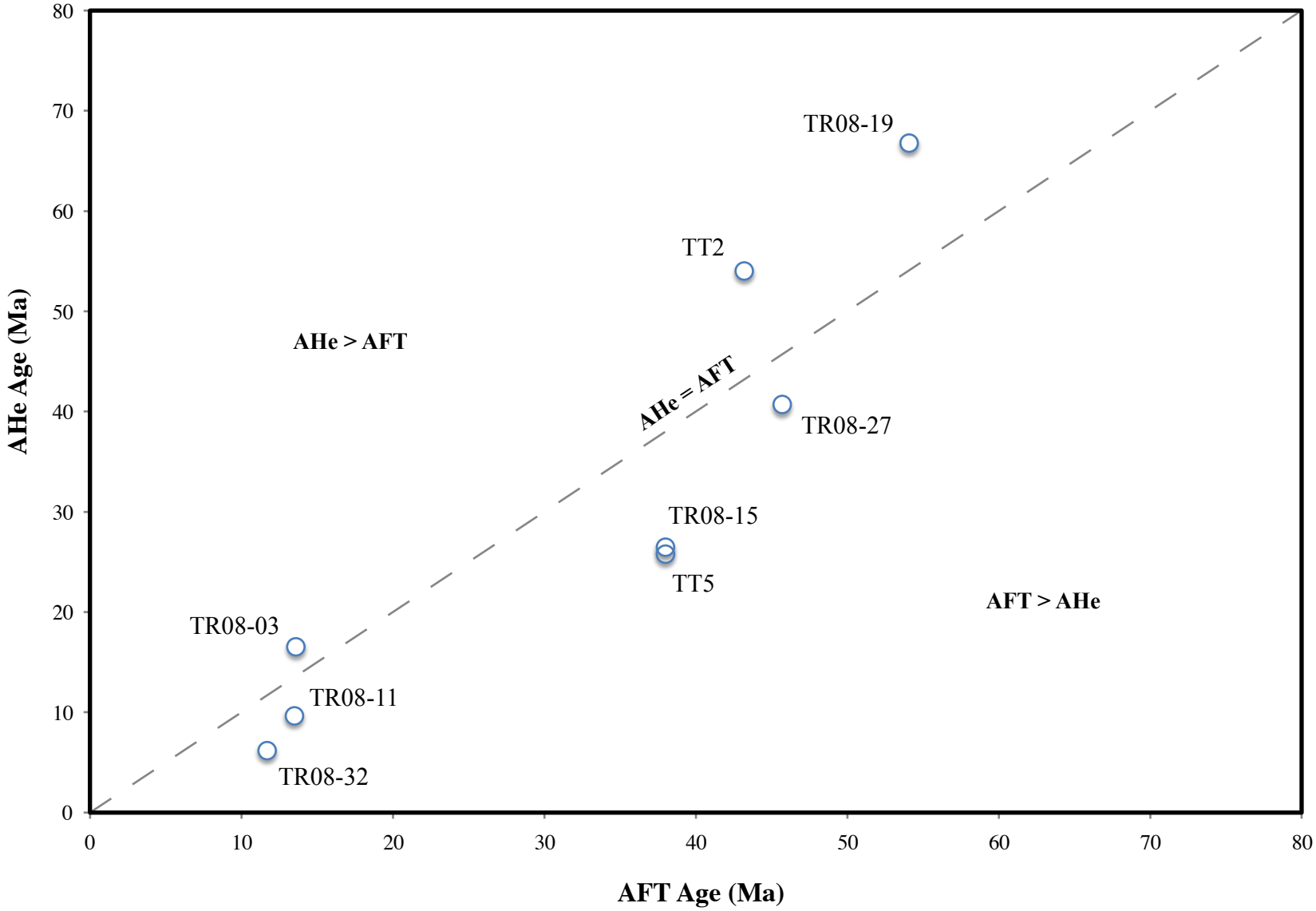

Figure 22. AFT vs. AHe with Uncorrected Sample Ages

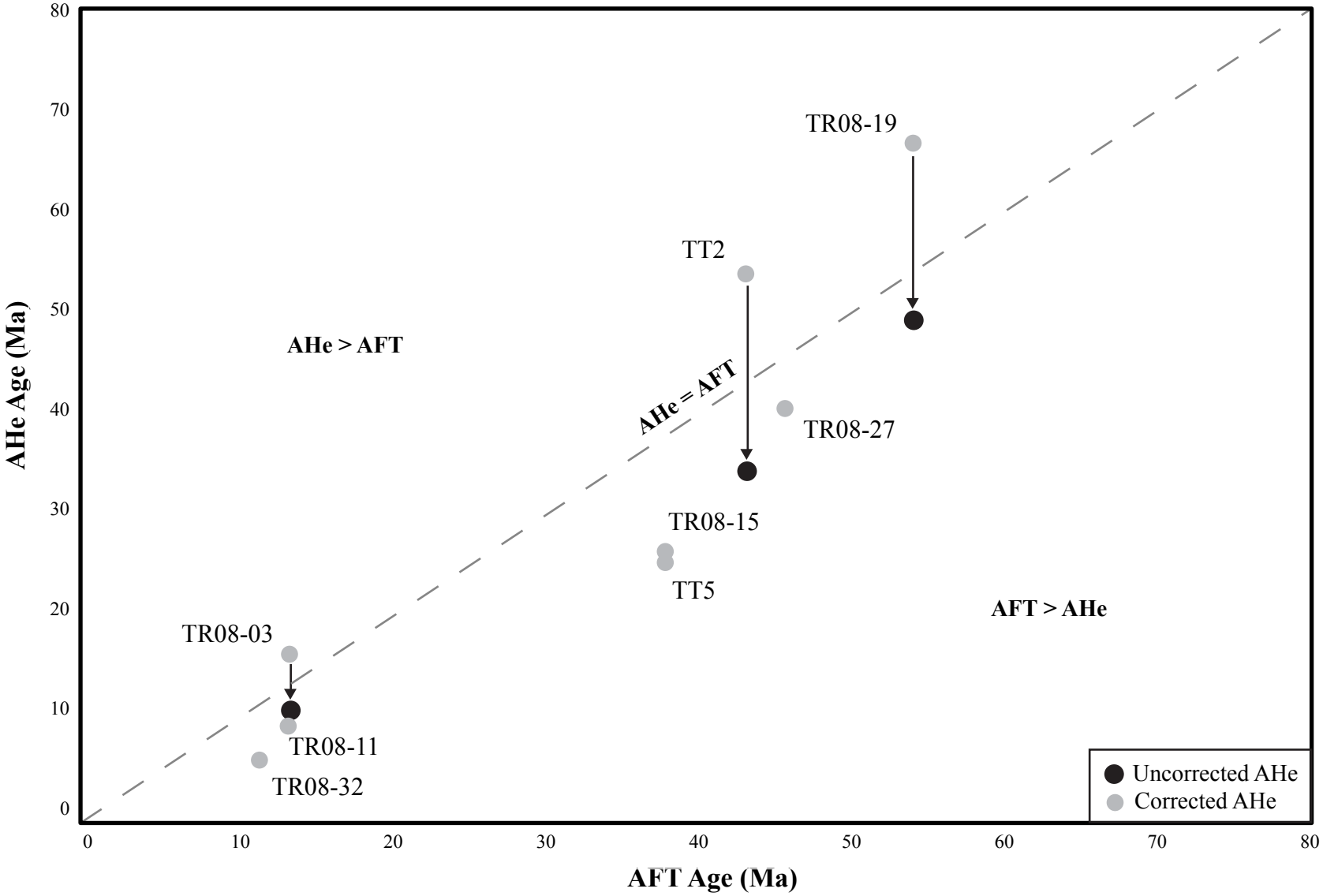

Figure 23. New AFT vs. Old AFT.

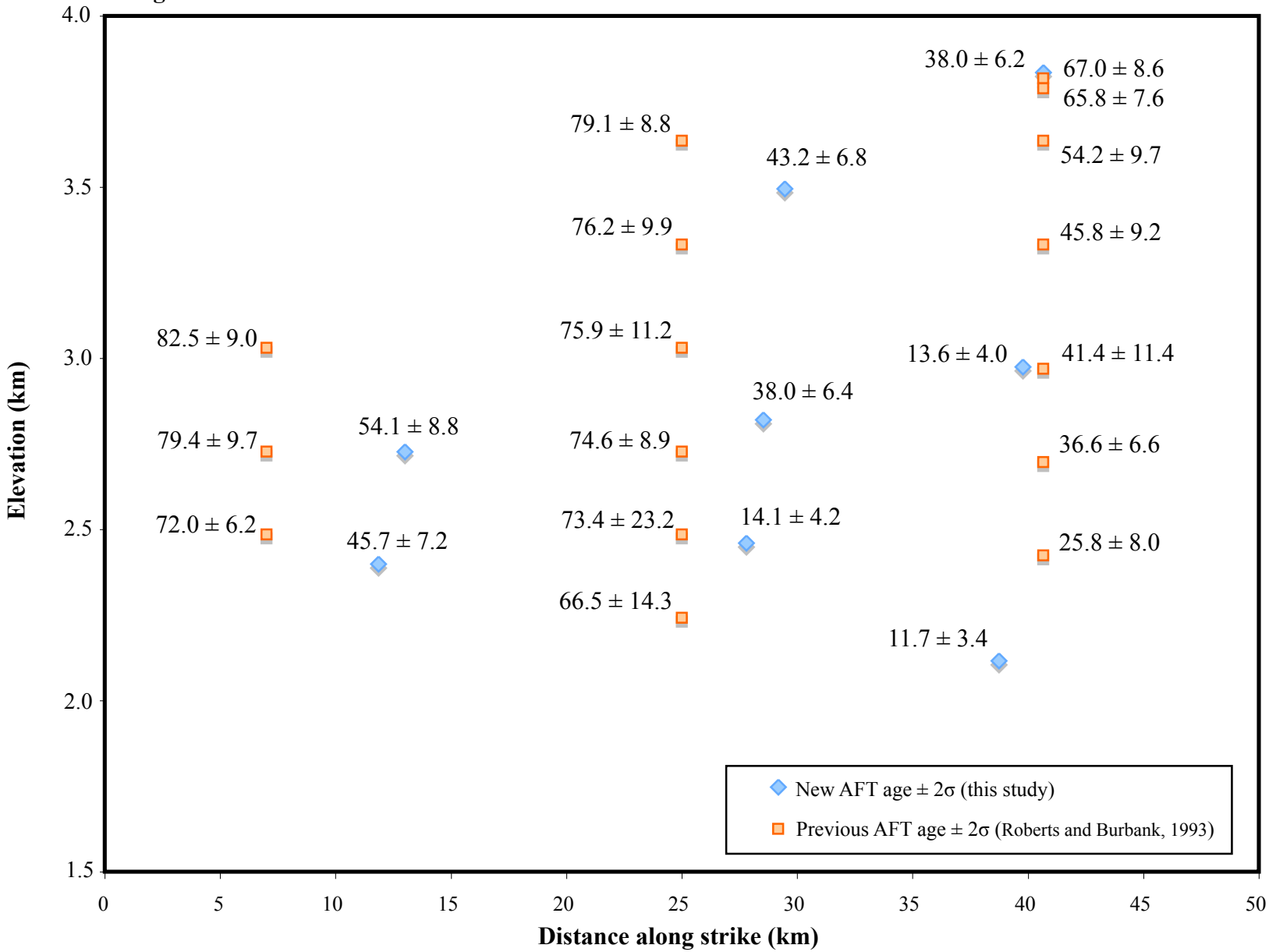

Figure 24. HeFTy modeling results for the Mount Moran transect.

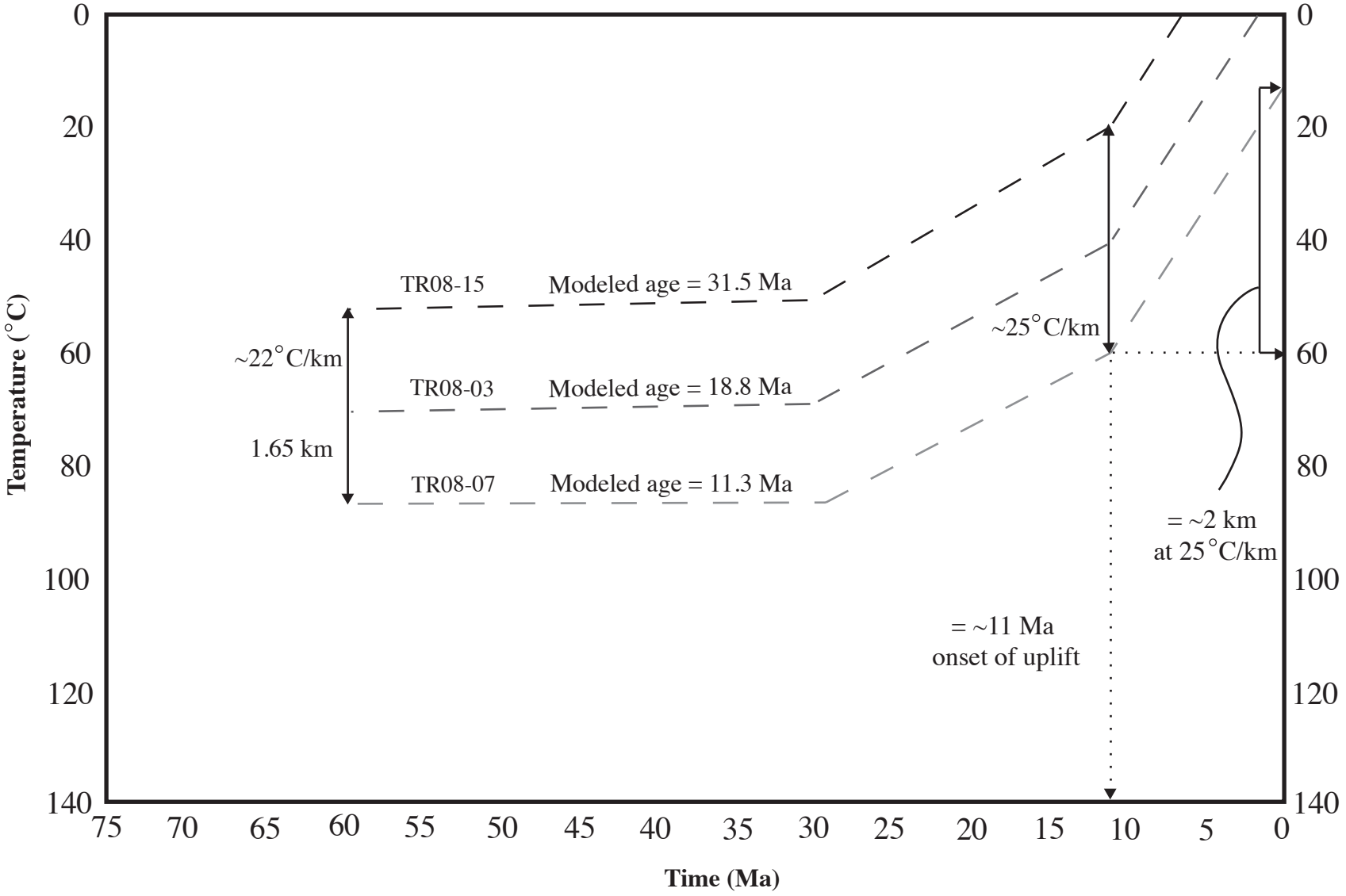

Figure 25. HeFTy modeling results for the Grand Teton transect.

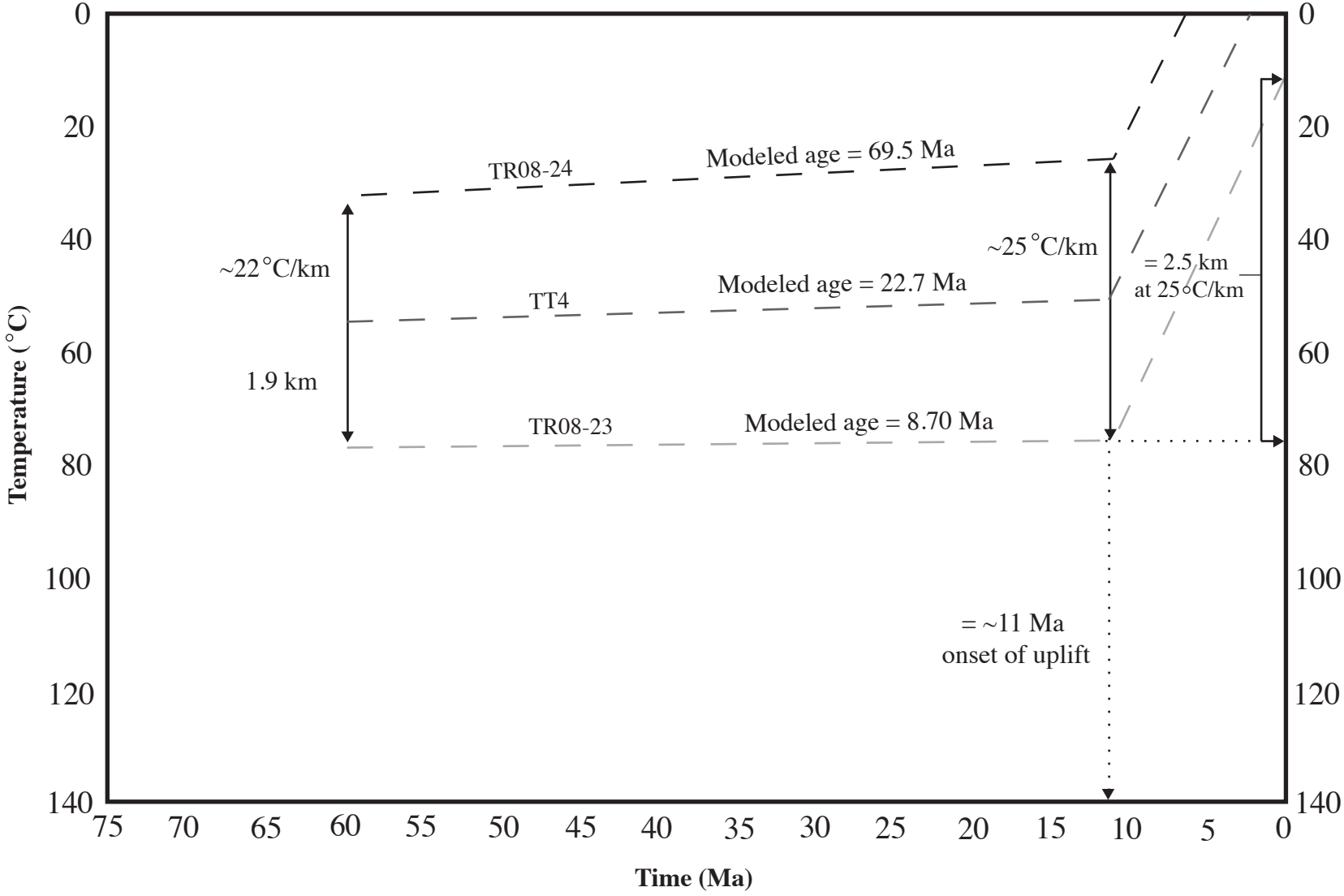

Figure 26. HeFTy modeling results for the Rendezvous Mountain transect.

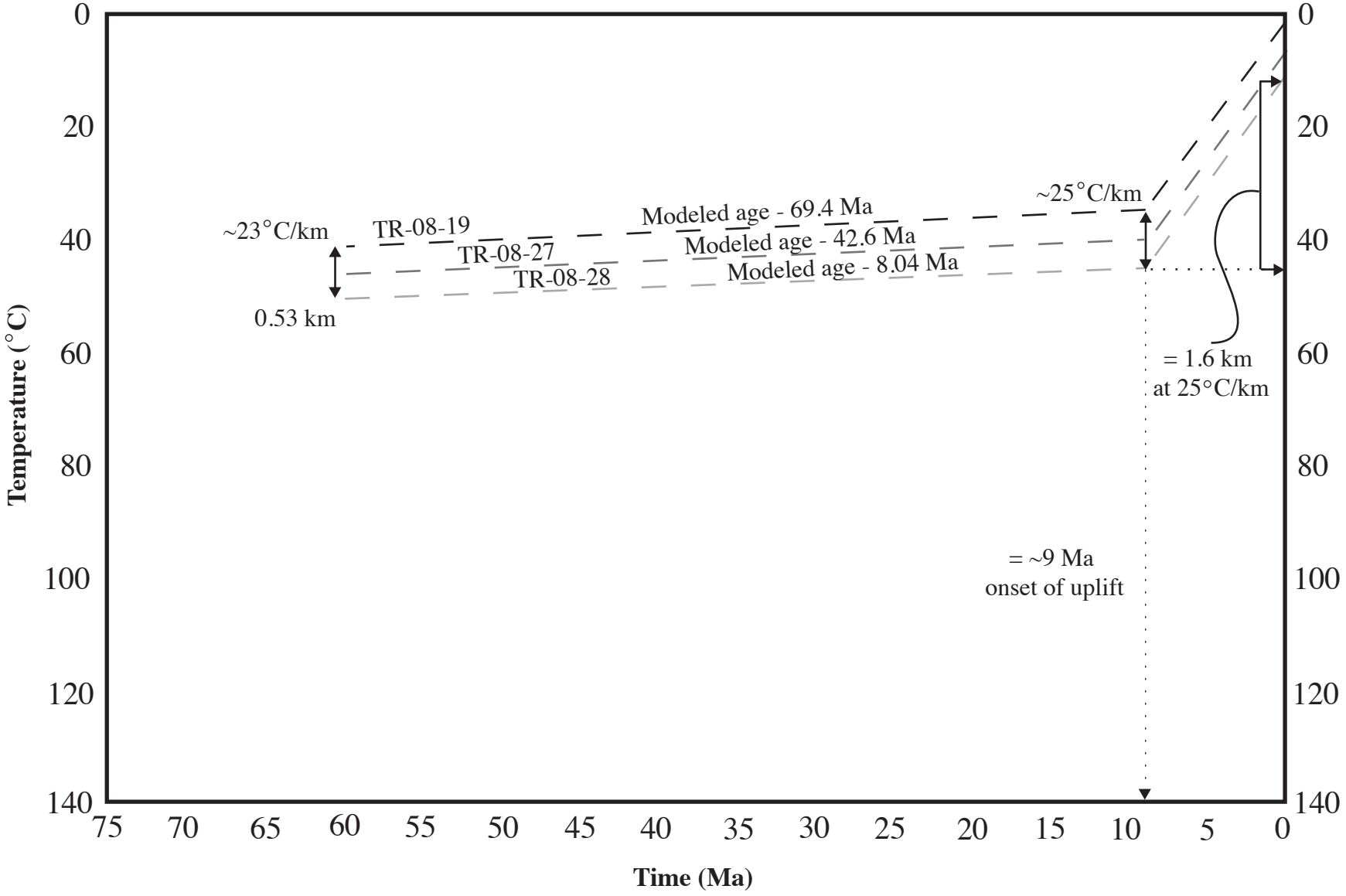

Figure 27. Cross sections in 3DMove.

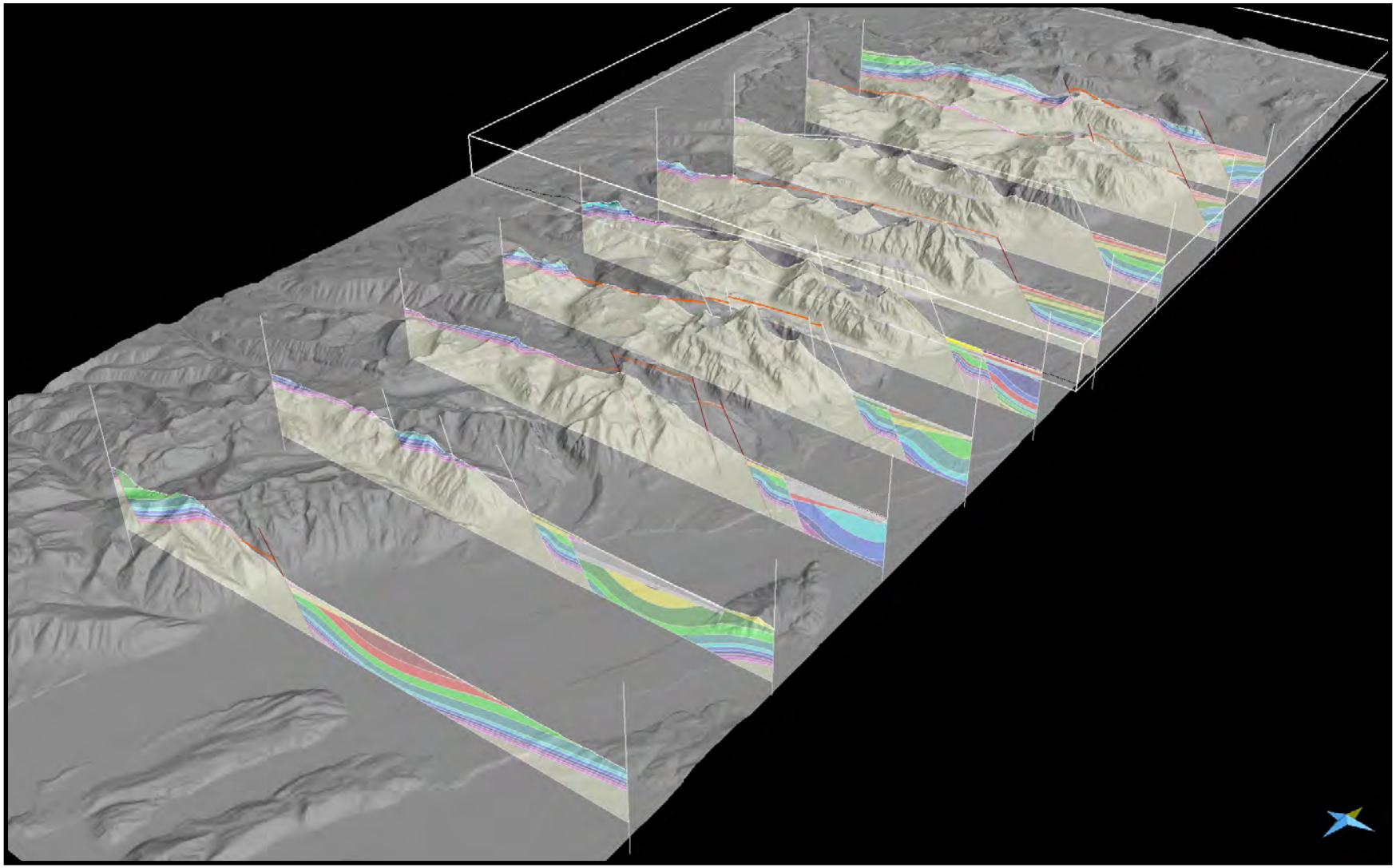

Figure 28. Domed character of the unconformity in 3DMove.

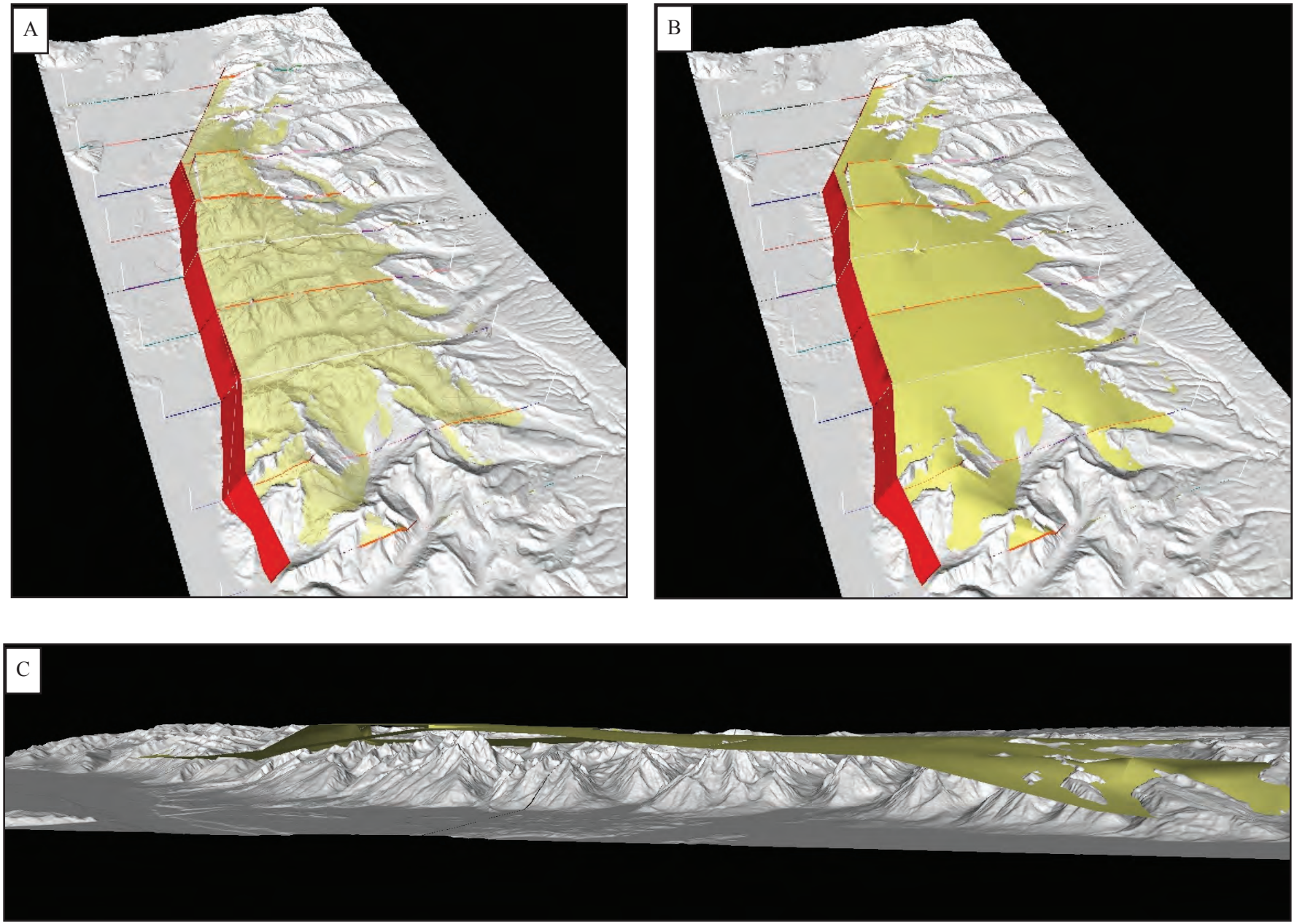

Figure 29. Structure contour map of the Precambrian-Paleozoic unconformity.

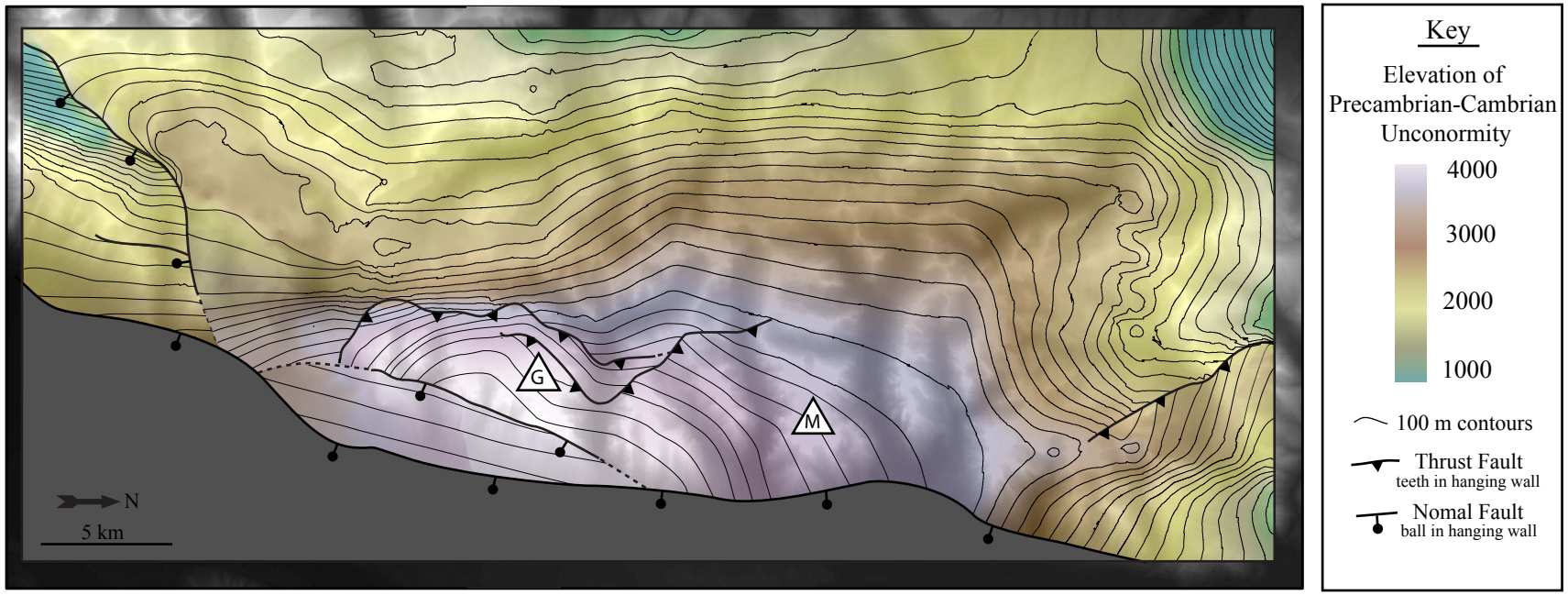

5. DISCUSSION

5.1 The Teton Fault

Low elevation AHe ages average 8.5 ± 1.9 Ma and although some variation is expected from sampling elevation, ages are reasonably consistent along strike. However, the age of the next highest sample in each transect varies, with the rate of age increase being most rapid at Rendezvous Mountain, and slowest at Mount Moran. Thus, the age consistency is unique to the low-elevation samples, most likely indicating that they define a minimum estimate for the onset of fault related uplift in the Tetons. A range of late fault onsets was modeled using HeFTy (5-8 Ma), however, was unsuccessful at producing the young low elevation ages. An ~8-11 Ma onset of uplift is comparable to early estimates of Teton fault initiation (Love and Reed, 1971; Barnosky, 1984) based on angular unconformities and the stratigraphic offsets between the Colter and Teewinot Formations and the Conant Creek Tuff. Recent estimates focus on uplift of the Teton Range in terms of when it became topographically significant (e.g. impeding deposition of the Kilgore Tuff; Morgan and McIntosh, 2005). It is possible that early Teton faulting did not produce significant topographic relief, and many have suggested that although the Teton fault initiated between ~8 to 12 Ma, that the majority of displacement occurred within the past 2 Myr (e.g. Byrd et al., 1994).

The pattern of faults radiating from the Yellowstone hotspot track suggests extension related to encroachment of the plume, leading some to propose that uplift of the Teton Range was a product of Yellowstone influence (e.g Pierce and Morgan, 2009). However, available evidence supports active extension in the Teton-Yellowstone region well before arrival of the Yellowstone hotspot. Chemical analyses of the tuff deposits in Jackson Hole suggest a transition from a compressional to an extensional regime between 18 and 13 Ma (Barnosky, 1984, 1986; Barnosky and Labar, 1989). Additionally, seismic velocity models indicate that the Teton fault might extend beneath the southern portion of the Yellowstone caldera, possibly as a remnant Basin and Range-type zone of weakness (Smith and Arabasz, 1991; White et al., 2009). At ~9 Ma the eruptive center of the Yellowstone hotspot was approximately 250 km from the present site of the Teton Range, too distal to directly influence extension in northwestern Wyoming (Pierce and Morgan, 1992). Thus, the ~9-11 Ma calculated initiation of the Teton fault is probably a reflection of typical late Cenozoic Basin and Range-type extension.

Two methods were used to determine the rate of uplift since the onset of faulting.

Extrapolation of the data to the expected zero age produced a rate of 0.27 mm/yr at Mount Moran, 0.22 mm/yr at the Grand Teton, and 0.24 mm/yr at Rendezvous Mountain. This method assumes that onset occurred exactly at the age of the lowest sample, although it could technically have occurred before then (but after the next highest, significantly older sample in each transect). The second method of obtaining uplift rates was through modeling using HeFTy (Ketcham, 2005). The models produced similar results, and all three transects suggest exhumation rates of ~0.2 mm/yr after the onset of faulting. It is important to note that these rates only account for exhumation of the footwall, and thus are an underestimation of slip rate for the entire Teton fault system. As the current estimates of slip rate across the Teton fault are 0.5-1.2 mm/yr (Love, 1977; Smith et al., 1993a; White et al., 2009) this suggests that the majority of slip is probably accommodated by hanging wall subsidence. Normal fault models indicate that the theoretical ratio of hanging wall subsidence to footwall uplift is about 4:1 (King et al, 1988; King and Ellis, 1990; Ellis and King, 1991). However, based on the gravity modeling results of Byrd et al. (1994), this ratio is probably closer to 3:1 for the Teton fault. This indicates ~2 km of footwall rock uplift (suggested by the extrapolation and HeFTy modeling) and ~6 km of hanging wall subsidence.

5.2 Differential Uplift

Samples within the Mount Moran transect exhibit significantly younger ages overall than those from the southern transects. Although this is in agreement with the differential uplift suggested by Roberts and Burbank (1993) it is important to reiterate that very small deviations of temperature within the HePRZ zone can lead to apparently large variation in ages. The results of the HeFTy modeling show that all three transects resided within the HePRZ for an extended period of time. Because the Mount Moran samples were slightly deeper before rapid Neogene uplift, the kinematics of He diffusion produced significantly younger ages. Additionally, HeFTy models suggest that the Mount Moran transect experienced an early cooling event at ~30 Ma, bringing the northern samples to a similar temperature as the Rendezvous and Grand Teton samples by ~11 Ma.

The decrease in ages northward is consistent in both the AHe and AFT datasets, documenting a distinctive cooling history for the northern Tetons. Although overall, the AHe and AFT data imply a similar cooling history, a few samples stray from the expected relationship

and suggest AHe ages that are "too old". It is likely that a combination of U-rich basement (Hendriks and Redfield, 2005; Soderland et al., 2005) and, more importantly, zoning contributed to the inverted age relationship. Tranel et al. (in review) documented that 73% of apatite contained some degree of zoning when extracted from the layered gneisses of the Precambrian. Zonation within apatite results in U and Th rich cores, and thus suggests that He diffusion might not reach the exterior of the grain, negating the need for diffusion corrections. As corrections assuming ejection out of the apatite grain increase the age, this results in a "too old" age. Since the majority of apatite analyzed for AHe originated in layered gneiss, the "too old" age probably extends beyond the few samples analyzed for both AHe and AFT. In the worst case, if 100% of the U and Th resided in the cores, the uncorrected AHe ages would be truly representative of the cooling history. Even if such drastic zoning was present within the Teton samples, the ages would be reduced by no more than ~25%, and thus would not necessarily alter our overall interpretations.

5.3 Old vs. New AFT

The fission track analytical techniques used in this study are the same as those employed by the Roberts and Burbank (1993) study, with some exceptions. In this study, apparent cooling ages represent the analysis of ~20 crystals per sample while the ages of Roberts and Burbank are calculated from as few as 5 crystals per sample. The larger sample size provides a better statistical representation of the actual cooling age. This study uses a different, temperature-controlled etch (5.5M HNO_3 at 21°C for 20 seconds as opposed to 7% HNO_3 at an unknown temperature for 60 seconds), to reveal spontaneous fission tracks. These etch conditions were selected because the annealing models used in HeFTy are calibrated using this etching protocol.

The main difference between the two studies is in the age calculation. Roberts and Burbank (1993) use an absolute approach whereas this study uses a standardized zeta calibration method (e.g., Hurford and Green, 1983; Hurford 1990). The absolute approach requires that a value for the fission decay constant (λ_f) be specified and the thermal neutron fluence (Φ) measured. Determinations of λ_f have a wide range of values from 6.9 x 10^{-17} yr^{-1} to 8.42 x 10-^{17} yr^{-1} with many studies, including Roberts and Burbank (1993), favoring 7.03 x 10^{-17} yr^{-1} (Hurford and Green, 1983). Additionally, an absolute, unique value for the thermal neutron fluence Φ is difficult to obtain. Roberts and Burbank (1993) used Durango apatite (FT standard; 31 Ma) to

verify their calibration of Φ for each sample; but unfortunately, no information is presented about their Φ measurements or the calibrations performed. Furthermore, thermal neutron irradiation was performed in one of the TRIGA reactors at the USGS (Denver, CO) or Oregon State University (Corvallis, OR). The reactor in which each sample was irradiated is not identified. The zeta calibration technique does not require a specification of λ_f nor Φ (Hurford and Green, 1983). Instead, a series of standards are used to establish a calibration factor, ζ or zeta, for a dosimeter glass of known ^{235}U concentration (i.e., ζ_{CN5}). This is the preferred method of calculating apparent cooling ages from data obtained using the external detector method. While the northward younging trend in AFT ages reported by Roberts and Burbank (1993) is still likely meaningful, the ages cannot be accepted in an absolute sense (Hurford and Green, 1983). Because of these variations in analytical techniques, and the advancement of fission track calibration, any conclusions based on the older AFT dataset require further examination.

Overall, the Roberts and Burbank (1993) model implies rapid, large-scale uplift of the Mount Moran section. However, there is no evidence of such uplift in the stratigraphic record, and there are no documented faults proximal to the Mount Moran section that could account for the additional uplift. As the relatively young Mount Moran ages were also observed in the AHe dataset, an alternative explanation is necessary. One reason could be a topographic high in the north that would have kept the present Mount Moran section at a greater depth. A thicker Mesozoic section in the north (following Laramide uplift) could have produced this 'extra' topography. Erosion prior to onset of rapid uplift would then explain the late pulse of cooling documented by the northern section. The other possibility, acknowledged by Roberts and Burbank, involves thermal effects from the Yellowstone magma chamber. They examined the possibility of thermal perturbation in the form of an adjacent intrusion affecting ages by partially annealing the fission tracks. It is more feasible that if Yellowstone affected the Mount Moran section, it was by increasing the geothermal gradient (i.e. a widespread magma source at depth below the Moran section). For example, if the magma chamber were tilted southward beneath the northern Tetons then it would be reflected in the geothermal gradient at Mount Moran. This is supported by the evidence of a volcanic vent located under northern Jackson Lake, which acted as the eruptive center for the Colter Formation (Barnosky, 1984). Thus, it is not possible to rule out thermal anomalies or extra topography as the source of younger ages in the Moran section.

5.4 Doming of the Unconformity

Roberts and Burbank (1993) proposed that doming of the unconformity occurred prior to onset of the Teton fault. This was based on the pattern of AFT ages at different stages throughout the Cretaceous, but many of the constraints applied to their model are non-unique. For example, the lowest sample from the Rendezvous Peak transect was interpreted to remain in the PAZ for a period of time based on the track length distribution; however, it was within error of other samples from Rendezvous Peak, and thus doesn't necessarily confirm that the base of Rendezvous remained within the PAZ. Also, the basal samples at Buck Mountain are minimum estimates, as the track length distributions indicate the samples resided within the PAZ. Therefore, ages from the Rendezvous Peak and Buck Mountain are nearly the same, and could just as easily have attained the difference in elevation as a result of doming in the Neogene.

To further investigate the timing of doming, the AHe data was plotted in the same manner Roberts and Burbank (1993) used to suggest Cretaceous warping of the unconformity. A series of "time slices" were constructed based on the conditions suggested by HeFTy modeling (Figure 30). Slow systematic exhumation was occurring between ~50 and ~30 Ma. This continued for the Rendezvous Mountain and Grand Teton transects until the onset of Teton faulting. However, the Mount Moran transect clearly experienced increased exhumation between ~30 and ~11 Ma, supporting the original hypothesis of Roberts and Burbank (1993). At ~10 Ma the unconformity was ~2 km below its present position and the onset of faulting rapidly increases the rate of rock uplift. The rate of uplift increased slightly during the last 5 Myr, bringing the unconformity and the summit samples to their current elevation. The effect of differential exhumation on the structure of the unconformity is evident. Although the unconformity was slightly warped before ~50 Ma, by ~15 Ma rapid cooling of the Mount Moran section "flattened" any preexisting north-south curvature. This implies that any of the doming present today is purely a result of displacement on the Teton fault. Thus, early warping most likely occurred during the Laramide, either a product of Gros-Ventre uplift or offset across the Buck Mountain Fault Zone. Models suggest that at ~50 Ma the top of the unconformity near the Grand Teton was ~1 km shallower than the depth of the unconformity at Rendezvous and Mount Moran. The exact offset of the Buck Mountain reverse fault is unclear, as it is only exposed within Precambrian rocks. However, estimates suggest that it is at least ~1 km (Smith, 1991). It

is possible that early deformation of the unconformity was associated with displacement across the Buck Mountain Fault Zone.

5.5 Implications for Normal Faulting

Densmore et al. (2004) proposed that a direct and consistent relationship exists for Basin and Range faults proximal to the Snake River Plain. The Teton Range was compared to 10 faults using an average throw of 3.5 km and a fault length of 100 km (from Byrd et al., 1994). Since the present day doming is a result of Teton fault displacement, the structure of the unconformity can be used as a proxy to the Teton fault. By comparing the restored footwall unconformity with the estimated depth to the unconformity in the hanging wall (Byrd et al., 1994), an average throw of 3.3 km was calculated across the Teton fault (Figure 31). Moreover, by extrapolating the unconformity in both the hanging wall and footwall, we calculated a fault length of ~100 km. This results in displacement to length ratio of 0.033 (Figure 32A), and is in agreement with values proposed by both Schlische et al. (1996) and Densmore et al. (2004). The relationship between maximum displacement and length of the Teton fault also coincides well with distributions modeled by Schultz and Fossen (2002) (Figure 32B). Other than scaling, it is difficult to make any regional scale interpretations regarding normal fault behavior on the basis of the Teton fault. For example, although HeFTy indicates a slightly earlier onset of uplift in the central and northern Tetons, this does not necessarily confirm that the Teton fault was shorter at 11 Ma than at 9 Ma, as suggested by the models of Walsh and Watterson (1988) and Cowie and Scholz (1992). Alternatively, the Teton fault could have initiated as a continuous zone of Basin and Range-type weakness (Walsh et al., 2002). Subsequent displacement across the fault would be more prominent at the center of the fault, producing the appearance of early onset near the Grand Teton section. The surface expression of the Teton fault is extremely segmented, and lacks any evidence for displacement deficits between segments. The smooth doming of the unconformity also suggests that the segments are behaving as one large structure, indicating that they have been linked for some time.

5.6 Bedrock Erosion

Reconstruction of the unconformity and calculation of eroded rock volume produced ~276 cubic kilometers. This is a reasonable estimate when compared to ~35 cubic kilometers

calculated for the area surrounding Mount Moran (Brown et al., 2008). Utilizing the area beneath the unconformity (~471 sq. km), this produced a spatially averaged depth to incision of 0.3 km. By adding the eroded Phanerozoic section we calculated a spatially averaged erosion rate of 0.18 mm/yr for 10 Myr. This is significantly higher than estimates of 0.02 to 0.05 mm/yr based on ^{10}Be and ^{26}Al surface exposure dating for both the Teton Range and Wind River Range (Small et al., 1997; Tranel et al., in review). However, our estimate is comparable to recent work documenting catchment averaged erosion rates of 0.16 to 0.27 mm/yr (Tranel et al., in review). While 0.18 mm/yr is an acceptable long-term estimate, the Teton Range is most likely best characterized by periods of increased erosion by glacial activity. Glacial erosion rates often exceed 1 mm/yr and can be as rapid as 30 mm/yr (Gardner and Jones, 1993; Hallet et al., 1996). When including possible erosion from river incision (5-10 mm/yr; Burbank et al, 1996) and bedrock landsliding (Hovius et al., 1997), it is clear that erosion from bare bedrock weathering (.05-0.20 mm/yr; Small et al., 1997; Bierman, 1994) is insufficient to erode the 276 cubic kilometers of rock missing from the Teton summits. Tranel et al. (in review) also measured talus volume, suggesting rates of 0.5 to 0.8 mm/yr since 13.5 ka. This, combined with our estimates and those of Foster et al. (2008, 2010), reaffirm the large role glaciers have played in shaping the Teton landscape.

Figure Captions

Figure 30: The uplift history of the Teton Range as derived from HeFTy models. At ~50 Ma, all three transects reside somewhat within the HePRZ with preexisting Laramide doming. From ~50 Ma to ~30 Ma, slow steady uplift occurs of all transects. Between ~30 and 11 Ma, differential cooling occurs, with faster exhumation of the northern Tetons. The rapid cooling of the Mount Moran section "flattens" any preexisting north-south doming. The Teton fault becomes active at ~11 Ma, resulting in rapid uplift of all three sections, and doming the unconformity.

Figure 31: Faulted unconformity reconstruction in the hanging wall and footwall. Reconstructed elevations of the unconformity along the Teton fault in the footwall (this study) are plotted with hanging wall subsurface unconformity depths from Byrd et al. (1994).

Figure 32: Comparison of Teton fault scaling to other normal faults. The Teton fault compares well to typical fault scaling distributions. A) Plot of average displacement versus length from Schlische et al. (1996) with the addition of data from the Teton fault (this study). The Teton fault plots on the regression line indicating a scaling ratio of 0.03. B) Plot of maximum displacement versus length from Schultz and Fossen (2002) with the addition of data from the Teton fault (this study).

Figure 30. The uplift history of the Teton Range as derived from HeFTy models.

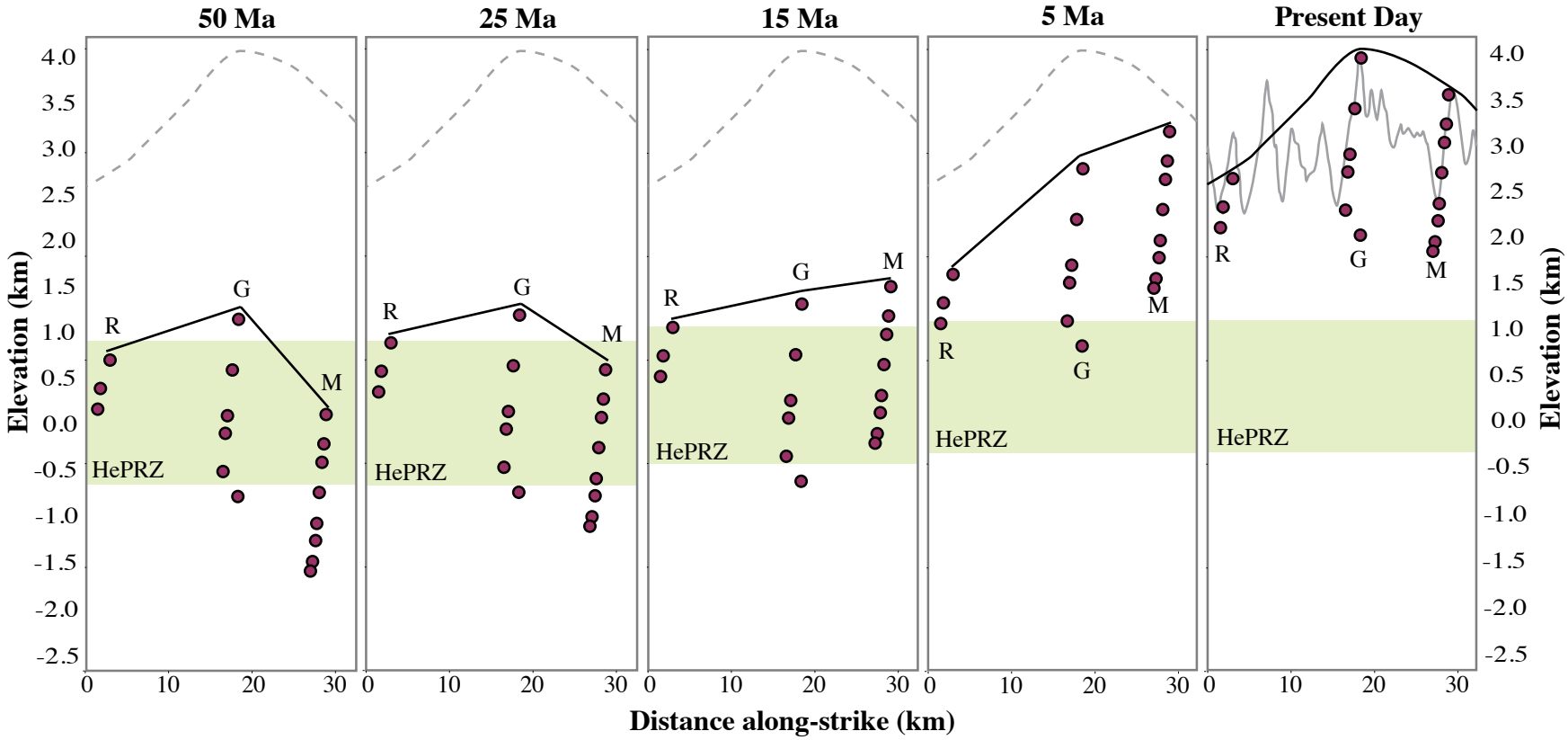

Figure 31. Faulted unconformity reconstruction in the hanging wall and footwall.

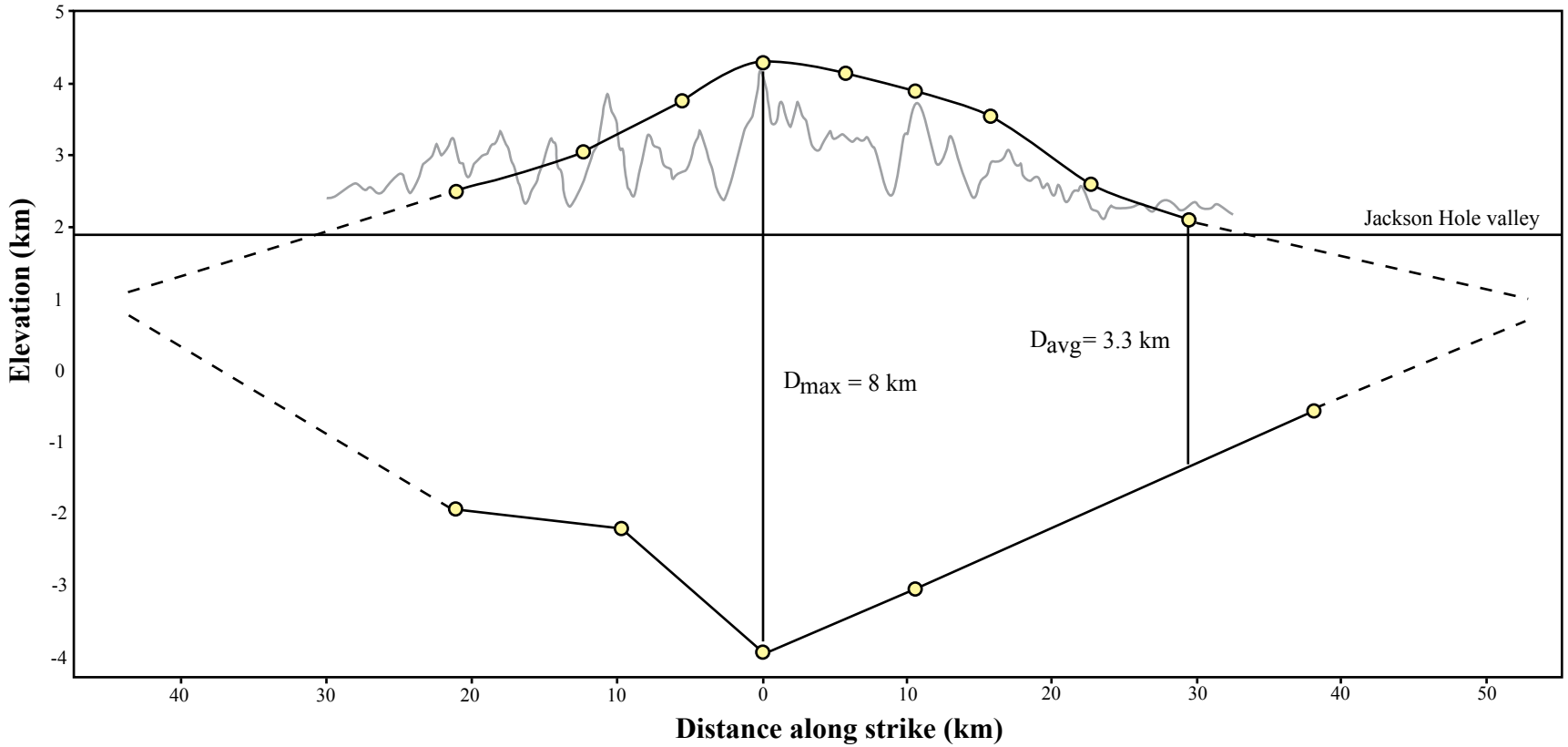

Figure 32. Comparison of Teton fault scaling to other normal faults.

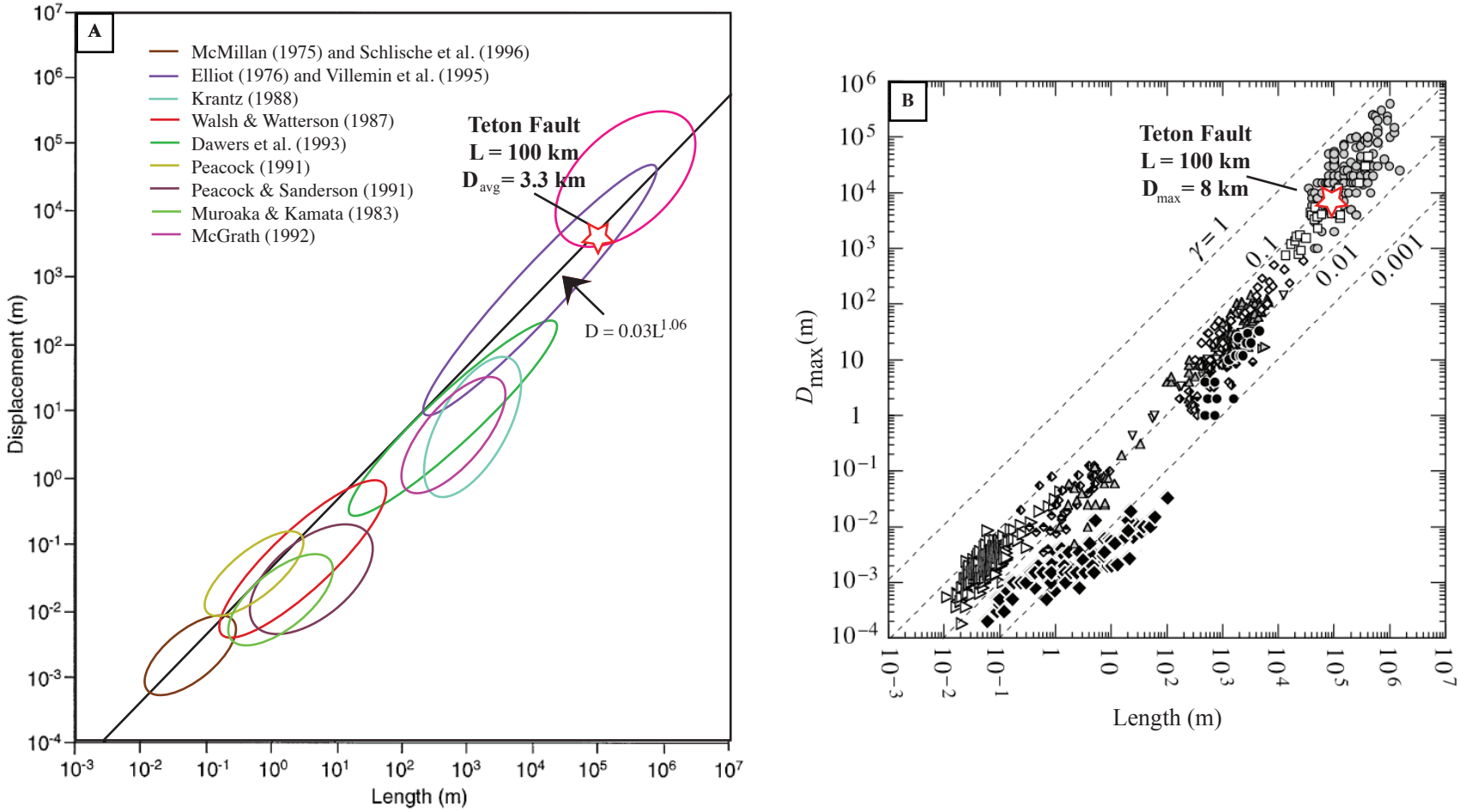

6. CONCLUSIONS

Young (~9 Ma) AHe cooling ages parallel the trace of the Teton fault and are interpreted as the minimum onset of Teton fault related uplift in the Teton Range. This is supported by the modeled histories from HeFTy, which suggest an onset of rapid uplift between 9 and 11 Ma. The Teton fault originated as a Basin and Range-type structure, but increased extension has occurred since the arrival of the Yellowstone hotspot. Model results also indicate an average of ~2 km of footwall exhumation. Taking into account the ~6 km of hanging wall subsidence indicated by previous work, this suggests a maximum throw of ~8 km near the Grand Teton. The average throw for the Teton fault is 3.3 km, and structural examination indicates a fault length of ~100 km. Thus, the Teton fault is comparable to models representing fault scaling in terms of both average and maximum displacement.

Inversion of the typical AHe-AFT relationship in a few of the Teton Range samples is a result of intense zoning, primarily in layered gneiss lithologies. Future work with samples from the Teton Range should pursue element mapping of U and Th concentrations across apatite grains to determine the appropriate amount of diffusion correction. Regardless, both the AHe and AFT ages consistently indicate differential uplift of the Tetons. Relatively rapid cooling of the Mount Moran section occurred between ~30 and 10 Ma, and is not apparent in the southern sections. As the Teton fault was not yet active, the increased exhumation could be explained by: (1) increased erosion of the northern section or (2) a higher geothermal gradient related to magmatic activity adjacent to the northern Teton Range. Both of these are plausible, although detailed examination of the Mount Moran ages and additional sampling north of the section line would be necessary to determine the cause. While a domed unconformity is evident prior to ~50 Ma, rapid cooling of the Mount Moran section resulted in a north-south flattening of this extensive horizon. Thus, displacement across the Teton fault, particularly in the central Tetons, produced the present domed shape of the uniformity.

Calculations of a long-term erosion rate based on the eroded volume of sediment from the Teton Range produced 0.18 mm/yr since 10 Ma, comparable to recent field-based estimates. This is less than the long-term footwall uplift of ~0.22 mm/yr since 10 Ma, thus providing a quantitative explanation for the modern Teton topography.

References Cited

Anders, M.H., Geissman, J.W., Piety, L.A., and Sullivan, J.T., 1989, Parabolic distribution of circumeastern Snake River Plain seismicity and latest Quaternary faulting: Migratory pattern and association with the Yellowstone hotspot: Journal of Geophysical Research, v.94, p. 1589-1621.

Anders, M.H. and Sleep, N.H., 1992, Magmatism and extension: the thermal and mechanical effects of the Yellowstone hotspot: Journal of Geophysical Research v. 97 (B11), p. 15379-15393.

Armstrong, P.A., Ehlers, T.A., Chapman, D.S., Farley, K.A., and Kamp, P.J.J., 2003, Exhumation of the central Wasatch Mountains, Utah: 1. Patterns and timing deduced from low-temperature thermochronology data: Journal of Geophysical Research, v. 108, doi:10.1029/2001JB001708.

Barnosky, Anthony D. 1984. The colter formation; evidence for miocene volcanism in Jackson Hole, Teton County, Wyoming. Earth Science Bulletin, v. 17, p. 49-97.

Barnosky, A.D. 1986, Arikareean, Hemingfordian, and Barstovian mammals from the Miocene Colter Formation, Jackson Hole, Teton County, Wyoming: Bulletin of Carnegie Museum Natural History, no. 26, p. 69.

Barnosky, A.D. and Labar, W.J., 1989, Mid-Miocene (Barstovian) environmental and tectonic setting near Yellowstone Park, Wyoming and Montana: Geological Society of America Bulletin, v. 101, p. 1448-1456.

Behrendt, J.C., Tibbets, B.L., Bonini, W.E., Lavin, P.M., Love, J.D., and Reed, J.C. Jr., 1968, A geophysical study in Grand Teton National Park and vicinity, Teton County, Wyoming, with sections on stratigraphy and structure and Precambrian rocks: U.S. Geol. Surv. Prof. Pap. 516-E.

Berger, A.L., Spotila, J.A., Chapman, J.B., Pavlis, T.L., Enkelmann, E., Ruppert, N.A., and Buscher, J.T., 2008, Architecture, kinematics, and exhumation of a convergent orogenic wedge: A thermochronological investigation of tectonic-climatic interactions within the central St. Elias orogen, Alaska: Earth and Planetary Science Letters, v. 270, p. 13-24.

Berger, A.L. and Spotila, J.A., 2008, Denudation and deformation in a glaciated orogenic wedge: Geology, v. 36, p.523-526, doi: 10.1130/G24883A.1.

Bierman, P.R., 1994, Using in-situ produced cosmogenic isotopes to estimate rates of landscape evolution: A review from the geomorphic perspective: Journal of Geophysical Research, v.99, p. 13,885-13,896.

Brown, S.J., Spotila, J., Thigpen, J.R., and Tranel, L.M., 2008, Refining the temporal and spatial evolution of the Teton Range, Wyoming, from integrated apatite (U-Th)/He and structural analyses: Abstracts with Programs- Geological Society of America: Houston, TX, United States, p. 148-149.

Brozovic, N., Burbank, D.W., and Meigs, A.J., 1997, Climatic Limits on Landscape Development in the Northwestern Himalaya: Science, v. 276, p. 571-574.

Burbank, D.W., Leland, J., Fielding, E., Anderson, R.S., Brozovic, N., Reid, M.R., and Duncan, C., 1996, Bedrock incision, rock uplift and threshold hillslopes in the northwestern Himalayas: Nature, v. 379, p. 505-510.

Byrd, J.O.D., 1995, Neotectonics of the Teton Fault, Wyoming: Salt Lake City, UT, University of Utah.

Byrd, J.O.D., Smith, R.B., and Geissman, J.W., 1994, The Teton fault, Wyoming: Topographic signature, neotectonics, and mechanisms of deformation: Journal of Geophysical Research, v. 99, no. B10, p. 20,095–20,122.

Cartwright, J.A., Trudgill, B.D., Mansfield, C.S., 1995, Fault growth by segment linkage: an explanation for scatter in maximum displacement and trace length data from the Canyonlands Grabens of SE Utah: Journal of Structural Geology, v. 17, p.1319-1326.

Cartwright, J.A., Mansfield, C., Trudgill, B., 1996, The growth of faults by segment linkage. In: *Modern Developments in Structural Interpretation, Validation and Modelling* (Ed. By P.G. Buchanan and D.A. Nieuwland): Spec. Publ. Geol. Soc. Lond., v. 99, p. 163-177.

Childs, D., Watterson, J., and Walsh, J.J., 1995, Fault overlap zones within developing normal fault systems. J. Geol. Soc. Lond., v. 152, p. 535-549.

Childs, C., Watterson, J., Walsh, J.J., 1996b, A model for the structure and development of fault zones. Journal of the Geological Society of London, v. 153, p .337-340.

Cowie, P.A. and Sholz, C.H., 1992, Displacement-length scaling relationship for faults: Data synthesis and discussion: Journal of Structural Geology, v.14, p. 1149-1156.

Dawers, N.H. and Anders, M.H., 1995, Displacement-length scaling and fault linkage: Journal of Structural Geology, v.17, p. 607-614.

Dawers, N.H., Anders, M.H., and Scholz, C.H., 1993, Growth of normal faults: Displacement-length scaling: Geology, v. 21, p. 1107-1110.

Densmore, A.L., Dawers, N.H., Gupta, S. Guidon, R., and Goldin, T., 2004, Footwall topographic development during continental extension: Journal of Geophysical Research, v.109, doi: 10.1029/2003JF000115.

Densmore, A.L., Dawers, N.H., Gupta, S., Guidon, R., 2005, What sets topographic relief in extensional footwalls?: Geological Society of America, Geology, v.33, p. 453-456.

Dodson, M.H., 1973, Closure temperatures in cooling geological and petrological systems: Contributions in Mineralogy and Petrology, v. 40, p. 259-274.

Donelick, R. A., Ketcham, R. A., and Carlson, W. D., 1999, Variability of apatite fission-track annealing kinetics: II. Crystallographic orientation effects: American Mineralogist, v. 84, no. 9, p. 1224-1234.

Doser, D.I. and Smith, R.B., 1983, Siesmicity of the Teton-Southern Yellowstone region, Wyoming: Bull. Seismol. Soc. Am.,v. 73, p. 1369-1394.

Ehlers, T.A., Armstrong, P.A., Chapman, D.S., 2001, Normal fault thermal regimes and the interpretation of low-temperature thermochronometers: Physics of the Earth and Planetary Interiors, v. 126, p.179-194.

Ehlers, T.A., Willett, S.D., Armstrong, P.A., and Chapman, D.S., 2003, Exhumation of the central Wasatch Mountains, Utah: 2. Thermokinematic model of exhumation, erosion, and thermochronometer interpretation: Journal of Geophysical Research, v. 108, no. B3, p. 2173.

Ehlers, T.A., Chaudri, T., Kumar, S., Fuller, S.W., Willett, S.D., Ketcham, R.A., Brandon, M.T., Belton, D.X., Kohn, B.P., Gleadow, A.J.W., Dunai, T.J., and Fu, F.Q., 2005, Computational tools for low-temperature thermochronometer interpretation: Rev Mineral Geochem, v. 58, p.589-.

Ehlers, T.A. and Farley, K.A., 2003, Apatite (U-Th)/He thermochronometry: methods and applications to problems in tectonic and surface processes: Earth and Planetary Science Letters, v. 206, p. 1-14.

Ellis, M. and King, G.C.P., 1991, Structural control of flank volcanism in continental rifts: Science, v. 254, p. 839-842.

Farley, K.A., 2000, Helium diffusion from apatite: general behavior as illustrated by Durango fluorapatite: Journal of Geophysical Research, v. 105, p. 2903-2914.

Farley, K.A., 2002, (U-Th)/He dating: techniques, calibrations and applications: Review in Mineralogy and Geochemistry, v. 47, p. 819-844.

Farley, K.A., Rushmore, M.E., and Bogue, S.W., 2001, Post-10 Ma uplift and exhumation of the northern Coast Mountains, British Columbia: Geology, v. 29, p. 99-102.

Farley, K.A. and Stockli, D.F., 2002, (U-Th)/He dating of phosphates; apatite, monazite, and xenotime, *in* Kohn, M.J.R., John; Hughes, John M, ed., Reviews in Mineralogy and Geochemistry, Volume 48: Washington, DC, Mineralogical Society of America and Geochemical Society, p. 559-577.

Fitzgerald, P.G., Fryxell, J.E., Wernicke, B.P., 1991, Miocene crustal extension and uplift in southeastern Nevada: Constraints from fission track analysis: Geology, v. 19, p. 1013- 1016.

Foster, D., Brocklehurst, S.H., and Gawthorpe, R.L., 2008, Small valley glaciers and the effectiveness of the glacial buzzsaw in the northern Basin and Range, USA: Geomorphology, v. 102, p.624-639.

Foster, D., Brocklehurst, S.H., and Gawthorpe, R.L., 2010, Glacial-topographic interactions in the Teton Range, Wyoming: J. Geophys. Res., v. 115, p. F01007.

Galbraith, R. F., and Laslett, G. M., 1993, Statistical-Models for Mixed Fission-Track Ages: Nuclear Tracks and Radiation Measurements, v. 21, no. 4, p. 459-470.

Gardner, J.S., and Jones, N.K., 1993, Sediment transport and yield at the Raikot glacier, Nanga Parbat, Punjab Himalaya, *in* Shroder, J.F., ed., Himalaya to the sea: London, Routledge, p. 184–197.

Gilbert, J.D., Ostenaa, D., and Wood, C., 1983, Seismotectonic study Jackson Lake Dam and Reservoir, Minidoka Project, Idaho-Wyoming: Seismotectonic Rep., v. 83-8, U.S. Bur. Of Reclam., Boise, Idaho, p.123.

Gillespie, P.A., Walsh, J.J., and Watterson, J., 1992, Limitations of dimension and displacement data from single faults and the consequences for data analysis and interpretation: J. Struct. Geol., v. 14, p. 1157-1172.

Gleadow, A.J.W., Duddy, I.R., Green, P.F., and Lovering, J.F., 1986, Confined fission track lengths in apatite: A diagnostic tool for thermal analysis: Contributions to Mineralogy and Petralogy, v. 94, p. 405–415.

Gleadow, A.J.W. and Duddy, I.R., 1981, A natural long-term track annealing experiment for apatite: Nucl Tracks ,v. 5, p. 169-174.

Green, P.F., Duddly, I.R., Gleadow, A.J.W., Tingate, P.R., Laslett, G.M., 1986, Thermal annealing of fission tracks in apatite. 1. A qualitive description: Chem. Geol., v. 59, p. 237-253.

Green, P.F., and Duddy, I.R., 2006, Interpretation of apatite (U-Th)/He ages and fission track ages from craton: Earth Planet. Sci. Lett., v. 244 (3-4), p. 541-547.

Hallet, B., Hunter, L. and Bogen, J., 1996, Rates of erosion and sediment evacuation by glaciers: A review of field data and their implications: Global and Planetary Change, v. 12, p. 213-235.

Hampel, A., Hetzel, R., and Densmore, A.L., 2007, Postglacial slip-rate increase on the Teton normal fault, northern Basin and Range Province, caused by melting of the Yellowstone ice cap and deglaciation of the Teton Range?: Geology, v. 35, no. 12, p. 1107.

Hauessler, P.J., O'Sullivan, P., Berger, A.L., and Spotila, J.A., 2008, Neogene exhumation of the Tordrillo Mountains, Alaska, and correlations with Denali (Mount McKinley), *in* Freymueller, J.T., Haeussler, P.J., Wesson, R.L., and Ekstrom, G., eds., Active tectonics and seismic potential of Alaska, Volume 179: Washington, DC, American Geophysical Union, p. 269-285.

Hendriks, B., and Redfield, T., 2005, Apatite fission track and (U-Th)/He data from Fennoscandia: an example of underestimation of fission track annealing in apatite. Earth Planet. Sci. Lett., v. 236, p. 443-458.

Hovius, N., Stark, C.P., and Allen, P.A., 1997, Sediment flux from a mountain belt derived by landslide mapping: Geology, v. 25, p. 231-234.

Hurford, A. J., and Green, P. F., 1983, The Zeta-Age Calibration of Fission-Track Dating: Isotope Geoscience, v. 1, no. 4, p. 285-317.

Ketcham, R. A., Donelick, R. A., and Carlson, W. D., 1999, Variability of apatite fission-track annealing kinetics: III. Extrapolation to geological time scales: American Mineralogist, v. 84, no. 9, p. 1235-1255.

Ketcham, R.A., Donelick, R.A., Carlson, W.D., 1999, Variability of apatite fission-track annealing kinetics III: Extrapolition to geological time scales: Am Mineral, v. 84, p. 1235-1255.

Ketcham, R.A., Donelick, R.A., Donelick, M.B., 2000, AFTSolve: A program for multi-kinetic modeling of apatite fission-track data: Geol Mat Res 2: (electronic).

Ketcham, R.A., 2005, Forward and Inverse Modeling of Low-Temperature Thermochronometry Data: Reviews in Mineralogy and Geochemistry, v. 58, p. 275-314.

King, G.C.P., Stein, R.S., Rundle, J.B., 1988, The growth of geological structures by repeated earthquakes: 1. Conceptual framework: J. Geophys. Res., v. 93(B11), p.13,307- 13,318, doi:10.1029/JB093iB11pl3307.

King, G.C.P., and Ellis, M., 1990, The origin of large local uplift in extensional regions: Nature, v. 348, p. 689-693.

Lageson, D.R., 1992, Possible Laramide influence on the Teton normal, western Wyoming, in Regional Geology of Eastern Idaho and Western Wyoming, edited by P.K. Link, M.A. Kuntz, and L.B. Platt: Mem. Geol. Soc. Am., v. 179, p. 183-195.

Lageson, D.R., Adams, D.C., Morgan, L.A., Pierce, K.L., and Smith, R.B., 1999, Neogene-Quaternary Tectonics and Volcanism of southern Jackson Hole, Wyoming and southeastern Idaho, *in* Hughes, S.S., Thackray, G.D., eds., Guidebook to the Geology of Eastern Idaho: Pocatello, Idaho Museum of Natural History, p. 115-130.

Lanphere, M.A., Champion, D.E., Christiansen, R.L., Obradovich, J.D., 2002, Revised ages for tuffs of the Yellowstone Plateau volcanic field; assignment of the Huckleberry Ridge Tuff to a new geomagnetic polarity event: Geological Society of America Bulletin, v. 114, p. 559-568.

Laslett, G.M., Gleadow, A.J.W., and Duddy, I.R., 1984, The relationship between fission-track length and density in apatite: Nucl. Tracks, v. 9, p. 29 – 38.

Lavin, P.M., 1957, Detailed gravity measurements in the Jackson Hole-Teton Mountains areas of northwestern Wyoming, B.S.E. thesis, Princeton, Univ. Princeton, N.J. p. 46.

Leopold, E.B., Liu, G., Love, J.D., Love, D.W., 2007, Plio-Pleistocene climatic transition and the lifting of the Teton Range, Wyoming: Quaternary Research, v. 67, p. 1-11.

Licciardi, J.M., Pierce, K.L., Kurz, M.D., Finkel, R.C., 2005, Refined chronologies of Yellowstone ice cap and Teton Range outlet glacier fluctuations during the late Pleistocene: Abstracts with Programs- Geological Society of America, v. 37, no.7, p. 41.

Love, J.D., 1977, Summary of upper Cretaceous and Cenozoic stratigraphy, and of tectonic and glacial events in Jackson Hole, northwest Wyoming: Wyoming Geological Association Guidebook, 29th Annual Field Conference, p. 585-593.

Love, J.D., 1997, Summary of the Upper Cretaceous and Cenozoic stratigraphy, and of tectonic and glacial events in Jackson Hole, northwest Wyoming *in* Heisey, E.L., et al., eds., Rocky Mountain Thrust Belt: Geology and Resources: Wyoming Geological Association Guidebook, 29th Annual Field Conference, p. 585-593.

Love, J.D., Christiansen, R.L., and Stacey, J.R., 1973, Geologic block diagram and tectonic history of the Teton region: U.S. Geological Survey Map I-370: Moose, Wyoming, Grand Teton National History Association.

Love, J.D., Reed, J.C., Jr., and Christiansen, A.C., 1992, Geological map of Grand Teton National Park, Teton County, Wyoming, *in* USGS, ed., Volume I-2031: Reston, VA, U.S. Geological Survey.

Love, J.D., Morgan, L.A., McIntosh, W.C., 1997, The Teewinot Formation: evidence for late Miocene basin formation in response to volcanism, faulting and uplift associated with Yellowstone hot spot?: Geological Society of America, Abstracts with Programs, v. 29 (6), A365.

Love, J.D., Reed, J.C., and Pierce, K.L., 2003, Creation of the teton landscape; a geologic chronicle of Jackson hole and the teton range: Grand Teton Natural History Association, Moose, Wyoming, USA. 2nd ed.

Love, J.D. and Albee, H.F., 1972, Geologic map of the Jackson Quadrangle, Teton County, Wyoming, scale 1:24,000: U.S. Geol. Surv. Map I-769A.

Love, J.D. and Reed, J.C., 1971, Creation of the Teton landscape: Moose, Wyoming, Grand Teton Natural History Association, p.120.

McDougall, I. and Harrison, T.M., 1999, Geochronology and thermochronology by the $^{40}Ar/^{39}Ar$ method. Oxford University Press, New York.

Machette, M.N., Pierce, K.L., McCalpin, J.P., Haller, K.M., and Dart, R.L., 2001, Map and data for Quaternary faults and folds in Wyoming: U.S. Geological Survey, p. 158.

Mitchell, S.G., and Montgomery, D.R., 2006, Influence of a glacial buzzsaw on the height and morphology of the Cascade Range in central Washington State, USA: Quaternary Research, v. 65, p.96-107.

Morgan, L.A. and McIntosh, W.C., 2005, Timing and development of the Heise volcanic field, Snake River Plain, Idaho, western USA: GSA Bulletin, v.117, no.3/4, p.288-306.

Morley, C.K., Nelson, R.A., Patton, T.L., and Munn, S.G., 1990, Transfer zones in the East African rift system and their relevance to hydrocarbon exploration in rifts: Bull. Am. Ass. Petrol. Geol., v. 74, p. 1234-1253.

Naeser, C.W., 1976, Fission-track dating: U.S. Geol. Surv. Open File Rep., 76-0190, p. 1-65.

Nash, D.B. and Beaujon, J.S., 2006, Modeling degradation of terrace scarps in Grand Teton National Park, USA: Geomorphology, v. 75, p. 400-407.

Perkins, M.E. and Nash, W.P., 1994, Tephrochronology of the Teewinot Formation, Jackson Hole, Wyoming: Geological Society of America, Abstracts with Programs, v. 26 (6), p. 58-59.

Pierce, K.L. and Morgan, L.A., 1992, The track of the Yellowstone hot spot: Volcanism, faulting and uplift, *in* Link, P.K., Kuntz, M.A., and Platt, L.B., eds., Regional Geology of Eastern Idaho and Western Wyoming: Geological Society of American Memoir, v. 179, p.1-53.

Pierce, K.L., and Morgan, L.A., 2009, Is the track of the Yellowstone Hot Spot driven by a deep mantle plume? Review of volcanism, faulting, and uplift in light of new data: Journal of Volcanology and Geothermal Research, v. 188, no. 1-3, p. 1-25.

Reed, J.C., and Zartman, R.E., 1973, Geochronology of Precambrian Rocks of the Teton Range, Wyoming: Geological Society of America Bulletin, v. 84, p. 561-582.

Reiners, P.W., Brady, R., Farley, K.A. Fryxell, J.E., Wernicke, B., and Lux, Daniel, 2000, Helium and argon thermochronometry of the Gold Butte block, south Virgin Mountains, Nevada: Earth and Planetary Science Letters, v. 178, p. 315-326.

Reiners, P.W., Ehlers, T.A., and Zeitler, P.K., 2005, Past, Present, and Future of Thermochronology, in Reiners, P.W. and Ehlers, T.A. (Eds.), Thermochronology: Reviews in Mineralogy and Geochemistry, v. 58, p. 1-18.

Reiners, P.W., and Farley, K.A., 2001, Influence of crystal size on apatite (U-Th)/He thermochronology: an example from the Bighorn Mountains, Wyoming: Earth and Planetary Science Letters, v. 188, p. 413-420.

Roberts, S.V., and Burbank, D.W., 1993, Uplift and thermal history of the Teton Range (northwestern Wyoming) defined by apatite fission-track dating: Earth and Planetary Science Letters, v. 118, p. 295-309.

Royse, F., Jr., 1983, Extensional faults and folds in the foreland thrust belt, Utah, Wyoming, Idaho: Geol. Soc. Am. Abstr. Programs, v.15, p. 295.

Sales, J.K., 1983, Collapse of Rocky Mountain forland uplifts, in *Rocky Mountain Foreland Basins and Uplifts*, edited by J.D. Lowell, Rocky Mountain Association of Geologists, Denver, Colo., p. 79-97.

Schlische, R.W., Young, S.S., Ackermann, R.V., and Gupta, A., 1996, Geometry and scaling relations of a population of very small rift-related normal faults: Geology, v.24, p. 683-686.

Schultz, R.A. and Fossen, H., 2002, Displacement-length scaling in three dimensions; the importance of aspect ratio and application to deformation bands: Journal of Structural Geology, v. 24, no.9, p. 1389-1411.

Shuey, R.T., Ugland, R.O., Schmidt, C.R., 1977, Magnetic properties and secular variation in cores from Yellowstone and Jackson Lakes, Wyoming: J. Geophys. Res., v. 82, p. 3739-3746.

Small, E.E., Anderson, R.S., Repka, J.L., Finkel, R., 1997, Erosion rates of alpine bedrock summit surfaces deduced from in situ (super 10) Be and (super 26) Al : Earth and Planetary Science Letters, v. 150, no. 3-4, p. 413-425.

Smith, D.J., 1991, Structural Geology and History of the Buck Mountain Fault and Adjacent Intra-Range Faults, Teton Range, Wyoming, Master's thesis, Montana State University, Bozeman, Montana.

Smith, R.B., Shuey, R.T., Pelton, J.R., and Bailey, J.P., 1977, Yellowstone hot spot: Contemporary tectonics and crustal properties from earthquake and aeromagnetic data: Journal of Geophysical Research, p. 3665-3676.

Smith, R.B., Byrd, J.O.D., Susong, D.D., 1993a, Seismotectonics, Quaternary history, and earthquake hazards of the Teton Fault, Wyoming, in *Geology of Wyoming, Memoir 5*, edited by A. Snoke et al., p. 628-667: Geol. Surv. of Wyo., Laramie, Wyo.

Smith, R. B., K. L. Pierce and R. J. Wold, 1993, Quaternary history and structure of Jackson Lake, Wyoming, from seismic reflection surveys, in A. W. Snoke, J. Steidtmann, and S. M. Roberts, editors "Geology of Wyoming": Geological Survey of Wyoming Memoir No. 5, p. 668-693.

Smith, R.B. and Arabasz, W.J., 1991, Seismicity of the Intermountain seismic belt, *in* Slemmons, D.B., Engdahl, E.R., Zoback, M.D., and Blackwell, D.D., eds., Neotectonics of North America: Geological Society of America, North America Decade Map, v.1, p.185-228.

Smith, R.B., and Seigel, L.J., 2000, Windows into the Earth – The Geologic Story of Yellowstone and Grand Teton National Parks: New York, Oxford University Press, p. 242.

Soderland, P., Juez-Larre, J., Page, L.M., Dunai, T.J., 2005, Extending the time range of apatite (U-Th)/He thermochronology in slowly cooled terranes: Paleozoic to Cenozoic exhumation history of southeast Sweden: Earth Planet. Sci. Lett., v. 239, p. 266-275.

Stewart, J.H., 1980, Regional tilt patterns of late Cenozoic basin-range fault blocks, western

United States: Geological Society of America Bulletin, v. 91, p. 460– 464.

Stockli, D.F., Farley, K.A., and Dumitru, T.A., 2000, Calibration of the (U-Th)/He thermochronometer on an exhumed fault block, White Mountains, California: Geology, v. 28, p. 983 – 986.

Strutt, R., 1908, On the accumulation of helium in geologic time: Proc Roy Soc London v. 81A, p. 272-277.

Tranel, L.M., Spotila, J.A., and Waller, C.M., in review, Spatial variation of erosion in a small, glaciated basin in the Teton Range, Wyoming, based on detrital apatite (U-Th)/He thermochronology: Basin Research.

Tranel, L.M. and Spotila, J.A., 2007, Uniformity of drainage basin erosion and relief based on detrital thermochronometry and landscape analysis of the Teton Range, Wyoming: Geological Society of America, Abstracts with Programs, v. 39, no. 6, p. 107.

Walsh, J.J., Nicol, A., Childs, C., 2002, An alternative model for the growth of faults: Journal of Structural Geology, v. 24, p. 1669-1675.

Walsh, J.J., Bailey, W.R., Childs, C., Nicol, A., and Bonson, C.G., 2003, Formation of segmented normal faults: a 3-D perspective: Journal of Structural Geology, v. 25, p. 1251-1262.

Walsh, J.J. and Watterson, J., 1988, Analysis of the relationship between displacements and dimensions of faults: J. Struct. Geol., v. 10, p. 239-247.

Wells, D.L. and Coppersmith, K.J., 1994, New empirical relationships among magnitude, rupture length, rupture width, rupture area, and surface displacement: Seismological Society of America Bulletin, v.84, p. 974-1002.

White, B.J.P., Smith, R.B., Husen, S., Farrell, J.M., Wong, I., 2009, Seismicity and earthquake hazard analysis of the Teton-Yellowstone region, Wyoming: J. Volcanol. Geotherm. Res., doi:10.1016/j.volgeores.2009.08.015.

Wolf, R.A., Farley, K.A., and Silver, L.T., 1996, Helium diffusion and low-temperature thermochronometry of apatite: Geochimica et Cosmochimica Acta, v. 60, p. 4231-4140.

Wolf, R.A., Farley, K.A., and Kass, D.M., 1998, Modeling of the temperature sensitivity of the apatite (U-Th)/He thermochronometer: Chemical Geology, v. 148, p. 105 – 114.

Zeitler, P.K., Herczeg, A.L., McDougall, I., and Honda, M., 1987, U-Th-He dating of apatite: a potential thermochronometer: Geochima et Cosmochimica Acta, v. 51, p. 2865 – 2868.